UNIVERSITY OF KWAZULU-NATAL
INYUVESI YAKWAZULU-NATALI

N- and S-donor pincer complexes of Ni and Cu: synthesis and application as catalysts in alkane oxidation

by

Lynette Soobramoney

2017

Dissertation submitted in fulfilment of the academic requirements for the degree of Doctor of Philosophy

School of Chemistry & Physics, College of Agriculture, Engineering and Science, University of KwaZulu-Natal, Durban

As the candidate's supervisors we have approved this dissertation for submission.

_____	_____
Prof. M. D Bala	Date
_____	_____
Prof. H. B. Friedrich	Date

Abstract

Pincer compounds have become increasingly popular over the last few decades as coordinating ligands due to various advantageous features that include stability, flexibility and structural variability. Hemilabile pincer ligands, in particular, are of interest because of dissimilarity in donor strengths, a feature that is especially beneficial in catalysis. In this study, a series of mixed donor N- and S-based pincer ligands were prepared and coordinated to first row transition metals, nickel and copper, for application in alkane oxidation.

Two series of flexible SNS ligands, differentiated on the basis of the N-donor substituent i.e. a methyl or a phenyl group, were prepared with a further variation in the type of S-donor substituents. The different types of substituents that were employed were: methyl, ethyl, butyl, cyclohexyl and *t*-butyl, to yield ten ligands. Six of the ligands were coordinated to nickel to yield six new complexes and all ten ligands were coordinated to copper. All the compounds were characterised by NMR, IR, HRMS, CHN analysis and single crystal X-ray diffraction for selected compounds.

Analysis of the single crystal X-ray data showed that the nickel complexes of the series containing the methyl N-substituted ligands crystallised as bimetallic dimers bridged through three chlorides, whereas the phenyl N-substituted complexes were five coordinate monomers. The copper complexes also crystallised as five coordinate monomeric species with a trigonal bipyramidal geometry around each copper(II) centre. The only exception is the complex containing ethyl substituents on the S-donor atoms (phenyl substituted N-donor), which crystallised in a dimeric fashion bridged through a $[CuCl_4]^{2-}$ anion.

All the complexes were applied as catalysts in the oxidation of *n*-octane using both *tert*-butyl hydroperoxide (TBHP) and hydrogen peroxide (H_2O_2) as the oxidants. The nickel complexes produced a mixture of octanols and octanones oxygenated at C-2 to C-4 (of the C-8 alkane chain) with yields of 6-10% at 48 h and a selectivity of up to 77% to the octanones, using TBHP. The copper catalysts were much more active, producing yields of up to 57% at 1 h and turnover numbers (TONs) of 2270- 3180 at 24 h, using H_2O_2. Selectivity to the terminal or

C(1) carbon was substantial (up to 27%) and the highest selectivity was to the secondary octanols, which formed as the major products (after reduction with PPh_3).

In addition, a series of NSN ligands were synthesised and applied in a 'one pot' *in situ* catalytic study with various metal salts, using H_2O_2 as the source of oxygen. An improvement in the product yield from 12% based on a $CuCl_2/H_2O_2$ system to 21-27% when the NSN ligands were utilised along with the Cu(II) salt, implies definite ligand effect. Furthermore, selectivity to C(1) products was enhanced by the addition of the NSN ligands *in situ*, with up to 27% C(1) functionalisation achieved.

Preface

The experimental work described in this thesis was performed in the School of Chemistry and Physics, University of KwaZulu-Natal, Durban, from July 2012 to May 2017, under the supervision of Prof M. D. Bala and Prof. H. B. Friedrich.

These studies represent original work by the author and have not otherwise been submitted in any form for any degree or diploma to any tertiary institution. The work of others that has been used in this study is duly acknowledged in the text.

Lynette Soobramoney
BSc-Honors (*cum laude*) (UKZN)
MSc (*cum laude*) (UKZN)

Declarations

Declaration 1: Plagiarism

I, Lynette Soobramoney, declare that:

1. The research reported in this thesis, except where otherwise indicated, is my original research.
2. This thesis has not been submitted for any degree or examination at any other university.
3. This thesis does not contain other persons' data, pictures, graphs or other information, unless specifically acknowledged as being sourced from other persons.
4. This thesis does not contain other persons' writing, unless specifically acknowledged as being sourced from other researchers. Where other written sources have been quoted, then:
    a. Their words have been re-written but the general information attributed to them has been referenced
    b. Where their exact words have been used, then their writing has been placed in italics and inside quotation marks, and referenced.
5. This thesis does not contain text, graphics or tables copied and pasted from the Internet, unless specifically acknowledged, and the source being detailed in the thesis and in the References sections.

Signed: _____ Date: _____

Lynette Soobramoney

Declaration 2: Publications

Publication 1: Coordination chemistry of Co complexes containing tridentate SNS ligands and their application as catalysts for the oxidation of *n*-octane

Lynette Soobramoney, Muhammad D. Bala* and Holger B. Friedrich*

Dalton Trans. **2014**, *43*, 15968

Publication 2: Utilisation of new NiSNS pincer complexes in paraffin oxidation

Lynette Soobramoney, Muhammad D. Bala* and Holger B. Friedrich*

Submitted for publication in Inorganica Chimica Acta
(Reference no.: ICA_2017_1388)

Publication 3: Flexible pincer backbone revisited: the case of new CuSNS complexes as efficient catalysts in paraffin oxidation

Lynette Soobramoney, Muhammad D. Bala* and Holger B. Friedrich*

In preparation for submission.

Publication 4: Application of thiophene-based NSN ligands in paraffin oxidation catalysis: *in situ* generation of the active catalyst

Lynette Soobramoney, Muhammad D. Bala* and Holger B. Friedrich*

In preparation for submission.

Contribution by authors:

Muhammad Bala and Holger Friedrich were the research supervisors.

I completed all of the experimental work, analysis of results and compilation of the manuscripts.

Signed: _____ Date: _____

Lynette Soobramoney

Declaration 3: Conference proceedings

Catalysis Society of South Africa (CATSA) 2012

Oral Presentation: Application of cobalt complexes containing pincer-type SNS ligands as catalysts for biomimetic paraffin activation
L. Soobramoney, M. D. Bala and H. B. Friedrich

Catalysis Society of South Africa (CATSA) 2013

Poster Presentation: Synthesis and applications of pincer type S- and N- donor ligands of iron group metals for paraffin activation
L. Soobramoney, M. D. Bala and H. B. Friedrich

41st International conference on coordination chemistry (ICCC41) 2014, Singapore.

Poster Presentation: Synthesis of tridentate S- and N- donor ligands of iron group metals for the activation of paraffins.
L. Soobramoney, M. D. Bala and H. B. Friedrich

Catalysis Society of South Africa (CATSA) 2015

Oral Presentation: Transition metal complexes of pincer type S- and N-donor ligands as catalysts for the oxidation of *n*-octane.
L. Soobramoney, M. D. Bala and H. B. Friedrich

This dissertation is dedicated to the love of my life… my husband, Jerome Soobramoney

Acknowledgements

I give thanks and honour to my Lord and Saviour, Jesus Christ, for without Him I would not be where I am today… "*Your grace is sufficient for me.*"

My heartfelt gratitude to my supervisors, Prof. Muhammad D. Bala and Prof. Holger B. Friedrich, for their constant guidance and exceptional supervision throughout my postgraduate studies.

I gratefully thank c* change and NRF for financial support.

I also thank Dr Hong Su, Dr Michael Pillay and Mr Sizwe Zamisa for X-ray crystallographic data collection and refinement.

My extended appreciation goes out to the (technical) staff at the School of Chemistry and Physics: Anita Naidoo, Dilip Jagjivan, Gregory Moodley, Kishore Singh, Malini Padayachee, Miler Nundkumar, Mpho Sehoto, Renee Naidoo, Raj Somaru, Unathi Bongoza and Vashti Reddy for their assistance and contributions.

Special thanks to my lab mates and friends: Michael Pillay, Veresha Dukhi, Ebrahim Kadwa, Reshreen Singh, Vashen Moodley, Drushan Padayachee, Revana Chanerika, Kershen Naicker, Fezile Potwana, Saravanan Thangavel, Chintan Patel and Hari Narayana, as well as the members of the Catalysis Research Group (CRG), for their unwavering help, support and valuable contributions.

I am forever grateful to my parents, extended family, pastors, Life International family and Lightbearers family for their love, prayers, support and constant motivation.

I especially thank my husband, Jerome, for being so understanding, patient and supportive throughout my postgraduate studies, and for believing in me even when I didn't.

And to my late mom, thank you for everything you've invested in me… I know you would have been so proud of where I am today.

List of ligands

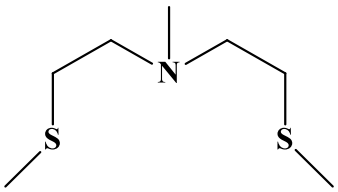

L1a*

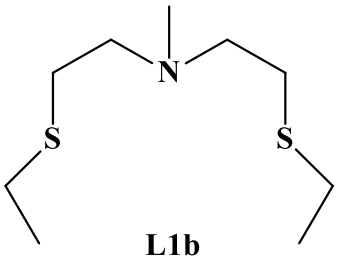

L1b

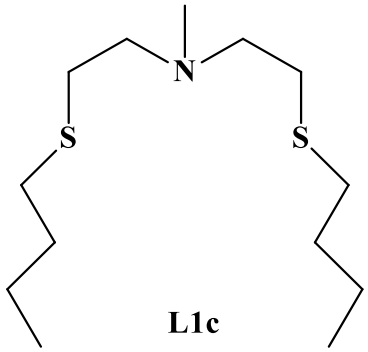

L1c

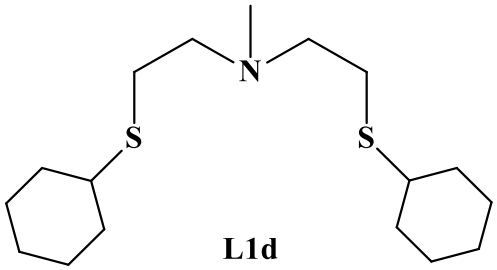

L1d

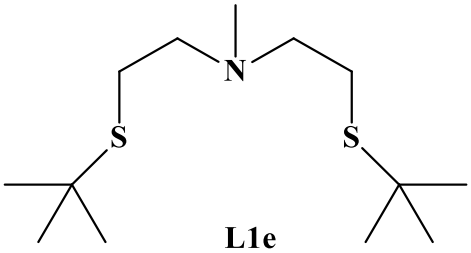

L1e

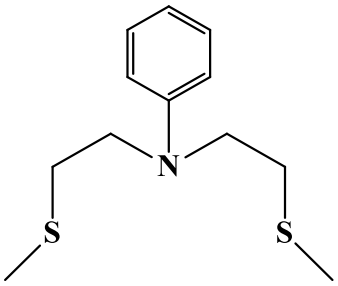

L2a

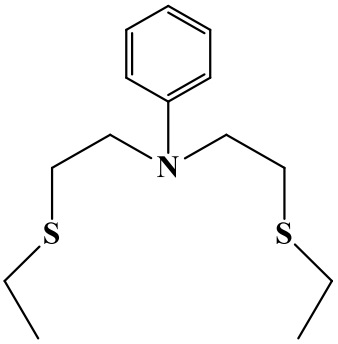

L2b*

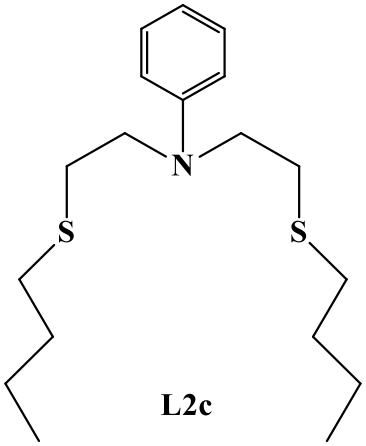

L2c

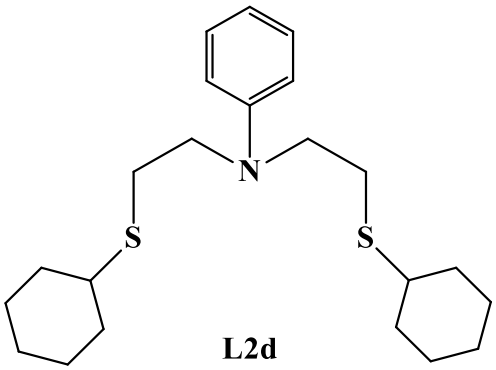

L2d

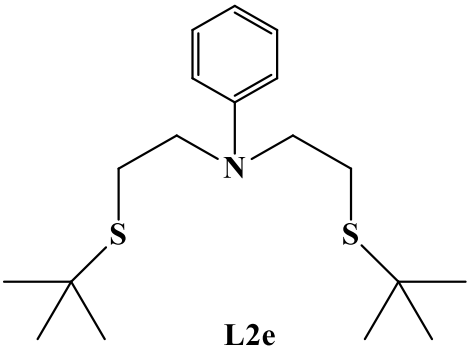

L2e

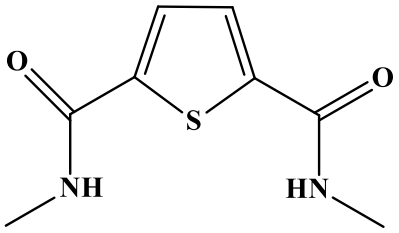

L3a

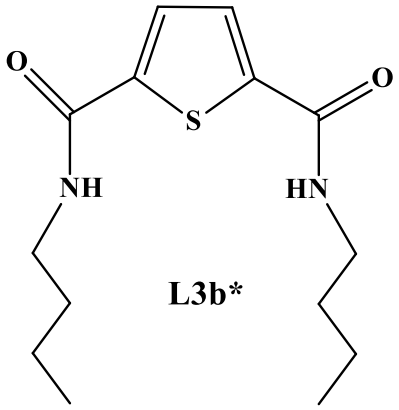

L3b*

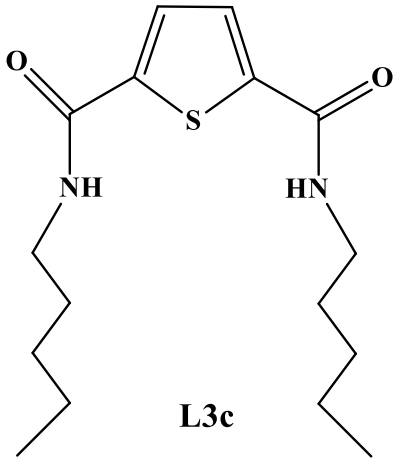

L3c

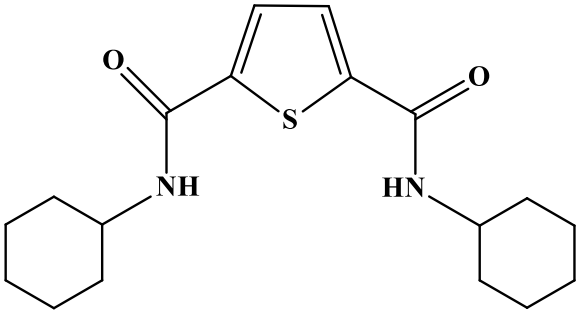

L3d

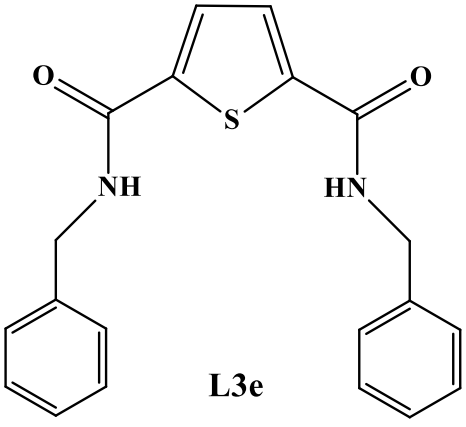

L3e

*These ligands have been reported before.

List of complexes

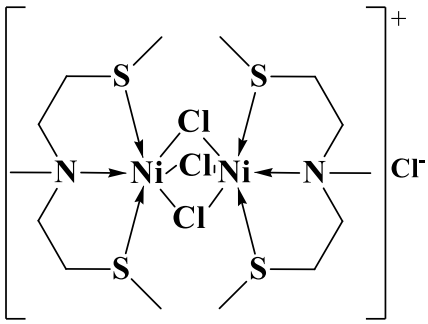

1.1a

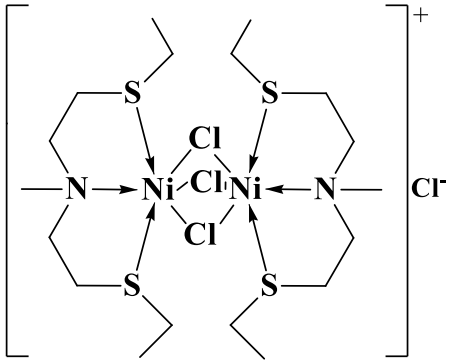

1.1b

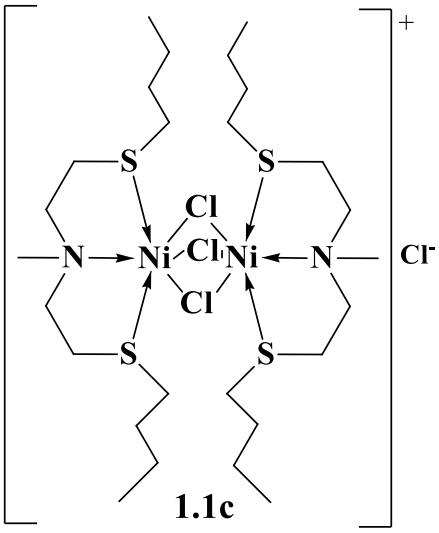

1.1c

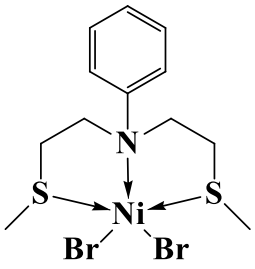

1.2a

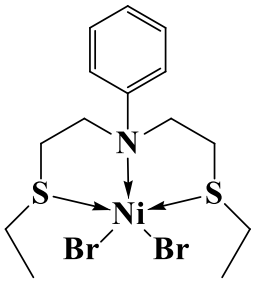

1.2b

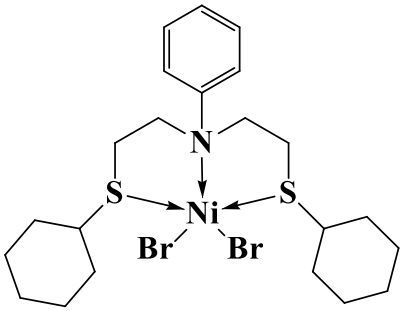

1.2d

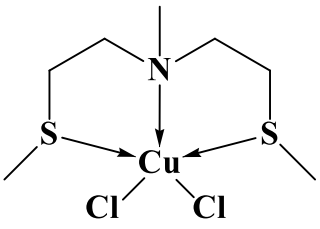

2.1a

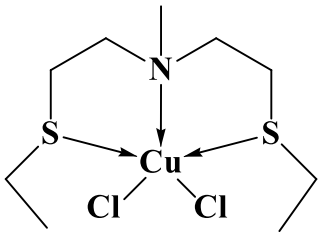

2.1b

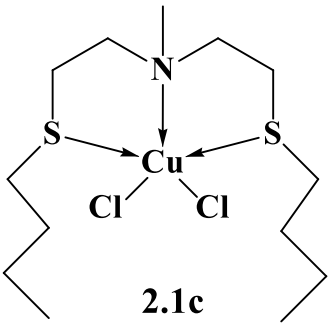

2.1c

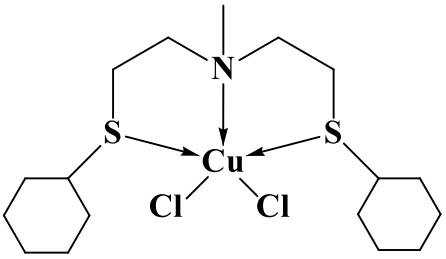

2.1d

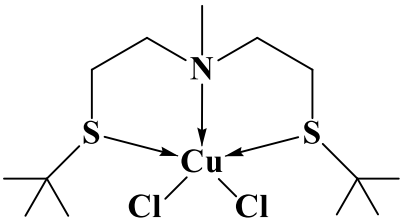

2.1e

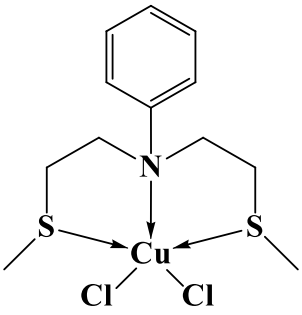

2.2a

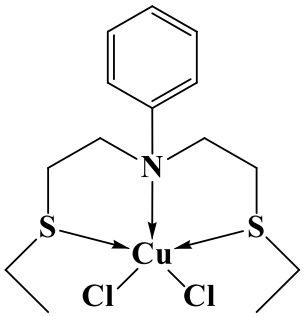

2.2b

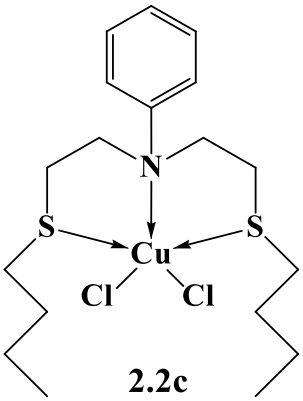

2.2c

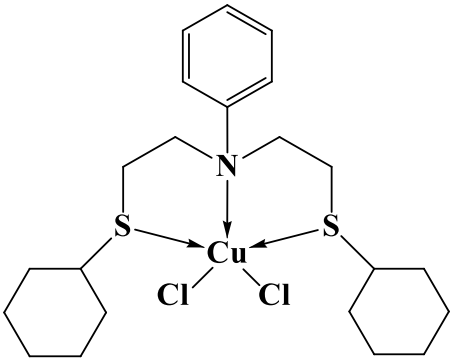

2.2d

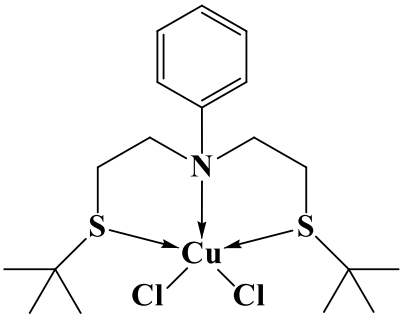

2.2e

List of Figures

List of Schemes

List of Tables

List of Abbreviations

APT		Attached proton test
ATR	-	Attenuated total reflectance
Bu	-	Butyl
CIF	-	Crystallographic information file
Cy	-	Cyclohexyl
CYPs	-	Cytochrome P450 monooxygenases
d	-	Doublet
DEPT	-	Distortionless enhancement by polarisation transfer
DFT	-	Density functional theory
DCM	-	Dichloromethane
ESI	-	Electron spray ionisation
Et	-	Ethyl
GC	-	Gas chromatography
IR	-	Infrared
L	-	Ligand
M	-	Metal
m	-	Multiplet
m-CBPA	-	*meta*-Chloroperoxybenzoic acid
Me	-	Methyl

MHz	-	Mega Hertz
MMO	-	Methane monooxygenase
mp	-	Melting point
N/A	-	Not applicable
NAD(P)H	-	Nicotinamide adenine dinucleotide phosphate
neg	-	Negative
NMR	-	Nuclear magnetic resonance
ORTEP	-	Oak ridge thermal ellipsoid plot
Ph	-	Phenyl
Ph-tos	-	Bis(2-tosylethyl)phenylamine
pos	-	Positive
RBF	-	Round bottom flask
s	-	Singlet
t	-	Triplet
TBHP	-	*tert*-Butyl hydroperoxide
THF	-	Tetrahydrofuran
TON	-	Turnover number
q	-	Quartet

Table of Contents

CHAPTER ONE

Introduction and Literature Review

1.1 Overview on pincer compounds

One of the earliest reports on pincer ligands dates back to 1976 by Moulton and Shaw.[1] Although not termed pincer at the time, their ligand exhibited a classic tridentate binding mode to the metal centre, which is a typical description of a pincer ligand. Since then, extensive research by a variety of groups has been devoted to the chemistry of pincer compounds.[2-5] A pincer ligand can be characteristically defined as a chelating agent that coordinates to a metal centre via three donor atoms. If one or more of the donor atoms on the ligand are carbons then a metal–carbon σ bond is usually formed which, being a strong bond, can limit or prevent dissociation of the ligand from the metal.[6] This is quite beneficial, especially in catalytic processes, as it confers a certain degree of stability upon the metal complex, particularly at high temperatures.[7,8]

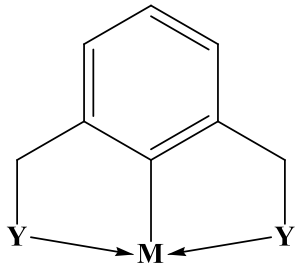

Figure 1.1: General structure of classic tridentate pincer ligands. Y = N, S, P, O; M = transition metal.

There are a wide variety of mixed-donor pincer systems ranging from the symmetrical ligands such as PCP[1,9-14], PNP[12,15] and ONO[16,17] to asymmetric hybrid systems like PNS[18,19], PNN[18-20] and PNO[19,21]. However, there have also been many reports on systems that contain identical donor atoms, e.g. NNN[22-24] and CCC[25,26]. A common type of pincer ligand contains an aromatic ring that

forms one σ bond with the metal and the *ortho* groups coordinate to the metal centre via various donor atoms (Fig. 1.1).[6] The vast number of modifications that pincer ligands can be subjected to makes them very desirable, especially in the area of homogeneous catalysis which this review will address in forthcoming sections.

1.1.1 Key features of pincer ligands

Not only can the steric and electronic features of the ligand be tuned, but the donor atoms can also be varied which subsequently influences factors such as hemilability and stability of any metal complex derived from it. In comparison to mono and bidentate ligands, pincer ligands bind to the metal centre via three bonds, which gives rise to the chelate effect and hence a relatively more stable complex.

Since the donor atoms in a pincer ligand can be varied (**E** and **Y**, Fig 1.2), the nature of the interaction between the donor atoms and the metal becomes important, as it determines the type of metal−ligand (M−L) coordination that may result. The M−L combination can determine if a coordination compound is likely to form, for instance, it is uncommon for hard metals and soft donors to coordinate. Late transition metals are known to be soft metals and therefore would interact readily with soft donors and hard early transition metals will preferentially bind hard donors. However, if a pincer skeleton contains only weak donor atoms, then the ligand will be labile, which means that it will form weak coordinative bonds with the metal and can easily dissociate, thus yielding an unstable complex. Hence, depending on the application of a pincer complex, mixed donor atoms with varying donor strengths are generally incorporated into the pincer backbone to modulate the reactivity of the metal centre.

Another important feature to consider is the spacer group linking the central donor group (or atom) **E** to the *ortho* donors **A** (Fig. 1.2). For pincers containing alkyl groups as linkers, the length of the spacer group can determine the degree of flexibility of the ligand. For example, an ethylene spacer is more flexible than a methylene group.[27] It has also been reported that the nature of the spacer group can enhance the solubility of a pincer compound.[28] Furthermore, hetero atoms such as O and N can be incorporated into the spacer to introduce chirality[12] or stability[29] amongst other properties.

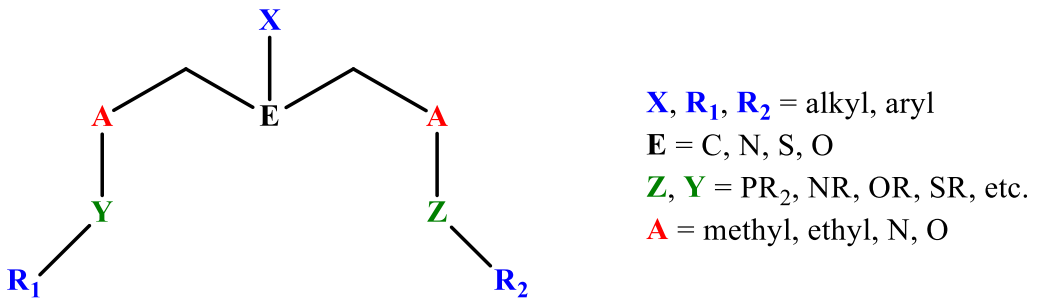

Figure 1.2: General structure of a pincer ligand showing the different variables.

Other factors that can affect the flexibility, stability and electronic properties of a pincer compound are the substituents $\mathbf{R_1}$, $\mathbf{R_2}$ directly attached to the donor atoms **Y**, **Z** (Fig. 1.2). For example, with alkyl substituents, as the chain length increases, an increase in electron density at the donor atom and increased flexibility of the pincer compound is observed, but stability is enhanced if more rigid aromatic groups are employed.

1.1.2 Applications of pincer complexes in homogeneous catalysis

Pincer complexes have been widely explored as homogeneous catalyst precusors in a variety of applications. The Heck reaction, which is a palladium catalysed reaction that involves C-C coupling between aryl or vinyl halides and activated alkenes in the presence of a base (Scheme 1.1), is an important reaction in organic synthesis. The first report on the use of palladium pincer complexes as catalysts for the Heck reaction was by Milstein *et al.* in 1997.[30] They synthesized and coordinated a range of phosphino PCP ligands to palladium and found that these complexes were highly efficient catalysts in the coupling of iodobenzene with methylacrylate, producing high yields at high turnover numbers. Moreover, the catalysts were very robust, since there was no decomposition observed at elevated temperatures, and the chelating pincer backbone enhanced the stability of the catalysts, thereby preventing degradation under an oxygen-rich atmosphere. Other reported pincer complexes of palladium used in the Heck reaction contained CCC,[28] CNC,[28,31] and SCS pincer ligands[32].

The Suzuki or Suzuki-Miyaura coupling reaction[33] is another popular application of pincer complexes which proceeds via a similar reaction pathway as the Heck reaction. Therefore, it is

very common that most of the catalysts utilized in the Heck reaction have also been applied in Suzuki coupling. Hence, palladium pincer PCP complexes have also shown exceptional activity in Suzuki reactions.[34]

A review by Younus *et al.* describes the catalytic applications of ruthenium pincer compounds in detail, focusing on oxidative dehydrogenation, direct hydrogenation and hydrogen transfer.[35]

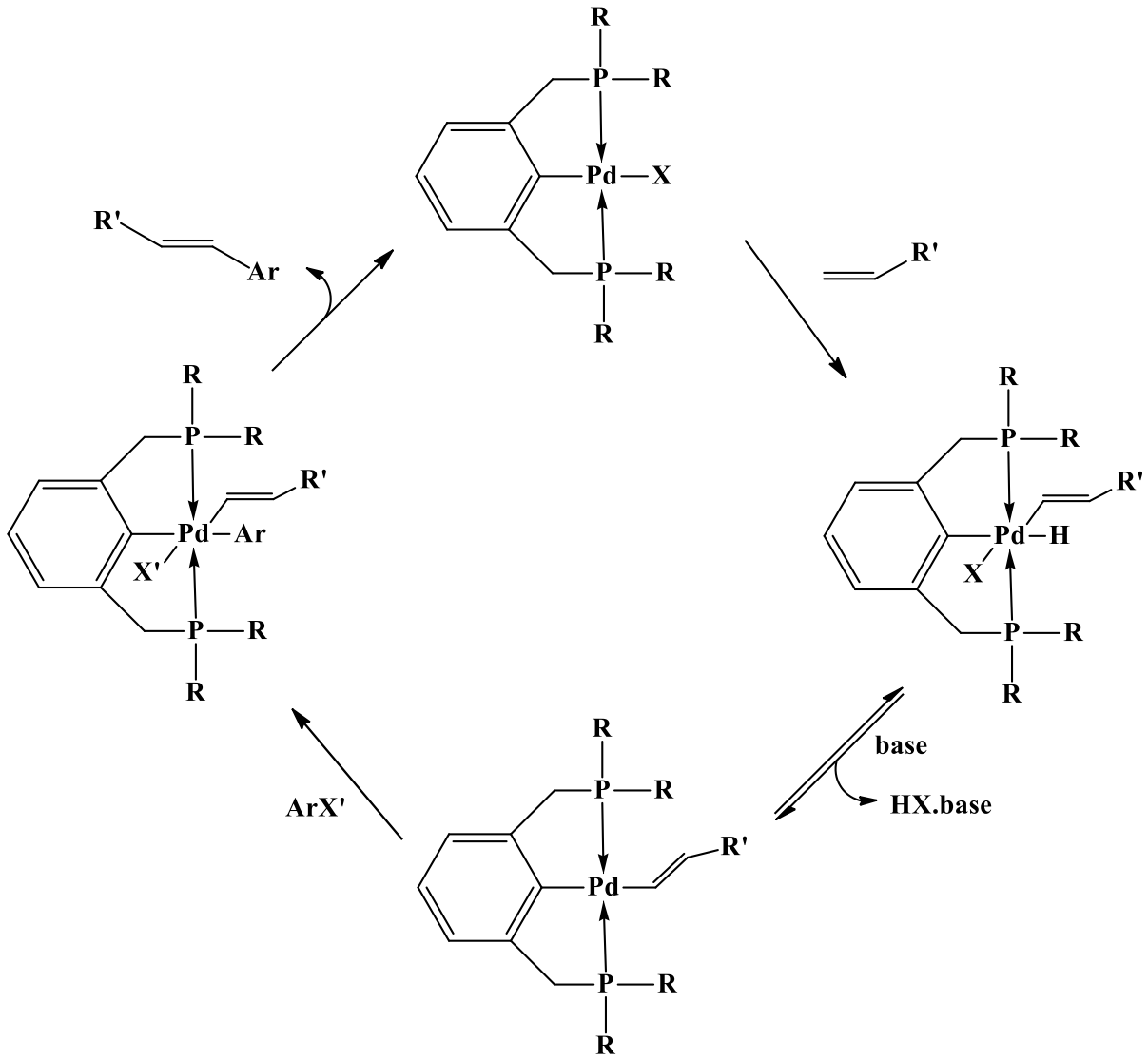

Scheme 1.1: General proposed mechanism of a Pd(PCP) catalyzed Heck reaction.[6]

1.2 Pincer complexes based on S- and N-donor atoms

Thus far, a general overview of pincer compounds has been presented, the following sections will more specifically focus on pincer compounds based on N- and S-donor atoms, the basis of this study. This class of pincer ligands has not been as extensively explored as that based on phosphines. However, due to the presence of mixed donor strengths i.e. soft S-donors and hard N-donors, these ligands are known to be hemilabile, which is an attractive feature that can be very useful, especially in catalytic applications. The two main classes that will be elaborated on are the SNS and NSN pincer ligands, along with their complexes.

1.2.1 SNS pincer compounds and their applications

Pincer complexes containing SNS ligand systems have received relatively less attention in comparison to other pincers like the popular PNP donor set. However, since the discovery of SNS complexes of chromium[36-41] as useful ethylene trimerisation catalysts, research exploring the SNS pincer backbone has advanced. To date, SNS pincer complexes of Cr,[36] Mo,[42] W,[43] Ru,[44-46] Co,[47] Ir,[48] Ni,[49] Pd,[50,51] Pt,[52,53] Cu,[54] Zn,[55-57] Cd,[58] and Hg[58] have been successfully synthesised and characterised. A SNS ligand consists of two relatively soft sulfur donors linked to a central hard nitrogen donor atom. The source of these donors can be varied, but most often the backbone is built from an *ortho* disubstituted pyridine ring. The synthesis of these compounds is generally straight forward and does not usually involve rigorous inert conditions as required for air sensitive phosphine-based pincer ligands. This is another reason for their increasing popularity.

There are various types of SNS backbone designs that have been reported in the literature, some of which are shown in Fig. 1.3. Ligand **A** features thioamide donor arms with a central pyridine backbone,[45,46,53] while ligand **B** contains two thiones as the S-donors that are directly attached to imidazole rings.[59] Ligands **C**[39,50,55,60] and **D**[49,61] are simpler designs with **C** containing a central pyridine donor and **D** employing a flexible amine backbone with an ethylene linker to the sulfide arms. In all of these ligands the R groups were varied, employing either alkyl or aromatic substituents. Each of these ligand systems exhibit different properties in terms of their stability,

flexibility and binding mode, which ultimately influence the performance and application of their metal complexes.[62]

The thioamide type SNS ligand **A** binds to metals via two different modes: either as the neutral thioamide or the anionic iminothiolate where there is a negative charge on the S-donor atom.[62] In the presence of a base, the thioamides are deprotonated to form the iminothiolate which reverts to the neutral form when an acid is added. The deprotonation creates an avenue for the formation of various multinuclear complexes which have been widely explored, especially with platinum and palladium transition metals forming square planar complexes.[63-70]

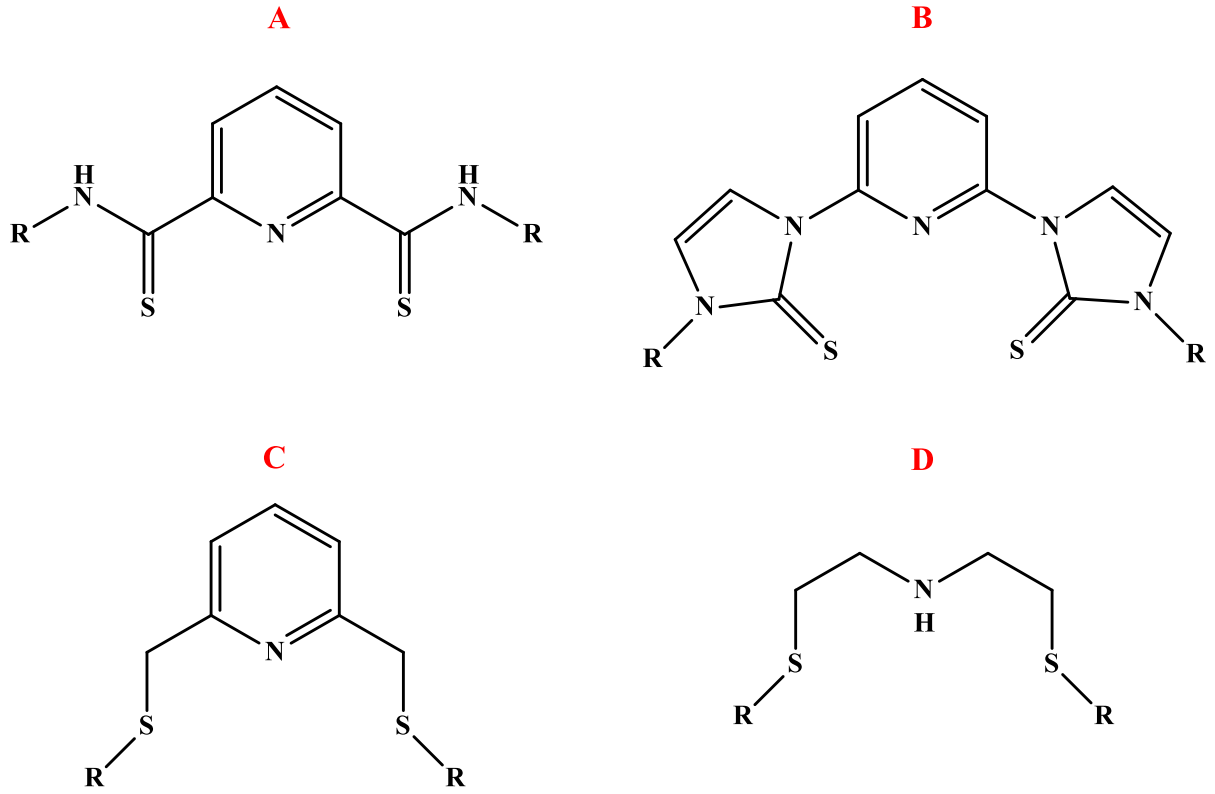

Figure 1.3: Examples of the different types of SNS ligands reported in the literature.

The type of substituents bonded to the N-donor atom also affects the binding mode of the ligand as demonstrated by Wang *et al.* (Scheme 1.2) where the SNS ligand **A** coordinated as a neutral dithioamide, when R = *t*-butyl, thus forming a charged complex **1**, while a neutral complex **2** containing a mixed thioamide-iminothiolate was formed when R = phenyl.[53]

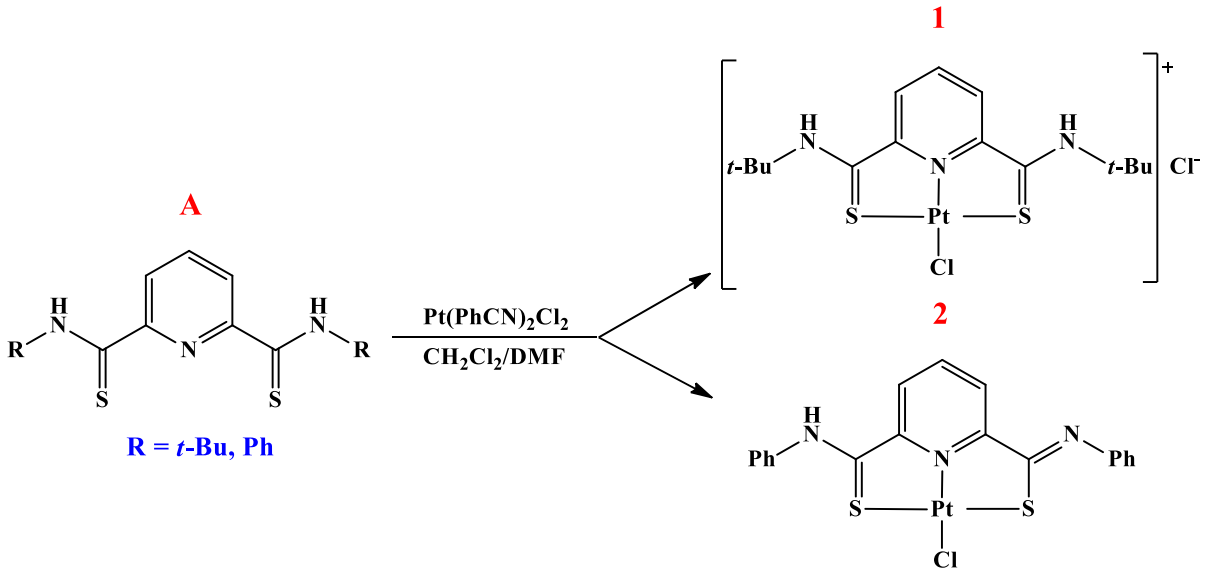

Scheme 1.2: Reaction pathway for PtSNS complexes bearing ligand type **A**.

Although ligand **B** is a pincer type ligand, when complexed to gold it coordinated in a bidentate fashion in order to form a stable complex as reported by Jia *et al*.[59] The complex was used to catalyse the reduction of 4-nitrophenol (an organic pollutant) to 4-nitroaniline with a TOF of 1.20 min^{-1}.[59]

According to a study by Page and co-workers, the catalytic application of ligand **C** coordinated to ruthenium has shown some promising results.[71] They applied the RuSNS complex as a catalyst in the transfer hydrogenation of acetophenone and obtained high activities, giving up to 96% conversion and TOF of circa 87000 h^{-1}.

This was a significant improvement over a reported phosphine-based RuPNP complex which achieved a TOF of 9000 h^{-1}.[72] However, the RuSNS catalysts underwent rapid deactivation ranging from 30 min to as low as 90 s. Work carried out by Shimokawa *et al.* employed a series of benzylpalladium complexes containing ligand **C** (with pyridine substituents coordinated to the sulphides) in the oxygenation of the benzyl ligand, using O_2, to organic products.[73]

Air-stable ruthenium complexes bearing the flexible SNS ligand **D** were reported by Gusev and co-workers (Fig 1.4). They replaced phosphorous with sulfide in Noyori-type catalysts in an attempt to overcome drawbacks associated with phosphine-based catalysts. Their results have shown that these RuSNS complexes are highly efficient catalysts in the hydrogenation of esters,

ketones and imines producing high TONs of up to 40000 under mild temperatures (23-40 °C) and low catalyst loadings (0.05 mol%).[74] However, a recent study was carried out by Chen and co-workers, who investigated the mechanism of the hydrogenation of ethyl acetate to produce ethanol computationally using DFT.[75] They employed Gusev's RuSNS catalyst and found that the actual catalyst in the reaction is the one in which the sulfurs are *trans* to one another, while the complex with the *cis*-sulfur atoms is more stable and can be considered as a resting state in the catalytic cycle. Their results also indicated that the catalytic cycle may be deactivated by the formation of a *fac*-SNS geometry.

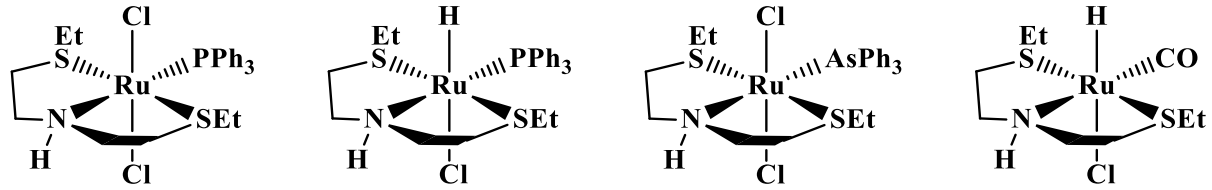

Figure 1.4: Ruthenium complexes containing the flexible SNS backbone **D**.

1.2.1.1 SNS complexes of late first row transition metals

SNS pincer complexes of first row transition metals, particularly those of iron, cobalt, nickel and copper are of importance since these metals are low cost, readily available and relatively non-toxic, thereby yielding economical complexes with a variety of applications. SNS complexes of these metals can also be regarded as biomimetic since these consist of common elements found in nature, particularly in enzymes.[76-78] The enzymes, as biological catalysts, exhibit incredible activity in biological processes that have inspired many areas of scientific research which copy enzymatic designs as a synthetic basis to numerous metal complexes. For example, cytochrome P450 is a well-known monooxygenase enzyme that contains iron as the active metal centre and has been an effective catalyst in hydroxylation reactions.[79-81]

As mentioned previously, S-donor atoms are regarded as soft donors and therefore are not likely to coordinate to hard metals such as iron unless they are electron rich. For this reason, it is quite rare to encounter FeSNS complexes, however, a recent article reports an asymmetric monoanionic thiolate ligand coordinated to iron.[82] This ligand undergoes ring opening when reacted with

$Fe(OTf)_2$ in the presence of NaO^tBu as the base to afford a trinuclear FeSNS complex as seen in Scheme 1.3. Furthermore, upon reaction with excess phosphine ($PMePh_2$), phosphite [$P(OMe)_3$] or 2,6-dimethylphenyl isocyanide, Baker and co-workers were able to synthesise diamagnetic dinuclear FeSNS complexes.[82] Another recent article describes the synthesis and characterisation of a pyridine-based SNS ligand and its coordination to iron, cobalt, nickel, copper and zinc together with the application of the complexes in antibacterial studies.[83]

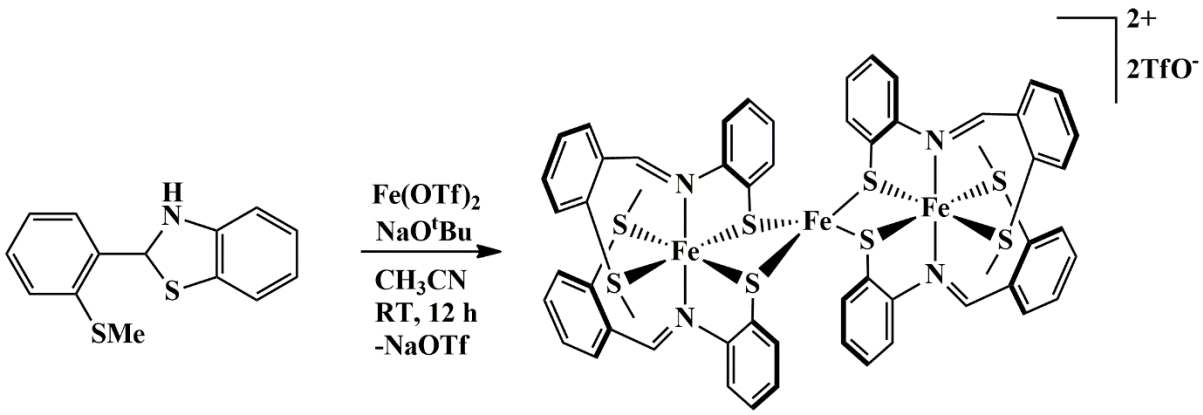

Scheme 1.3: Synthesis of a trinuclear iron complex containing a monoanionic SNS ligand.

Apart from this one report on CoSNS complexes[83], to the best of our knowledge, our previously reported work is the only other literature available that describes complete synthesis and characterisation of such compounds.[47] Also, the SNS pincer complexes of nickel and copper have not been extensively explored, however, there are a few reports available in the literature, and these are highlighted below.

NiSNS complexes may exhibit four-, five- or six-coordination of the donor atoms to the metal centre depending on the ligand and nickel salt used.[32,84-86] A four-coordinate NiSNS complex was reported by Koizumi *et al.* which contained a thioamide-based SNS ligand with a pyrrole ring as the N-donor source (Fig. 1.5a).[84] A five-coordinate complex displaying a distorted square pyramidal geometry has also been reported in which the crystal structure revealed that the SNS ligand coordinated in a meridional fashion (Fig. 1.5b).[86]

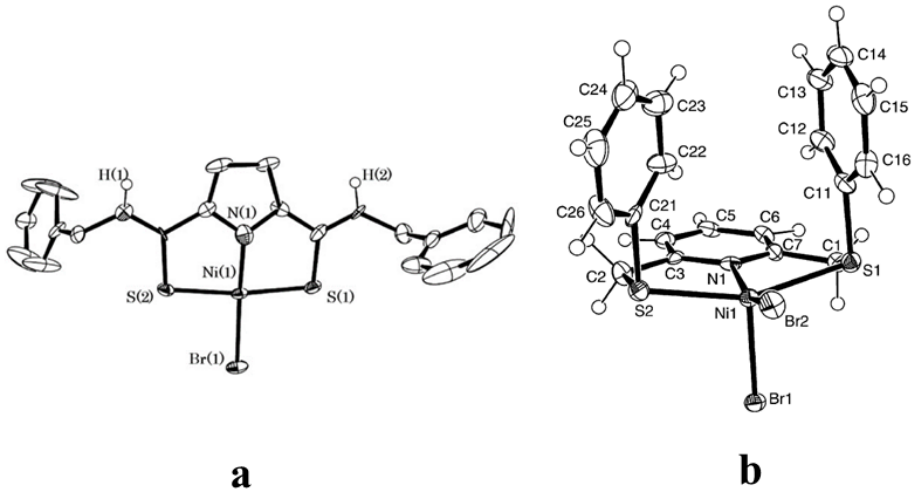

Figure 1.5: Crystal structures of a thioamide based (a) and pyridine based (b) NiSNS complexes.[84,86]

Hahn *et al.* reported a set of copper(II) complexes containing an aliphatic SNS ligand with either a methyl or benzyl substituent (or both) bonded to the S-donors.[87] The prepared complexes exhibited five coordinate, square pyramidal geometry around the metal centres with one forming a dinuclear nitrato-bridged complex (Fig. 1.6a). They found that the axial position was taken up by a chlorido ligand or, in the case of the bridged complex, the nitrato group, while the tridentate SNS ligand occupied the equatorial sites along with the other chlorido group. A similar complex with cyclohexyl substituents on the S-donor atoms has also been reported which displayed intermolecular hydrogen bonding interactions (Fig. 1.6b).[88] This complex was applied as a catalyst in a one-pot azide-alkyne cycloaddition reaction showing exceptional activity.[88]

Earlier work by Bai *et al.* prepared S-benzyl substituted CuSNS catalysts containing either Cl, Br, I or OTf ligands, also for application in azide-alkyne cycloadditions.[54] All of the prepared catalysts were found to be active at room temperature with up to 98% isolated yields.[54] Another relatively recent report by Hajifatheali *et al.* shows the synthesis of a novel SNS ligand functionalised with a methyl and a dodecyl substituent on the N- and S-donor atoms respectively.[89] In combination with copper, they developed an effective catalyst for the atom transfer radical polymerization of methyl methacrylate, the first of its kind.

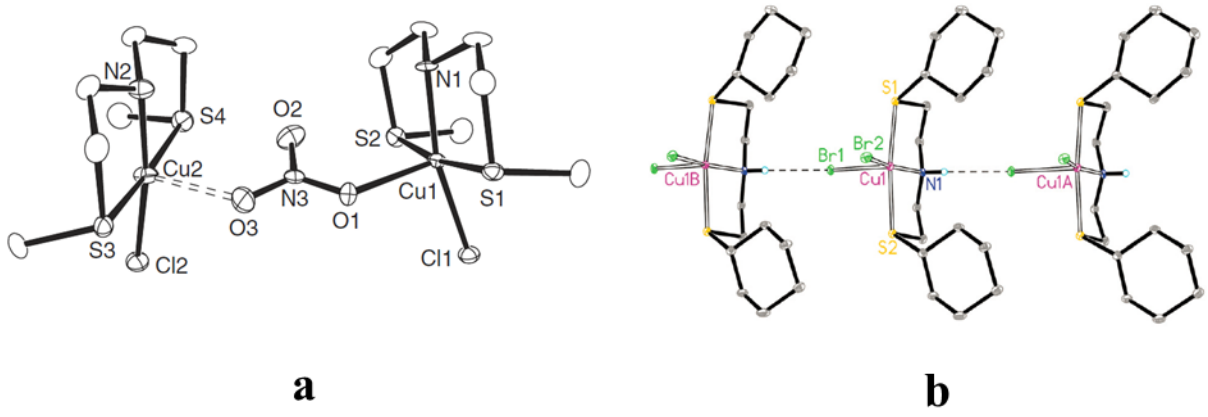

Figure 1.6: CuSNS complexes containing a bridging nitrato ligand (a) and a cyclohexyl-substituted ligand (b).[87,88]

As opposed to the flexible complexes discussed above, a more rigid system was reported by Miecznikowski and co-workers based on the combination of an imidazolyl/triazolyl and pyridyl backbone, containing bis-thiones coordinated to Cu(I) and Cu(II).[90,91]

1.2.2 NSN pincer compounds and their applications

The NSN pincer backbone contains two hard nitrogen donors and a central soft sulfur donor making this a more robust and thermally stable ligand in comparison to the hemilabile SNS moiety. However, despite these features, this particular type of pincer ligand system has probably been the least investigated amongst the pincer family because of the synthetic challenges and limitations arising from the combination of this donor set. Nevertheless, there are a few reports that describe the synthesis of different NSN compounds along with their applications.[92-94]

Interesting work carried out by Mylonas *et al.* describes the preparation of a novel asymmetric NSN ligand containing pyridyl and secondary amine moieties as the nitrogen sources with a central thioether functionality (Scheme 1.4).[95] They coordinated this ligand to rhenium (Re) and technetium (Tc) for potential application in radiopharmaceuticals. A crystal structure of the

ReNSN complex revealed a six coordinate, distorted octahedral geometry around the metal centre with the tridentate ligand and the CO groups bound facially.[95]

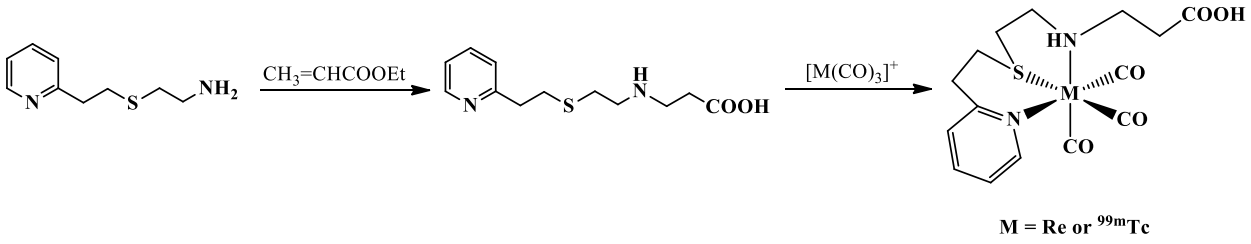

Scheme 1.4: Synthesis of novel asymmetric NSN ligand and complexes.

NSN ligands based on the diamidophenyl sulfide backbone have been reported with coordination to zirconium (Zr) and tantalum (Ta) to yield distorted trigonal bipyramidal/square pyramidal or pseudooctahedral complexes respectively. [96,97] A representative five-coordinate ZrNSN complex, Fig. 1.7a, exhibits a square pyramidal geometry around the Zr metal centre with a methyl substituent in the apical position, while the six coordinate TaNSN complex, Fig. 1.7b, showed the N-donors and two chlorido ligands residing in the equatorial plane and the S-donor, together with the Cp* ring, occupying axial positions. These complexes, along with other reported derivatives, have been fully characterized and form a series of novel compounds based on the tridentate NSN backbone.[96,97]

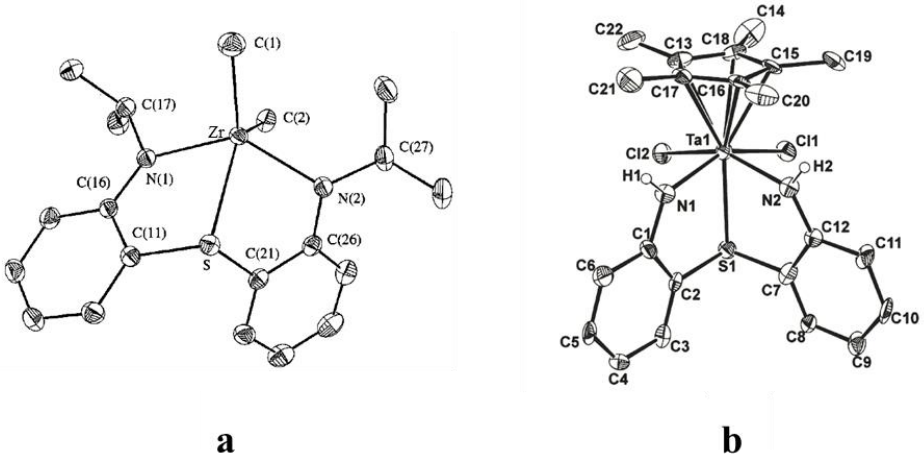

Figure 1.7: Crystal structures of ZrNSN (a) and TaNSN (b) complexes containing the diamidophenyl sulfide ligand.[96,97]

1.3 Oxidation of alkanes

Alkanes, also known as paraffins, are regarded as relatively inert compounds because they contain localised C−C and C−H bonds and also lack empty orbitals of low energy or filled orbitals of high energy required for the progression of chemical reactions.[98] These form major components of crude oil and natural gas and are therefore present in great quantity, particularly from petroleum industries.

Most often, these hydrocarbons are exploited for energy production in combustion reactions, and although it is possible to convert them into more reactive products, usually harsh reaction conditions are required, including extremely elevated temperatures and pressures, subsequently leading to uncontrollable reactions and unwanted by-products.[99] For this reason systems have been, and are continually being, developed to activate and functionalise the inert alkanes to more valuable or reactive products that have wider applications at industrial level.[99-101]

It is pertinent at this point that the terms activation and functionalisation be defined within the context of this discussion. Firstly, activation refers to the C−H bond of the hydrocarbon substrate binding to the active site of a catalyst, usually, but not always, resulting in the cleavage of that bond, whereas functionalisation occurs when a hydrogen is substituted with (a) non-hydrogen atom/s.[102] One of these processes involves selectively inserting e.g. oxygen into the hydrocarbon chain to yield, in this instance, oxygenated products such as alcohols, carboxylic acids, aldehydes and ketones. This type of catalytic reaction is commonly termed paraffin or alkane oxidation and can be carried out using biological, heterogeneous or homogeneous catalytic systems, but for the purpose of this discussion only the former and latter will be emphasized in subsequent sections of this chapter.

The activation step in alkane oxidation is followed by the addition of a single oxygen atom from a suitable oxidant to the activated hydrocarbon to obtain the functionalised oxygenated product. The most common oxygen sources are hydrogen peroxide (H_2O_2), *tert*-butyl hydroperoxide (TBHP) or molecular oxygen (O_2). Some reports involving metal oxo species have shown that the oxygen ligands on the metal could directly serve as the oxidant without the need for an added external oxidant.[103] These reactions, however, are stoichiometric and not catalytic.

Oxidation of paraffins is usually dominated by radical pathways in which case a hydrogen atom is removed, thus forming a radical which is functionalised to yield the product as demonstrated in Eq. 1.1.[98,104]

$$RH + O{=}M^{n+} \longrightarrow R^{\bullet} + HO{-}M^{(n-1)+} \longrightarrow ROH + M^{(n-2)+} \qquad \mathbf{1.1}$$

Both thermodynamic and kinetic factors affect the activity and selectivity of the catalytic system. Additionally, the strength of the C–H bond generally influences the efficiency of these radical reactions, therefore the terminal position of the alkane is difficult to activate because it has the highest bond energy in the hydrocarbon chain (e.g. 104 kcal.mol^{-1} for methane).[98,105] This is one of the drawbacks of most radical initiated alkane oxidation reactions, because products of terminal C-H activation are more desired than those of internal activation in the oxidation process.

1.3.1 Alkane oxidation by enzymes

The enzymatic oxidation of alkanes has been extensively investigated. This is because biological catalysts typically operate under mild reaction conditions with up to 100% selectivity to the desired product. Enzymes have, hence, offered inspiration for the development of commercial analogues of chemical compounds capable of catalysing the activation of C−H bonds of hydrocarbons and subsequently converting them into value-added products.[106-109] A class of oxidation enzymes found in nature comprise the group of monooxygenases responsible for selective catalysis that incorporates an oxygen atom from molecular oxygen into an organic substrate.[79,81,110] A variety of monooxygenases essential in metabolic processes of both eukaryotes and prokaryotes are known. The two types that are relevant to this study are briefly highlighted in the following discussion.

Firstly, the widely explored cytochrome P450 monooxygenases (CYPs) is an enzyme that contains a heme group with iron as the active metal centre.[111-114] Apart from participating in the conversion of relatively inert substrates into more reactive compounds, CYPs are also able to reduce the toxicity of certain compounds in a series of biological processes. [80] One of the roles that CYPs play is in the biosynthesis of progesterone, by oxidising the aliphatic side chain on cholesterol.[81]

Scheme 1.5 shows the proposed mechanism for the hydroxylation of alkanes by cytochrome P450 with the pathway followed to achieve the hydroxylated product at the active metal iron centre highlighted.[81] The initial step involves the generation of a Fe^{III}–OO• intermediate, when the Fe^{II} species binds O_2, thereby leading to the formation of Fe^{III}–OOH from the transfer of an electron and a proton to the active site. This subsequently produces the Fe^{IV}=O species which is responsible for the oxidation of the substrate to yield the hydroxylate product with the Fe^{II} centre regenerated.[80,81] The Fe^{III} centre can also be transformed to the high valent species via a peroxide shunt.

Second is methane monooxygenase (MMO), an enzyme commonly found in microorganisms such as methanotrophs, which convert methane into methanol during metabolism.[81,115] There are two types of MMOs: a soluble form (sMMO) containing a catalytic diiron centre and a particulate or membrane-bound form (pMMO) that uses a copper active site.[115,116] Three protein components make up the sMMO enzyme system. These are a hydroxylase (MMOH which contains the diiron metal cluster), a reductase (MMOR that facilitates electron transfer between nicotinamide adenine dinucleotide NADH and the diiron cluster) and a regulatory protein that is without any cofactors (MMOB).[117]

The MMOH active site (Fig. 1.8) has a carboxylate-rich dinuclear structure containing six coordinate, octahedral iron centres bridged by a hydroxide ion and two bidentate carboxylate ligands (one of which is a glutamate carboxylate).[118] The reaction pathway for the hydroxylation of methane is initiated by the splitting of the O–O bond of O_2 by two reducing equivalents of the coenzyme nicotinamide adenine dinucleotide phosphate or NAD(P)H. One of the oxygen atoms is incorporated into the substrate to yield the alcohol product, whereas the other oxygen atom is reduced to form water.[118,119]

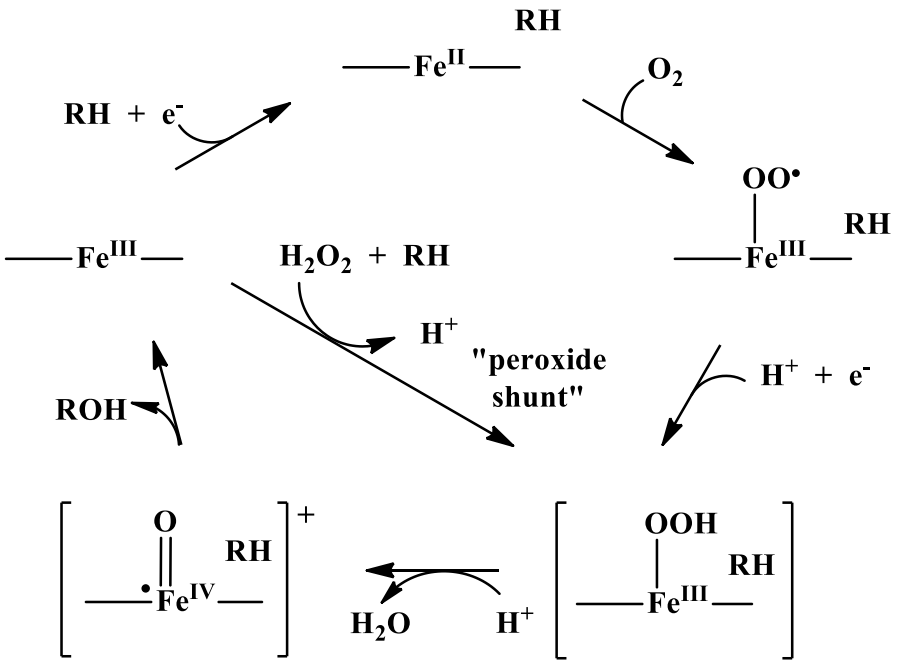

Scheme 1.5: Proposed catalytic cycle for the hydroxylation of alkanes by cytochrome P450.

The instability of pMMO and difficulties with purification has restricted the characterisation of its components.[120] The advantage offered by MMO is that it is not limited to a specific substrate, but rather is able to catalyse reactions containing a diverse range of substrates including carbohydrates.[118]

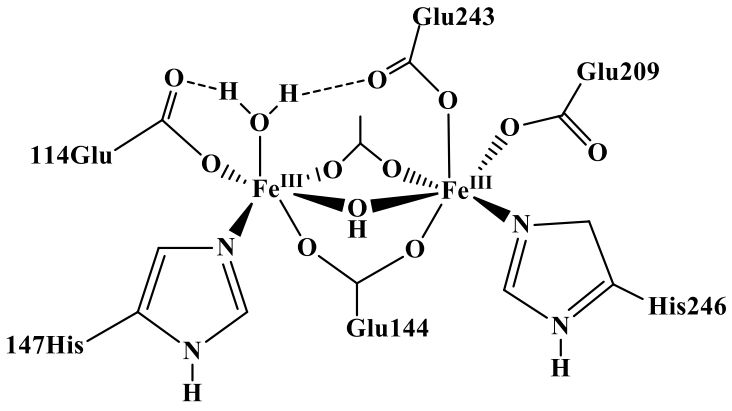

Figure 1.8: Structure of the active site of methane monooxygenase obtained from Methylococcus capsulatus.

1.3.2 Alkane oxidation by transition metal complexes

A substantial amount of research has been carried out over the last few decades concerning the use of transition metal complexes for the activation of paraffins.[102,104,107,121-131] During this time a variety of metal complexes have been developed that exhibit activity in paraffin or C–H activation, however, this review focuses on those directly related to straight chain or *n*-alkane oxidation. The initial studies carried out by Shilov and co-workers have essentially laid the foundation of alkane oxidation which much of the succeeding literature has expounded upon. In one of their early discoveries in 1972, they reported that platinum(II) salts were able to homogeneously catalyse the conversion of methane to methanol in solution. This system remains among the few examples to achieve selective alkane functionalisation under relatively mild conditions. [101,104,128] Following Shilov's work, Shul'pin and co-workers have greatly impacted the field of alkane oxidation achieving substantial progress over the past 30 years.[127,132-140] In addition, the Gif system, developed by Barton and co-workers, created an alternative avenue for the functionalisation of saturated hydrocarbons.[141-150]

The activation of a saturated hydrocarbon requires cleavage of the C−H bond and three possible mechanisms proposed by Shilov and Shul'pin account for this.[104,127] In the first mechanism, a metal−carbon σ-bond is formed during the catalytic cycle or as a final product and the C−H bond is cleaved via oxidative addition (eq. 1.2) or electrophilic substitution (eq. 1.3). This mechanism is often referred to as 'true' or 'organometallic' activation of the C−H bond.[127] Oxidative addition is favoured by metals in low and high oxidation states, while electrophilic substitution occurs with high oxidation state metals.[104]

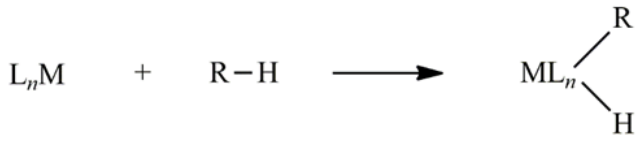

1.2

1.3

In the second mechanism, the C−H bond is cleaved by the metal complex, however, a metal−carbon σ-bond is not produced at any time during the catalytic cycle. The actual role of the

metal complex involves abstracting a hydrogen atom or an electron from the hydrocarbon chain thereby generating reactive radicals or radical ions which interact with other species, such as oxygen, to give rise to oxygenated products.

The third and final mechanism involves the activation of a specific reagent, such as an oxidant source, e.g. H_2O_2 or TBHP, to produce reactive species which are directly responsible for the activation and functionalization of the hydrocarbon independent of the metal complex. Fenton chemistry is a classic example of this mechanism, whereby the reaction pathway is radical based.[151] The actual mechanism followed in a particular reaction is dependent on the type of metal complex used as the catalyst.

A comprehensive review on metal-catalysed alkane oxidation has been provided by Shul'pin, which details the effect of additives on the reaction rates and gives some mechanistic insights into the catalytic systems.[100] The addition of certain acids, such as sulfuric acid, oxalic acid, acetic acid, etc. promotes oxidation of the substrate leading to higher activities.[129,130,152] It was found that the oxidation of saturated hydrocarbons with a manganese-based catalyst and H_2O_2 as the oxidant increased significantly upon the addition of a small amount of a carboxylic acid to the reaction mixture.[153-156] Whereas in the absence of the acid promoter, the alkane substrate is not oxidised. The role of the acid additive has not been fully established, however studies imply that the acid participates in proton-transfer steps as well as promotes unsaturation of the metal centers.[157]

Much research has been carried out on a variety of metals as catalysts for alkane oxidation, however, the focus of this review will now concentrate on those of late first row transition metal complexes, particularly iron, cobalt, nickel and copper.

1.3.2.1 Iron and cobalt

Fenton's reagent, which is a combination of H_2O_2 and ferrous iron, was one of the earliest discoveries made using iron for alkane oxidation.[102,104,151] The reaction of iron(II) with H_2O_2 produces reactive hydroxyl radicals as shown in Eqs. 1.4 – 1.10, with the iron(II) regenerated in the mechanism.[102,151]

$$Fe^{2+} + H_2O_2 \longrightarrow Fe^{3+} + HO^{\bullet} + OH^{-} \quad \textbf{1.4}$$

$$RH + HO^{\bullet} \longrightarrow R^{\bullet} + H_2O \quad \textbf{1.5}$$

$$R^{\bullet} + O_2 \longrightarrow ROO^{\bullet} \quad \textbf{1.6}$$

$$Fe^{2+} + HO^{\bullet} \longrightarrow Fe^{3+} + HO^{-} \quad \textbf{1.7}$$

$$HO^{\bullet} + H_2O_2 \longrightarrow HO_2^{\bullet} + H_2O \quad \textbf{1.8}$$

$$HO_2^{\bullet} + Fe^{2+} \longrightarrow Fe^{3+} + HO_2^{-} \quad \textbf{1.9}$$

$$O_2^{\bullet} + Fe^{3+} \longrightarrow Fe^{2+} + O_2 \quad \textbf{1.10}$$

These hydroxyl radicals react with the alkane (R−H) to produce alkyl radicals ($R^{\bullet}$) and water (eq. 1.5) and upon reaction with oxygen the alkylperoxy ($ROO^{\bullet}$) radical is formed (eq. 1.6) which then goes on to produce the alcohol and ketone products. The disadvantage with these free radical pathways is that they are not selective and often the activity is low.

Work by Barton and co-workers demonstrated the use of iron compounds with H_2O_2 in the oxidation of cyclohexane.[143,147] They discovered that the Fe^{II}-Fe^{IV} manifold was involved in the transformation of the substrate.

Pombeiro *et al*. reported the oxidation of cyclic alkanes (cyclopentane and cyclohexane) using an Fe(III)N_2S_2 complex with H_2O_2 as the oxidant and pyrazinecarboxylic acid as the promotor or co-catalyst.[158] With this system, they were able to achieve respectively TONs and yields of up to 490 and 13% (based on the substrate) at room temperature after 6 h. Furthermore, by utilizing radical scavengers they were able to confirm that the reaction pathway follows a radical mechanism.

Tripodal tetradentate nitrogen ligands coordinated to iron(II) have been used for the oxidation of cyclohexane with H_2O_2.[159] Of the five catalysts reported, three displayed reactivity distinct from Fenton-type chemistry, inferring a possible metal-based reaction mechanism. This was attributed to the pyridine substituents contained in the tripodal ligand.[159]

The oxidation of cyclohexane and cyclooctane by sandwich-type tungstophosphates with iron and cobalt (as well as manganese) was carried out by Santos *et al*. using H_2O_2.[160] The reactions with the iron complex as the catalyst were faster in comparison to the other catalysts and yielded TONs

of nearly 2000. However, one of the cobalt-based catalysts gave a selectivity and conversion of 83 and 92% respectively for the oxidation of cyclooctane to cyclooctanone.[160]

In 1985, Saussine *et al*. reported a series of novel cobalt(III) alkylperoxy complexes with application in the oxidation of a variety of hydrocarbon substrates, including cyclohexane and *n*-octane amongst others, using TBHP as the oxidant.[161] Product yields of up to 24% (cyclohexanone) and 12% (2-octanone) were achieved for the oxidation of cyclohexane and *n*-octane respectively.

In contrast, with the cobalt peroxide complex [Co(Py_3P)(OO^tBu)] a total yield of 59% was obtained for the oxidation of cyclohexane to cyclohexanol, cyclohexanone and cyclohexyl chloride products using TBHP as the oxidant and dichloromethane as the solvent.[162] The reaction pathway assumed a radical mechanism via the generation of a *t*-butoxy radical from the homolysis of the O−O bond present in the catalyst, which then reacts with the cyclohexane substrate, subsequently leading to the formation of a cyclohexyl radical.[162] The presence of this radical was evident from the formation of a large amount of cyclohexyl chloride in the reaction mixture.

Nam and co-workers demonstrated the use of simple metal perchlorate salts as catalysts for hydrocarbon oxidation with *m*-chloroperbenzoic acid (*m*-CPBA) as the oxidant.[163] Their results show that cobalt perchlorate was the most active among the three salts tested producing yields of up to ~90% for the oxidation of *cis*-1,2-dimethylcyclohexane to *cis*-1,2-dimethylcyclohexanol.

1.3.2.2 Nickel and copper

Not many elaborate studies have been carried out using nickel for alkane oxidation, however, available literature mainly describes the use of nickel complexes containing tripodal 4N ligands as catalysts in these reactions. Nagataki *et al*. reported on the hydroxylation of cyclohexane with *m*-CBPA as the oxidant using Ni(TPA) (where TPA = tris(2-pyridylmethyl)amine) as the catalyst (Fig. 1.9).[164] A TON of 656 was attained within 1 h with an oxidant efficiency of 71%. In comparison to similar cobalt, iron and manganese complexes, the nickel catalyst was more active. The authors also suggested the possible involvement of nickel-oxo species in the reaction mechanism.[164] Similar TONs were reported for nickel complexes containing derivatives of the same tripodal 4N ligand TPA under analogous conditions.[165]

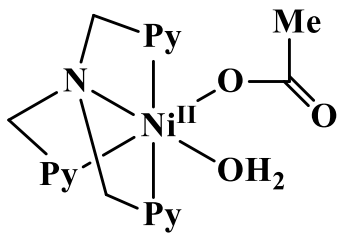

Figure 1.9: Structure of Ni(TPA) complex reported by Nagataki *et al*..[164]

Balamurugan and co-workers also carried out alkane oxidation studies using nickel tripodal 4N complexes, with *m*-CBPA as the oxidant, and they found TONs of 340-620 with good alcohol selectivity for cyclohexane as the alkane substrate.[166] Metal-based oxidation was suggested instead of the involvement of free radicals because of the higher alcohol selectivity. A mechanism for the reaction was proposed showing the activation of the oxidant and the formation of the products. (Scheme 1.6).[166] It is suggested that the oxidant *m*-CPBA replaces an acetonitrile ligand on the Ni(II) catalyst to form **1** which, upon hydrolysis of the O−O bond, leads to the formation of the reactive intermediate species **2** and the *m*-chlorobenzoic acid radical **3**. The intermediate species **2** then reacts with the substrate to form the oxygenated products, while **3** produces chlorobenzene (greater than 60% yield) upon decarboxylation.

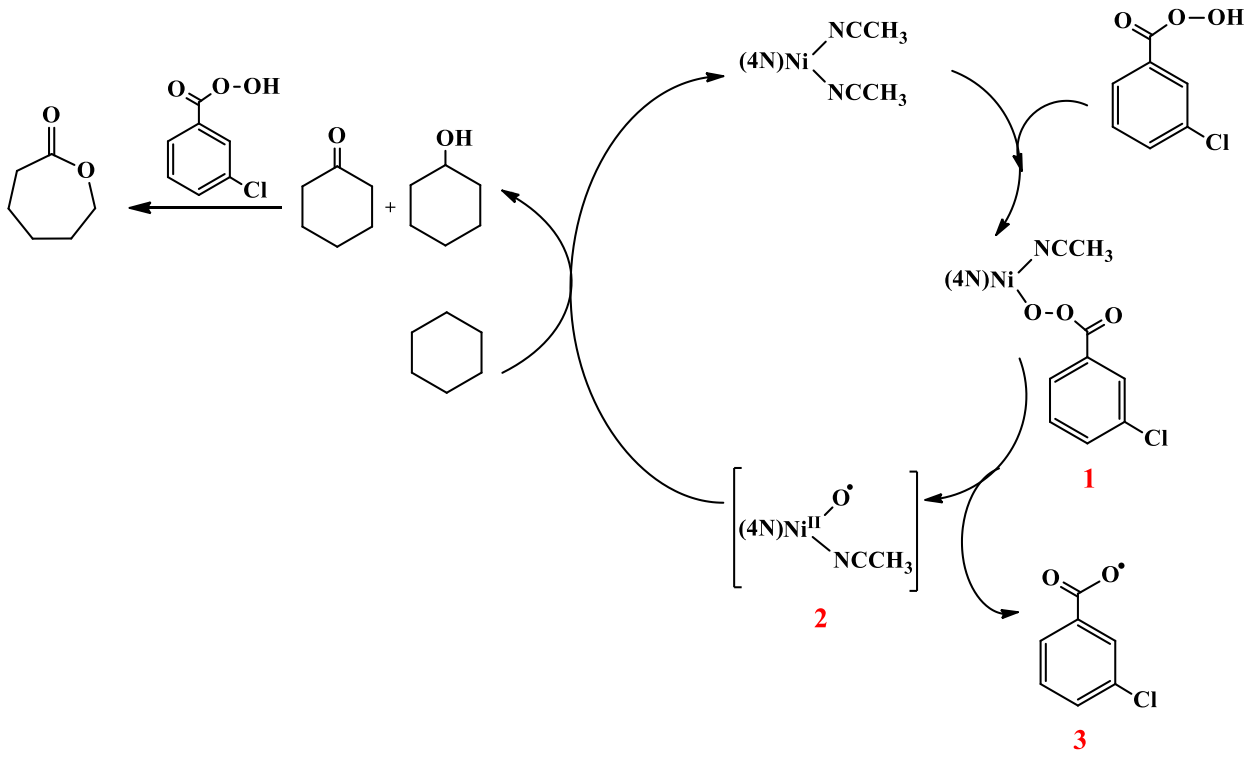

Scheme 1.6: Proposed reaction mechanism for the oxidation of cyclohexane.

Nickel and copper complexes containing a similar tripodal 4N ligand system, reported by Tordin *et al*., showed significantly lower TONs in comparison to the systems discussed previously. The copper catalyst was completely inactive, while the nickel catalyst gave a TON of 31, however, the selectivity remained towards the alcohol product.[167]

In general, copper systems have been investigated to a greater extent in comparison to those of nickel and some studies have shown promising results.[168,169] Much like iron, copper is found in the active site of pMMO and therefore is considered to be a biomimetic metal. The development of catalysts similar in construction or inspired by those of pMMO and other enzymatic systems has been an interesting subject which has motivated much research.[77]

The Gif system, developed by Barton and co-workers, illustrated the use of copper salts for the oxidation of cyclohexane using H_2O_2.[146] The reaction was performed in the presence of pyridine and yielded cyclohexanone as the only product. However, this system was not as efficient as the iron systems which they had previously reported.[143,147]

A tridentate pincer-type NNN ligand (bis-(2-pyridylmethyl)amine) or BMPA coordinated to copper(II) has been employed for the oxidation of cyclohexane with H_2O_2 and TBHP as oxidants.[170] Total yields of up to 68.9% were attained with H_2O_2, while the systems using TBHP gave only a highest yield of 11.2% within 24 h. Furthermore, it was found that selectivity to the alcohol product was higher with H_2O_2, and TBHP yielded more ketones.[170]

Pombeiro and co-workers have employed multinuclear copper triethanolamine complexes for alkane oxidation under mild reaction conditions.[157,171-173] A convenient and comprehensive review is also provided which discusses the application of these multinuclear copper complexes in the functionalisation of alkane substrates.[174] An example of a multinuclear triethanolamine complex is represented in Fig. 1.10.

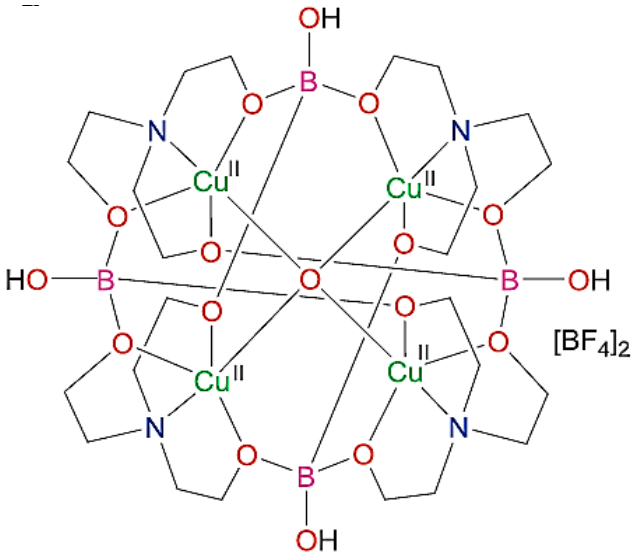

Figure 1.10: Representation of a multinuclear copper triethanolamine complex.[157]

The effect of an acid promotor was investigated and the results showed an enhancement in the catalytic activity with the addition of various acids. Hydrochloric acid had the most positive effect for the systems using H_2O_2, whereas no significant effect was observed in the reactions with TBHP as the oxidant.[157,173]

Schiff-base copper(II) complexes reported by Roy and Manassero, showed substantial activity in the oxidation of cyclohexane with H_2O_2.[175] Total yields of up to 38% were obtained, with a 63%

selectivity to cyclohexanol. Moreover, they also verified the use of nitric acid to enhance the activity of the catalytic system.

A more recent study reported by Kirillov and co-workers developed new water soluble dicopper aminoalcoholate complexes, which as catalysts in the presence of trifluoroacetic acid and H_2O_2 gave a maximum total product yield of 34%. [176]

1.4 Conclusion

The oxidation of saturated hydrocarbons is a field that has advanced over the last few decades. The fundamental understanding of the catalytic systems has progressed, however, there still remains room for improvement. Scientists have incorporated a variety of catalysts ranging from simple metal salts to multinuclear complexes, though the challenge of developing a system that is both highly active and selective has not yet been overcome. This review has highlighted the potential of the first row transition metals, particularly iron, cobalt, nickel and copper in the oxidation of various alkanes. However, the latter two metals have not been studied as much as iron and cobalt. Research has also demonstrated the importance of the ligand system coordinated to the metal, as well as the choice of the oxidant. With so many factors to consider in the development of the ideal catalytic system, the scope of this field remains unlimited.

1.5 Project aims, scope and chapter summaries

The motivation for this work stems from challenges still faced by chemists worldwide in the development of efficient homogeneous catalytic systems for the oxidation of saturated alkanes. This is even more important for systems that are capable of operating under mild reaction conditions that closely mimic nature. Towards the attainment of this goal, considerate and clever catalyst design is important. Key features to be considered in metal catalyst design include the type of ligands to be used, architecture of the ligands and very importantly, the metal(s). The ligand in particular plays a significant role in modulating the activity of the catalyst, whence catalytic

properties may be altered by fine tuning the various components and moieties that compose the ligand structure.

The aim of this project is to develop economically viable catalysts that are efficient in the oxidation of alkanes and capable of functioning under mild conditions. Therefore, relatively cheap metals such as nickel and copper with bio-inspired pincer-type ligand systems were chosen. The pincer ligand design was selected because it is structurally tridentate, meaning it coordinates to the metal centre via three donors, thereby inducing greater stability as well as variable electronic and steric effects that may be easily altered to optimise the catalyst.

In this study, two different types of SNS ligands were synthesised with a flexible ethylene backbone in which there is a variation of substituent on the N-donor atom i.e. a methyl (**L1**) or a phenyl (**L2**) group. The substituents bonded to the S-donor atoms were also varied in order to investigate any potential steric and/or electronic effects. These are straight chained substituents, such as methyl (**a**), ethyl (**b**), and butyl (**c**) groups, cyclic groups such as cyclohexyl (**d**) and branched substituents such as the *t*-butyl (**e**) group. The structures of **L1** and **L2** sub-groupings are shown in Figs. 1.11 and 1.12 respectively. The majority of the ligands synthesised in this work are new.

The synthesised ligands were then coordinated to nickel and copper to yield novel complexes which were characterised by various techniques. The resulting complexes were then employed as catalysts for the oxidation of *n*-octane as the hydrocarbon substrate. Reason for the choice of this particular substrate is that there is limited work on its oxidation studies. Furthermore, it is an example of a medium chain alkane which forms a major component of crude oil. Due to its low value and large excess in petroleum refining industries, there is a need to convert it into value added products. The catalytic conditions were optimised by varying the reaction temperature, octane:oxidant ratio and reaction time in order to obtain the best yield and selectivity.

Furthermore, a range of NSN ligands were synthesised (Fig. 1.13), which were applied in a ‘one pot’ *in situ* catalysis using salts of iron, cobalt, nickel and copper.

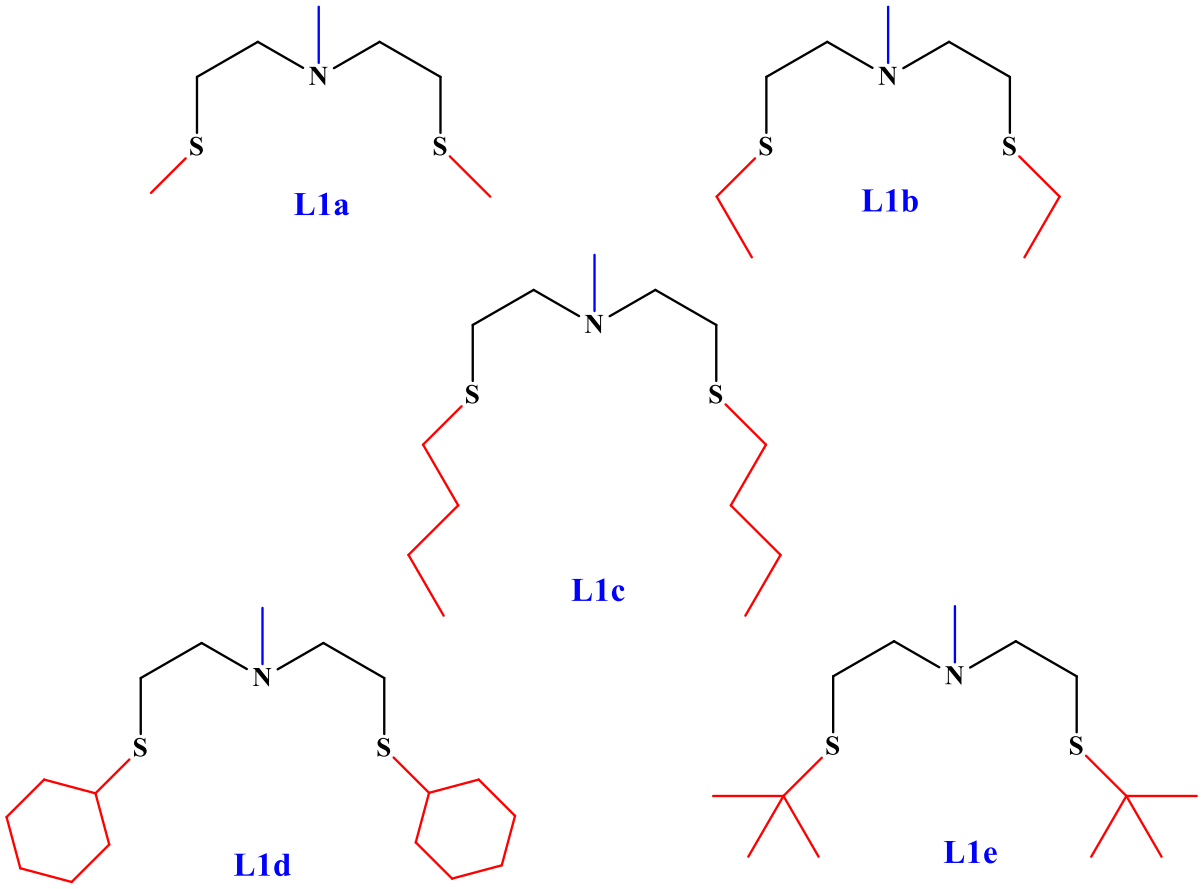

Figure 1.11: Structures of the SNS ligands **L1** containing a methyl on the N-donor and various substituents on the S-donor atoms.

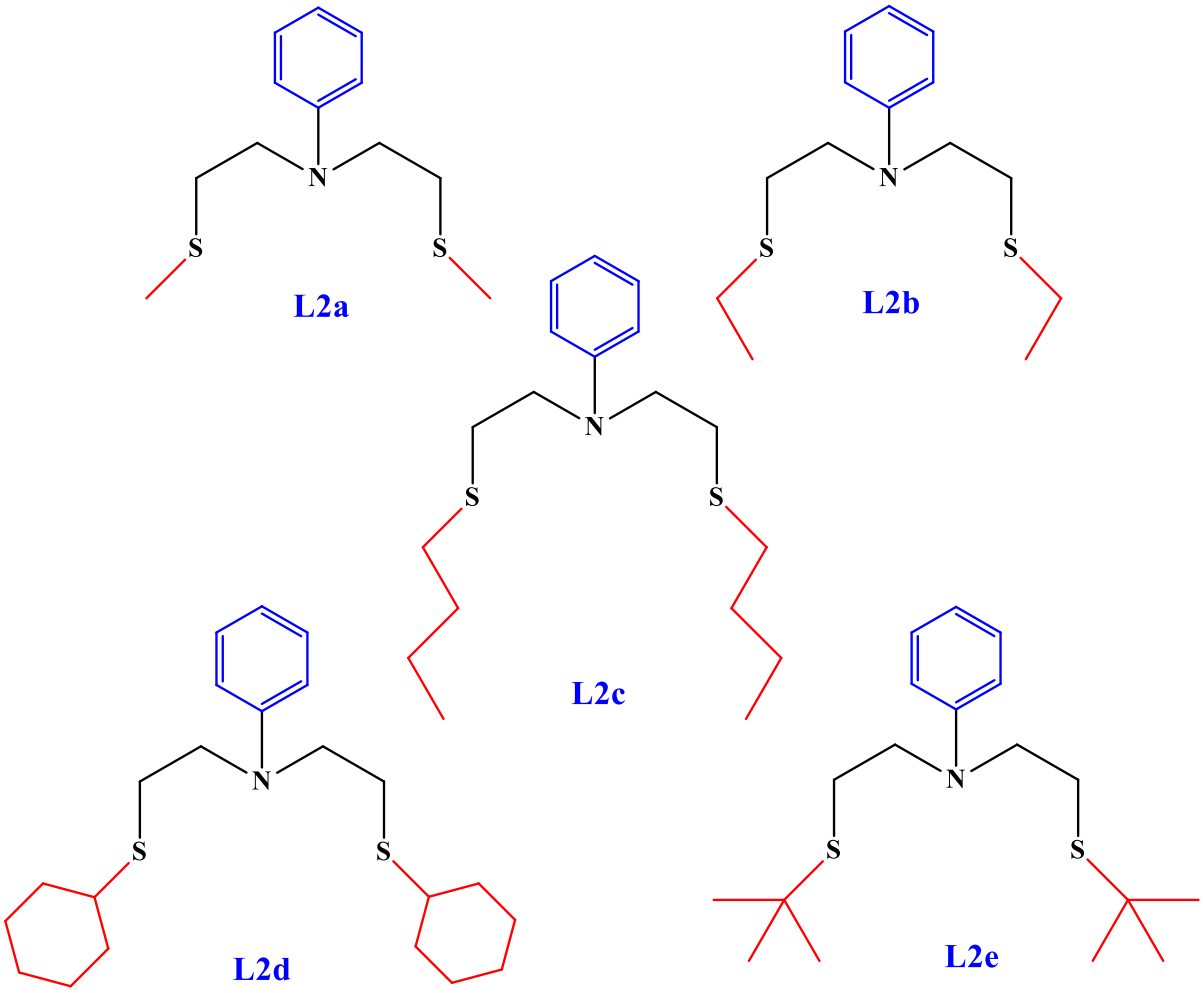

Figure 1.12: Structures of the SNS ligands **L2** containing a phenyl on the N-donor and various substituents on the S-donor atoms.

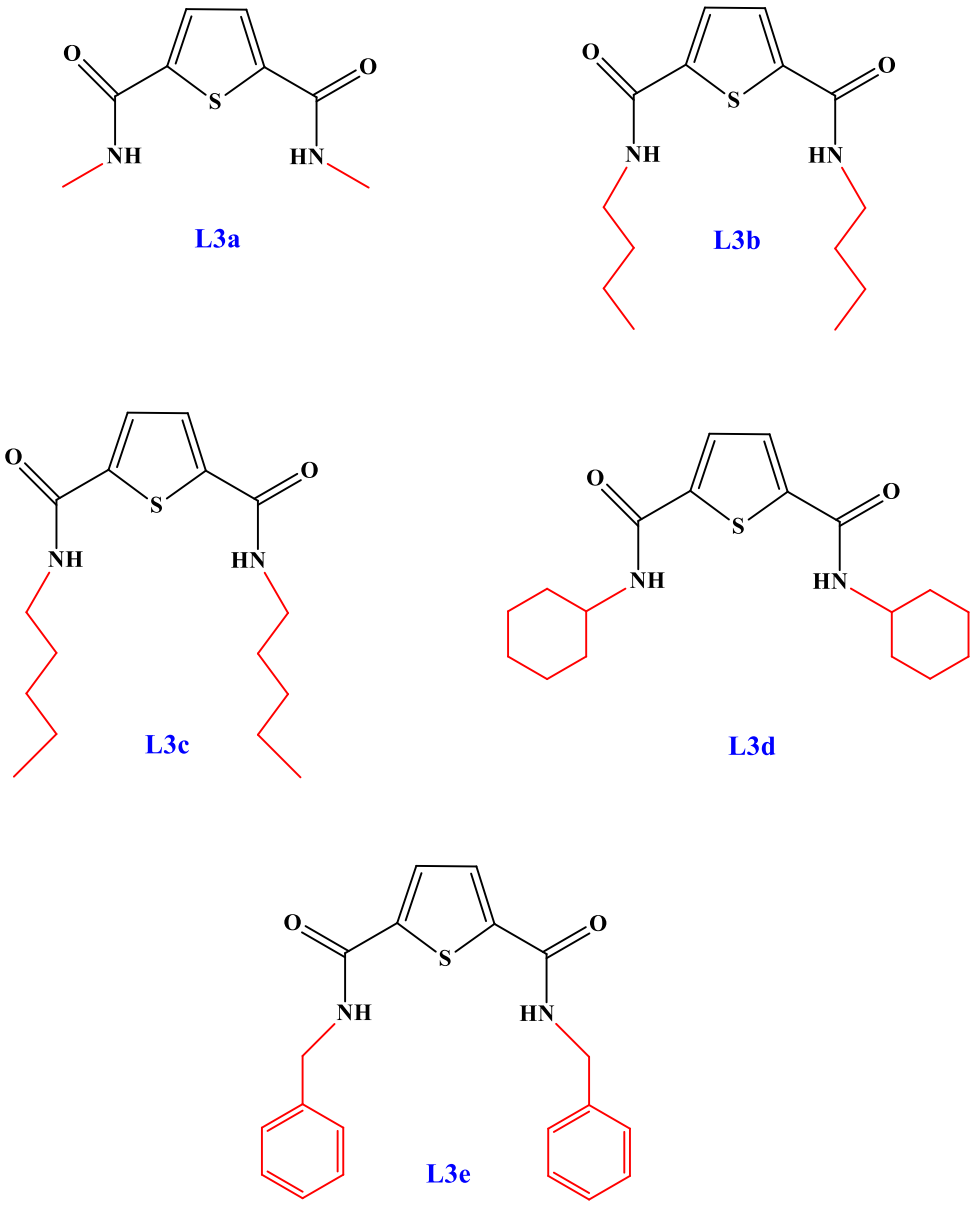

Figure 1.13: Structures of the NSN ligands **L3** synthesised containing a thiophene backbone and various substituents on the N-donor atoms.

To conclude, this work describes the synthesis of novel catalysts based on cheap and environmentally benign transition metals, such as nickel and copper, containing pincer-type ligands. Their application in oxidation catalysis is also a new study and to the best of our knowledge, there are no published literature reports on the use of nickel or copper SNS complexes for this type of application. The SNS ligands, as well as the prepared NSN ligands, were also

employed *in situ* combined with iron, cobalt, nickel and copper salts as catalysts for alkane oxidation.

Chapter two is dedicated to the synthesis and characterisation of the SNS ligands, the nickel SNS complexes and their application in the oxidation of *n*-octane. Chapter three focuses on the synthesis and characterisation of the copper SNS complexes, as well as their application in the oxidation of *n*-octane. Chapter four outlines the preparation of the NSN ligands, as well as *in situ* catalysis with salts of iron, cobalt, nickel and copper, while the final chapter presents the summary and conclusions of this dissertation. A graphical summary of chapters two-four is provided below.

Chapter 2: Utilisation of novel NiSNS complexes in paraffin oxidation

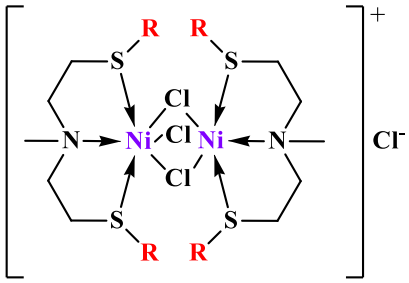

1.1

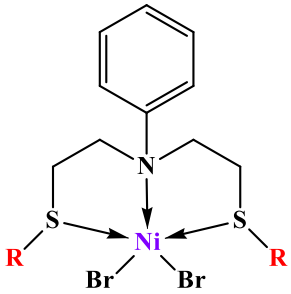

1.2

R = methyl, ethyl, butyl, cyclohexyl and *t*-butyl

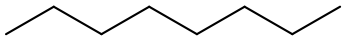

1.1 and 1.2

50 °C, TBHP, MeCN

octanols + octanones

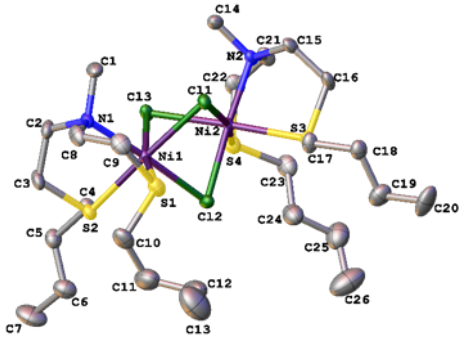

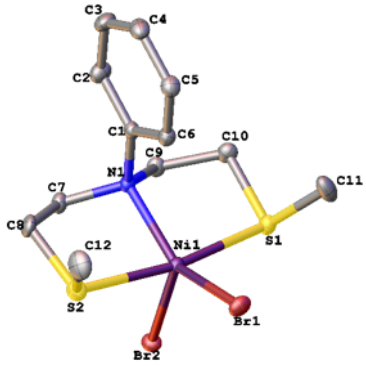

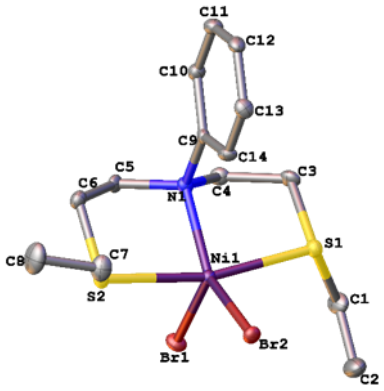

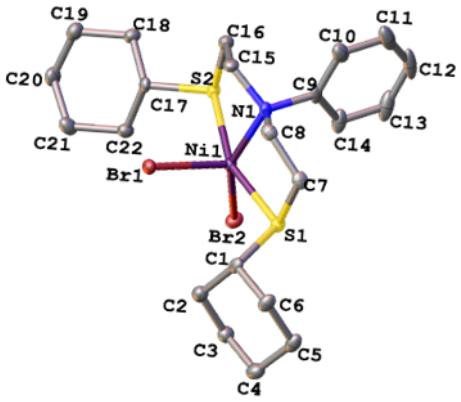

Chapter 3: Flexible pincer backbone revisited: the case of CuSNS complexes as efficient catalysts in paraffin oxidation

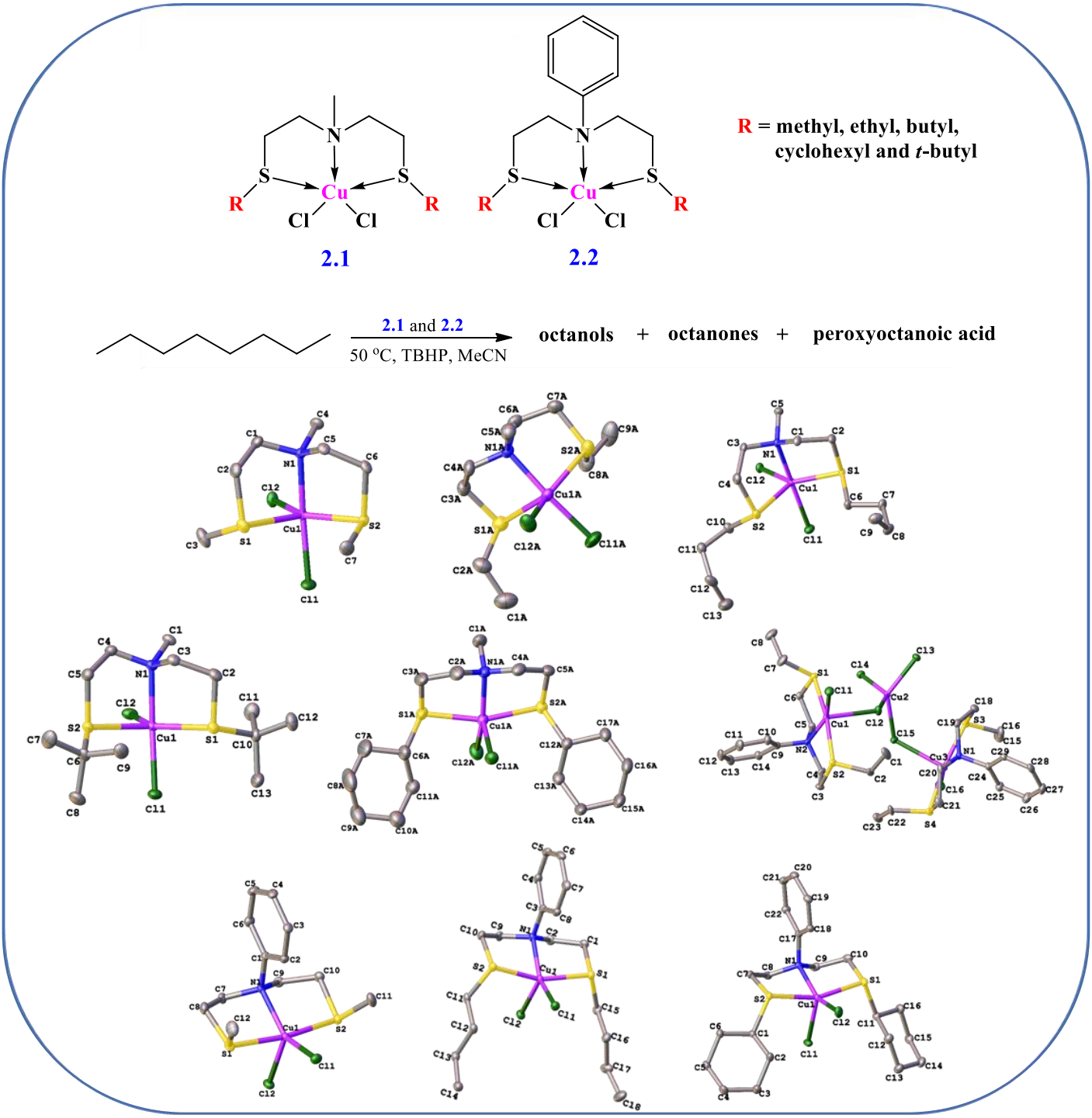

Chapter 4: Synthesis and characterisation of new NSN ligands and their *in situ* application in oxidation catalysis

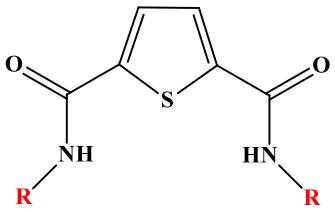

L3

R = methyl, butyl, pentyl, cyclohexyl and benzyl

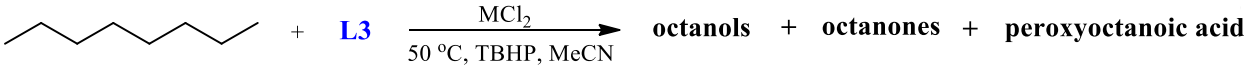

M = Fe, Co, Ni, Cu

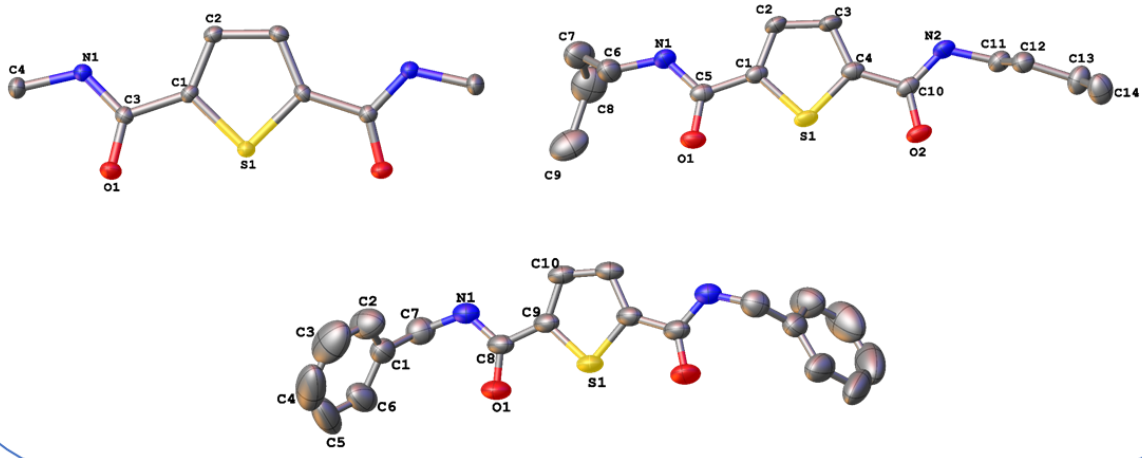

1.6 References

(1) Moulton, C. J.; Shaw, B. L. *J. Chem. Soc., Dalton Trans.* **1976**, 1020.

(2) Rahman, M. S.; Prince, P. D.; Steed, J. W.; Hii, K. K. *Organometallics* **2002**, *21*, 4927.

(3) Hermann, D.; Gandelman, M.; Rozenberg, H.; Shimon, L. J. W.; Milstein, D. *Organometallics* **2002**, *21*, 812.

(4) Zhang, J.; Gandelman, M.; Shimon, L. J. W.; Rozenberg, H.; Milstein, D. *Organometallics* **2004**, *23*, 4026.

(5) Ben-Ari, E.; Leitus, G.; Shimon, L. J. W.; Milstein, D. *Journal of the American Chemical Society* **2006**, *128*, 15390.

(6) Singleton, J. T. *Tetrahedron* **2003**, *59*, 1837.

(7) Carlson, A. R., University of Florida, 2007.

(8) Albrecht, M.; van Koten, G. *Angewandte Chemie International Edition* **2001**, *40*, 3750.

(9) Kanzelberger, M.; Singh, B.; Czerw, M.; Krogh-Jespersen, K.; Goldman, A. S. *J. Am. Chem. Soc.* **2000**, *122*, 11017.

(10) van der Boom, M. E.; Milstein, D. *Chem. Rev.* **2003**, *103*, 1759.

(11) Vigalok, A.; Uzan, O.; Shimon, L. J. W.; Ben-David, Y.; Martin, J. M. L.; Milstein, D. *J. Am. Chem. Soc.* **1998**, *120*, 12539.

(12) Benito-Garagorri, D.; Kirchner, K. *Accounts of Chemical Research* **2008**, *41*, 201.

(13) Lee, D. W.; Jensen, C. M.; Morales-Morales, D. *Organometallics* **2003**, *22*, 4744.

(14) Baber, R. A.; Bedford, R. B.; Betham, M.; Blake, M. E.; Coles, S. J.; Haddow, M. F.; Hursthouse, M. B.; Orpen, A. G.; Pilarski, L. T.; Pringle, P. G.; Wingad, R. L. *Chem. Commun.* **2006**, *0*, 3880.

(15) Meiners, J.; Friedrich, A.; Herdtweck, E.; Schneider, S. *Organometallics* **2009**, *28*, 6331.

(16) Pascualini, M. E.; Di Russo, N. V.; Quintero, P. A.; Thuijs, A. E.; Pinkowicz, D.; Abboud, K. A.; Dunbar, K. R.; Christou, G.; Meisel, M. W.; Veige, A. S. *Inorganic Chemistry* **2014**, *53*, 13078.

(17) Bellone, D. E.; Bours, J.; Menke, E. H.; Fischer, F. R. *Journal of the American Chemical Society* **2015**, *137*, 850.

(18) Lagaditis, P. O.; Sues, P. E.; Sonnenberg, J. F.; Wan, K. Y.; Lough, A. J.; Morris, R. H. *Journal of the American Chemical Society* **2014**, *136*, 1367.

(19) Xu, W.; Langer, R. *Dalton Transactions* **2015**.

(20) Zell, T.; Langer, R.; Iron, M. A.; Konstantinovski, L.; Shimon, L. J. W.; Diskin-Posner, Y.; Leitus, G.; Balaraman, E.; Ben-David, Y.; Milstein, D. *Inorganic Chemistry* **2013**, *52*, 9636.

(21) Kumar, P.; Kashid, V. S.; Reddi, Y.; Mague, J. T.; Sunoj, R. B.; Balakrishna, M. S. *Dalton Transactions* **2015**, *44*, 4167.

(22) Abbenhuis, R. A. T. M.; del Río, I.; Bergshoef, M. M.; Boersma, J.; Veldman, N.; Spek, A. L.; van Koten, G. *Inorganic Chemistry* **1998**, *37*, 1749.

(23) Ghorai, D.; Kumar, S.; Mani, G. *Dalton Transactions* **2012**, *41*, 9503.

(24) DeMott, J. C.; Dekarske, J. R.; McCulloch, B. J.; Ozerov, O. V. *Inorganic Chemistry Frontiers* **2015**, *2*, 912.

(25) Knapp, S. M. M.; Shaner, S. E.; Kim, D.; Shopov, D. Y.; Tendler, J. A.; Pudalov, D. M.; Chianese, A. R. *Organometallics* **2014**, *33*, 473.

(26) Chianese, A. R.; Drance, M. J.; Jensen, K. H.; McCollom, S. P.; Yusufova, N.; Shaner, S. E.; Shopov, D. Y.; Tendler, J. A. *Organometallics* **2014**, *33*, 457.

(27) Lee, H. M.; Zeng, J. Y.; Hu, C.-H.; Lee, M.-T. *Inorganic Chemistry* **2004**, *43*, 6822.

(28) Gründemann, S.; Albrecht, M.; Loch, J. A.; Faller, J. W.; Crabtree, R. H. *Organometallics* **2001**, *20*, 5485.

(29) Göttker-Schnetmann, I.; White, P.; Brookhart, M. *Journal of the American Chemical Society* **2004**, *126*, 1804.

(30) Ohff, M.; Ohff, A.; van der Boom, M. E.; Milstein, D. *Journal of the American Chemical Society* **1997**, *119*, 11687.

(31) Peris, E.; Loch, J. A.; Mata, J.; Crabtree, R. H. *Chemical Communications* **2001**, 201.

(32) Basauri-Molina, M.; Hernández-Ortega, S.; Morales-Morales, D. *European Journal of Inorganic Chemistry* **2014**, *2014*, 4619.

(33) Suzuki, A. *Journal of Organometallic Chemistry* **1999**, *576*, 147.

(34) Bedford, R. B.; Draper, S. M.; Noelle Scully, P.; Welch, S. L. *New Journal of Chemistry* **2000**, *24*, 745.

(35) Younus, H. A.; Su, W.; Ahmad, N.; Chen, S.; Verpoort, F. *Advanced Synthesis & Catalysis* **2015**, *357*, 283.

(36) McGuinness, D. S.; Wasserscheid, P.; Keim, W.; Morgan, D.; Dixon, J. T.; Bollmann, A.; Maumela, H.; Hess, F.; Englert, U. *J. Am. Chem. Soc.* **2003**, *125*, 5272.

(37) McGuinness, D. S.; Wasserscheid, P.; Morgan, D. H.; Dixon, J. T. *Organometallics* **2005**, *24*, 552.

(38) McGuinness, D. S.; Brown, D. B.; Tooze, R. P.; Hess, F. M.; Dixon, J. T.; Slawin, A. M. Z. *Organometallics* **2006**, *25*, 3605.

(39) Temple, C. N.; Gambarotta, S.; Korobkov, I.; Duchateau, R. *Organometallics* **2007**, *26*, 4598.

(40) Jabri, A.; Temple, C.; Crewdson, P.; Gambarotta, S.; Korobkov, I.; Duchateau, R. *Journal of the American Chemical Society* **2006**, *128*, 9238.

(41) Temple, C.; Jabri, A.; Crewdson, P.; Gambarotta, S.; Korobkov, I.; Duchateau, R. *Angewandte Chemie* **2006**, *118*, 7208.

(42) Downing, S. P.; Hanton, M. J.; Slawin, A. M. Z.; Tooze, R. P. *Organometallics* **2009**, *28*, 2417.

(43) Shaffer, D. W.; Szigethy, G.; Ziller, J. W.; Heyduk, A. F. *Inorganic Chemistry* **2013**, *52*, 2110.

(44) Viñas, C.; Anglès, P.; Sánchez, G.; Lucena, N.; Teixidor, F.; Escriche, L.; Casabó, J.; Piniella, J. F.; Alvarez-Larena, A.; Kivekäs, R.; Sillanpää, R. *Inorg. Chem.* **1998**, *37*, 701.

(45) Teratani, T.; Koizumi, T.-a.; Yamamoto, T.; Tanaka, K.; Kanbara, T. *Dalton Transactions* **2011**, *40*, 8879.

(46) Komiyama, Y.; Kuwabara, J.; Kanbara, T. *Organometallics* **2014**, *33*, 885.

(47) Soobramoney, L.; Bala, M. D.; Friedrich, H. B. *Dalton Transactions* **2014**, *43*, 15968.

(48) Klerman, Y.; Ben-Ari, E.; Diskin-Posner, Y.; Leitus, G.; Shimon, L. J. W.; Ben-David, Y.; Milstein, D. *Dalton Trans.* **2008**, 3226.

(49) Konrad, M.; Meyer, F.; Heinze, K.; Zsolnai, L. *J. Chem. Soc., Dalton Trans.* **1998**, 199.

(50) Canovese, L.; Chessa, G.; Marangoni, G.; Pitteri, B.; Uguagliati, P.; Visentin, F. *Inorg. Chim. Acta* **1991**, *186*, 79.

(51) Zhang, B.-S.; Wang, W.; Shao, D.-D.; Hao, X.-Q.; Gong, J.-F.; Song, M.-P. *Organometallics* **2010**, *29*, 2579.

(52) Pitteri, B.; Bortoluzzi, M. *Polyhedron* **2008**, *27*, 2259.

(53) Wang, Q.-Q.; Ara Begum, R.; Day, V. W.; Bowman-James, K. *Inorganic Chemistry* **2012**, *51*, 760.

(54) Bai, S.-Q.; Koh, L. L.; Hor, T. S. A. *Inorg. Chem.* **2009**, *48*, 1207.

(55) Teixidor, F.; Escriche, L.; Casabo, J.; Molins, E.; Miravitlles, C. *Inorg. Chem.* **1986**, *25*, 4060.

(56) Jia, W.-G.; Li, D.-D.; Zhang, H.; Dai, Y.-C.; Sheng, E.-H. *Journal of Coordination Chemistry* **2014**, *68*, 220.

(57) Miecznikowski, J. R.; Lo, W.; Lynn, M. A.; Jain, S.; Keilich, L. C.; Kloczko, N. F.; O'Loughlin, B. E.; DiMarzio, A. P.; Foley, K. M.; Lisi, G. P.; Kwiecien, D. J.; Butrick, E. E.; Powers, E.; Al-Abbasee, R. *Inorganica Chimica Acta* **2012**, *387*, 25.

(58) Lai, W.; Berry, S. M.; Bebout, D. C.; Butcher, R. J. *Inorganic Chemistry* **2006**, *45*, 571.

(59) Jia, W.-G.; Dai, Y.-C.; Zhang, H.-N.; Lu, X.; Sheng, E.-H. *RSC Advances* **2015**, *5*, 29491.

(60) Teixidor, F.; Sanchez-Castello, G.; Lucena, N.; Escriche, L.; Kivekas, R.; Sundberg, M.; Casabo, J. *Inorg. Chem.* **1991**, *30*, 4931.

(61) Kumar, S. *Dalton Transactions* **2013**, *42*, 16939.

(62) Sola, J.; López, A.; Coxall, Robert A.; Clegg, W. *European Journal of Inorganic Chemistry* **2004**, *2004*, 4871.

(63) Okamoto, K.; Kuwabara, J.; Kanbara, T. *Journal of Organometallic Chemistry* **2011**, *696*, 1305.

(64) Akaiwa, M.; Kanbara, T.; Fukumoto, H.; Yamamoto, T. *Journal of Organometallic Chemistry* **2005**, *690*, 4192.

(65) Okamoto, K.; Kanbara, T.; Yamamoto, T.; Wada, A. *Organometallics* **2006**, *25*, 4026.

(66) Okamoto, K.; Yamamoto, T.; Akita, M.; Wada, A.; Kanbara, T. *Organometallics* **2009**, *28*, 3307.

(67) Kuwabara, J.; Munezawa, G.; Okamoto, K.; Kanbara, T. *Dalton Transactions* **2010**, *39*, 6255.

(68) Begum, R. A.; Powell, D.; Bowman-James, K. *Inorganic Chemistry* **2006**, *45*, 964.

(69) Kozlov, V. A.; Aleksanyan, D. V.; Nelyubina, Y. V.; Lyssenko, K. A.; Gutsul, E. I.; Puntus, L. N.; Vasil'ev, A. A.; Petrovskii, P. V.; Odinets, I. L. *Organometallics* **2008**, *27*, 4062.

(70) Aleksanyan, D. V.; Kozlov, V. A.; Nelyubina, Y. V.; Lyssenko, K. A.; Puntus, L. N.; Gutsul, E. I.; Shepel, N. E.; Vasil'ev, A. A.; Petrovskii, P. V.; Odinets, I. L. *Dalton Transactions* **2011**, *40*, 1535.

(71) Page, M. J.; Wagler, J.; Messerle, B. A. *Organometallics* **2010**, *29*, 3790.

(72) Dani, P.; Karlen, T.; Gossage, R. A.; Gladiali, S.; van Koten, G. *Angewandte Chemie International Edition* **2000**, *39*, 743.

(73) Shimokawa, R.; Kawada, Y.; Hayashi, M.; Kataoka, Y.; Ura, Y. *Dalton Transactions* **2016**.

(74) Spasyuk, D.; Smith, S.; Gusev, D. G. *Angewandte Chemie International Edition* **2013**, *52*, 2538.

(75) Chen, X.; Jing, Y.; Yang, X. *Chemistry – A European Journal* **2016**, *22*, n/a.

(76) Belle, C.; Rammal, W.; Pierre, J.-L. *Journal of Inorganic Biochemistry* **2005**, *99*, 1929.

(77) Arends, I. W. C. E.; Gamez, P.; Sheldon, R. A. In *Advances in Inorganic Chemistry*; Eldik, R. v., Reedijk, J., Eds.; Academic Press: 2006; Vol. Volume 58, p 235.

(78) Mugesh, G.; du Mont, W. W. *Chemistry–A European Journal* **2001**, *7*, 1365.

(79) Torres Pazmino, D. E.; Winkler, M.; Glieder, A.; Fraaije, M. W. *Journal of Biotechnology* **2010**, *146*, 9.

(80) Guengerich, F. P. *Chemical Research in Toxicology* **2001**, *14*, 611.

(81) Costas, M.; Chen, K.; Que Jr., L. *Coordination Chemistry Reviews* **2000**, *200-202*, 517.

(82) Das, U. K.; Daifuku, S. L.; Gorelsky, S. I.; Korobkov, I.; Neidig, M. L.; Le Roy, J. J.; Murugesu, M.; Baker, R. T. *Inorganic Chemistry* **2016**, *55*, 987.

(83) AbdEl-Halim, H. F.; Mohamed, G. G.; Hofmann, K.; Albert, B. *Comptes Rendus Chimie* **2015**, *18*, 619.

(84) Koizumi, T.-a.; Teratani, T.; Okamoto, K.; Yamamoto, T.; Shimoi, Y.; Kanbara, T. *Inorganica Chimica Acta* **2010**, *363*, 2474.

(85) Márquez, V. E.; Anacona, J. R.; Hurtado, R. J.; Díaz de Delgado, G.; Roque, E. M. *Polyhedron* **1999**, *18*, 1903.

(86) Ball, R. J.; Genge, A. R. J.; Radford, A. L.; Skelton, B. W.; Tolhurst, V.-A.; White, A. H. *Journal of the Chemical Society, Dalton Transactions* **2001**, 2807.

(87) Blomenkemper, M.; Schröder, H.; Pape, T.; Hahn, F. E. *Inorganica Chimica Acta* **2012**, *390*, 143.

(88) Bai, S.-Q.; Jiang, L.; Zuo, J.-L.; Hor, T. S. A. *Dalton Transactions* **2013**, *42*, 11319.

(89) Hajifatheali, H.; Ahmadi, E.; Wojtczak, A.; Jaglicic, Z. *Macromolecular Research* **2015**, *23*, 977.

(90) Miecznikowski, J. R.; Lynn, M. A.; Jasinski, J. P.; Lo, W.; Bak, D. W.; Pati, M.; Butrick, E. E.; Drozdoski, A. E. R.; Archer, K. A.; Villa, C. E.; Lemons, E. G.; Powers, E.; Siu, M.; Gomes, C. D.; Bernier, N. A.; Morio, K. N. *Polyhedron* **2014**, *80*, 157.

(91) Miecznikowski, J. R.; Lynn, M. A.; Jasinski, J. P.; Reinheimer, E.; Bak, D. W.; Pati, M.; Butrick, E. E.; Drozdoski, A. E. R.; Archer, K. A.; Villa, C. E.; Lemons, E. G.; Powers, E.; Siu, M.; Gomes, C. D.; Morio, K. N. *Journal of Coordination Chemistry* **2014**, *67*, 29.

(92) Pedras, B.; Santos, H. M.; Fernandes, L.; Covelo, B.; Tamayo, A.; Bértolo, E.; Capelo, J. L.; Avilés, T.; Lodeiro, C. *Inorganic Chemistry Communications* **2007**, *10*, 925.

(93) Liu, B.; Li, L.; Sun, G.; Liu, J.; Wang, M.; Li, S.; Cui, D. *Macromolecules* **2014**, *47*, 4971.

(94) Coles, S. J.; Gale, P. A.; Hursthouse, M. B.; Light, M. E.; Warriner, C. N. *Supramolecular Chemistry* **2004**, *16*, 469.

(95) Mylonas, I.; Triantis, C.; Panagiotopoulou, A.; Patsis, G.; Raptopoulou, C. P.; Terzis, A.; Psycharis, V.; Komiotis, D.; Pelecanou, M.; Pirmettis, I.; Papadopoulos, M. *Inorganica Chimica Acta* **2013**, *400*, 2.

(96) Graf, D. D.; Schrock, R. R.; Davis, W. M.; Stumpf, R. *Organometallics* **1999**, *18*, 843.

(97) Fandos, R.; Fernández-Gallardo, J.; Otero, A.; Rodríguez, A.; Ruiz, M. a. J. *Organometallics* **2011**, *30*, 1551.

(98) Labinger, J. A.; Bercaw, J. E. *Nature* **2002**, *417*, 507.

(99) Conley, B. L.; Tenn Iii, W. J.; Young, K. J. H.; Ganesh, S. K.; Meier, S. K.; Ziatdinov, V. R.; Mironov, O.; Oxgaard, J.; Gonzales, J.; Goddard Iii, W. A.; Periana, R. A. *Journal of Molecular Catalysis A: Chemical* **2006**, *251*, 8.

(100) Shul'pin, G. B. *Journal of Molecular Catalysis A: Chemical* **2002**, *189*, 39.

(101) Crabtree, R. H. *J. Organomet. Chem.* **2004**, *689*, 4083.

(102) Crabtree, R. H. *J. Chem. Soc., Dalton Trans.* **2001**, 2437.

(103) Chavez, F. A.; Mascharak, P. K. *Accounts of Chemical Research* **2000**, *33*, 539.

(104) Shilov, A. E.; Shul'pin, G. B. *Chem. Rev.* **1997**, *97*, 2879.

(105) Sen, A. *Accounts of Chemical Research* **1998**, *31*, 550.

(106) Kille, S.; Zilly, F. E.; Acevedo, J. P.; Reetz, M. T. *Nat Chem* **2011**, *3*, 738.

(107) Kamata, K.; Yonehara, K.; Nakagawa, Y.; Uehara, K.; Mizuno, N. *Nat Chem* **2010**, *2*, 478.

(108) Fish, R. H.; Konings, M. S.; Oberhausen, K. J.; Fong, R. H.; Yu, W. M.; Christou, G.; Vincent, J. B.; Coggin, D. K.; Buchanan, R. M. *Inorganic Chemistry* **1991**, *30*, 3002.

(109) Fish, R. H.; Oberhausen, K. J.; Chen, S.; Richardson, J. F.; Pierce, W.; Buchanan, R. M. *Catalysis Letters* **1993**, *18*, 357.

(110) Yoshizawa, K.; Shiota, Y. *Journal of the American Chemical Society* **2006**, *128*, 9873.

(111) Wong, L.-L. *Current Opinion in Chemical Biology* **1998**, *2*, 263.

(112) Mansuy, D. *Comptes Rendus Chimie* **2007**, *10*, 392.

(113) Mansuy, D. *Pure and Applied Chemistry* **1990**, *62*, 741.

(114) Coon, M. J. *Annual Review of Pharmacology and Toxicology* **2005**, *45*, 1.

(115) Semrau, J. D.; DiSpirito, A. A.; Yoon, S. *FEMS Microbiology Reviews* **2010**, *34*, 496.

(116) Ross, M. O.; Rosenzweig, A. C. *JBIC Journal of Biological Inorganic Chemistry* **2016**, 1.

(117) Banerjee, R.; Meier, K. K.; Münck, E.; Lipscomb, J. D. *Biochemistry* **2013**, *52*, 4331.

(118) Westerheide, L.; Pascaly, M.; Krebs, B. *Current Opinion in Chemical Biology* **2000**, *4*, 235.

(119) Friedle, S.; Reisner, E.; Lippard, S. J. *Chemical Society Reviews* **2010**, *39*, 2768.

(120) Merkx, M.; Kopp, D. A.; Sazinsky, M. H.; Blazyk, J. L.; Müller, J.; Lippard, S. J. *Angewandte Chemie International Edition* **2001**, *40*, 2782.

(121) Parshall, G. W. *Acc. Chem. Res.* **1975**, *8*, 113.

(122) Chatt, J.; Davidson, J. M. *Journal of the Chemical Society (Resumed)* **1965**, 843.

(123) Janowicz, A. H.; Bergman, R. G. *Journal of the American Chemical Society* **1982**, *104*, 352.

(124) Rappe, A. K.; Goddard, W. A. *Journal of the American Chemical Society* **1982**, *104*, 3287.

(125) Labinger, J. A. *Fuel Process. Technol.* **1995**, *42*, 325.

(126) Pozzi, G.; Cavazzini, M.; Quici, S.; Fontana, S. *Tetrahedron Letters* **1997**, *38*, 7605.

(127) Shul'pin, G. B. *C.R. Chim.* **2003**, *6*, 163.

(128) Goldman, A. S.; Goldberg, K. I. In *Activation and Functionalization of C- H Bonds*; Goldberg, K. I., Goldman, A. S., Eds.; American Chemical Society: 2004; Vol. 885, p 1.

(129) Gupta, S.; Kirillova, M. V.; Guedes da Silva, M. F.; Pombeiro, A. J. L. *Applied Catalysis A: General* **2013**, *460–461*, 82.

(130) Kozlov, Y. N.; Nizova, G. V.; Shul'pin, G. B. *J. Phys. Org. Chem.* **2008**, *21*, 119.

(131) Shul'pin, G. B. *Mini-Reviews in Organic Chemistry* **2009**, *6*, 95.

(132) Shilov, A. E. e.; Shul'pin, G. B. *Russian Chemical Reviews* **1987**, *56*, 442.

(133) Shul'pin, G. *Izvestiya Akademii Nauk SSSR, Seriya Khimicheskaya* **1988**, 2653.

(134) Shul'pin, G. B.; Suss-Fink, G.; Shul'pina, L. S. *J. Mol. Catal. A: Chem.* **2001**, *170*, 17.

(135) Shul'pin, G. B.; Shilov, A. E.; Suss-Fink, G. *Tetraheron Letters* **2001**, *42*, 7253.

(136) Shul'pin, G. B. *Pet. Chem.* **2001**, *41*, 405.

(137) Süss-Fink, G.; Gonzalez, L.; Shul'pin, G. B. *Applied Catalysis A: General* **2001**, *217*, 111.

(138) Shul'pin, G. B.; Golfeto, C. C.; Suss-Fink, G.; Shul'pina, L. S.; Mandelli, D. *Tetrahedron Letters* **2005**, *46*, 4563.

(139) Shul'pin, G. B.; Kudinov, A. R.; Shul'pina, L. S.; Petrovskaya, E. A. *Journal of Organometallic Chemistry* **2006**, *691*, 837.

(140) Shul'pin, G. B.; Kozlov, Y. N.; Shul'pina, L. S.; Petrovskiy, P. V. *Applied Organometallic Chemistry* **2010**, *24*, 464.

(141) Barton, D. H. R.; Gastiger, M. J.; Motherwell, W. B. *Journal of the Chemical Society, Chemical Communications* **1983**, 41.

(142) Barton, D. H. R.; Doller, D. *Accounts of Chemical Research* **1992**, *25*, 504.

(143) Barton, D. H. R.; Chabot, B. M. *Tetrahedron* **1996**, *52*, 10287.

(144) Barton, D. H. R.; Beviere, S. D.; Chavasiri, W.; Csuhai, E.; Doller, D.; Liu, W. G. *Journal of the American Chemical Society* **1992**, *114*, 2147.

(145) Barton, D. H. R.; Chabot, B. M.; Hu, B. *Tetrahedron* **1996**, *52*, 10301.

(146) Barton, D. H. R.; Delanghe, N. C.; Patin, H. *Tetrahedron* **1997**, *53*, 16017.

(147) Barton, D. H. R.; Costas Salgueiro, M.; MacKinnon, J. *Tetrahedron* **1997**, *53*, 7417.

(148) Barton, D. H. R. *Synlett* **1997**, *1997*, 229.

(149) Barton, D. H. R.; Delanghe, N. C. *Tetrahedron* **1998**, *54*, 4471.

(150) H.R. Barton, D.; Boivin, J.; Ozbalik, N.; M. Schwartzentruber, K.; Jankowski, K. *Tetrahedron Letters* **1985**, *26*, 447.

(151) Dunford, H. B. *Coordination Chemistry Reviews* **2002**, *233–234*, 311.

(152) Shul'pina, L. S.; Kirillova, M. V.; Pombeiro, A. J. L.; Shul'pin, G. B. *Tetrahedron* **2009**, *65*, 2424.

(153) Shul'pin, G. B.; Süss-Fink, G.; Shul'pina, L. S. *Journal of Molecular Catalysis A: Chemical* **2001**, *170*, 17.

(154) Shul'pin, G. B.; Lindsay-Smith, J. R. *Russian Chemical Bulletin* **1998**, *47*, 2379.

(155) Lindsay Smith, J. R.; Shul'pin, G. B. *Tetrahedron Letters* **1998**, *39*, 4909.

(156) Shul'pin, G. B.; Süss-Fink, G.; Lindsay Smith, J. R. *Tetrahedron* **1999**, *55*, 5345.

(157) Kirillova, M. V.; Kozlov, Y. N.; Shul'pina, L. S.; Lyakin, O. Y.; Kirillov, A. M.; Talsi, E. P.; Pombeiro, A. J. L.; Shul'pin, G. B. *Journal of Catalysis* **2009**, *268*, 26.

(158) Fernandes, R. R.; Kirillova, M. V.; da Silva, J. A. L.; Fraústo da Silva, J. J. R.; Pombeiro, A. J. L. *Applied Catalysis A: General* **2009**, *353*, 107.

(159) Britovsek, G. J. P.; England, J.; White, A. J. P. *Inorganic Chemistry* **2005**, *44*, 8125.

(160) Santos, I. C. M. S.; Gamelas, J. A. F.; Balula, M. S. S.; Simões, M. M. Q.; Neves, M. G. P. M. S.; Cavaleiro, J. A. S.; Cavaleiro, A. M. V. *Journal of Molecular Catalysis A: Chemical* **2007**, *262*, 41.

(161) Saussine, L.; Brazi, E.; Robine, A.; Mimoun, H.; Fischer, J.; Weiss, R. *Journal of the American Chemical Society* **1985**, *107*, 3534.

(162) Chavez, F. A.; Nguyen, C. V.; Olmstead, M. M.; Mascharak, P. K. *Inorganic Chemistry* **1996**, *35*, 6282.

(163) Nam, W.; Ryu, J. Y.; Kim, I.; Kim, C. *Tetrahedron Letters* **2002**, *43*, 5487.

(164) Nagataki, T.; Tachi, Y.; Itoh, S. *Chemical Communications* **2006**, 4016.

(165) Nagataki, T.; Ishii, K.; Tachi, Y.; Itoh, S. *Dalton Transactions* **2007**, 1120.

(166) Balamurugan, M.; Mayilmurugan, R.; Suresh, E.; Palaniandavar, M. *Dalton Transactions* **2011**, *40*, 9413.

(167) Tordin, E.; List, M.; Monkowius, U.; Schindler, S.; Knör, G. *Inorganica Chimica Acta* **2013**, *402*, 90.

(168) Gava, R.; Olmos, A.; Noverges, B.; Varea, T.; Álvarez, E.; Belderrain, T. R.; Caballero, A.; Asensio, G.; Pérez, P. J. *ACS Catalysis* **2015**, *5*, 3726.

(169) Martins, L.; Nasani, R.; Saha, M.; Mobin, S.; Mukhopadhyay, S.; Pombeiro, A. *Molecules* **2015**, *20*, 19203.

(170) Silva, A. C.; Fernández, T. L.; Carvalho, N. M. F.; Herbst, M. H.; Bordinhão, J.; Jr, A. H.; Wardell, J. L.; Oestreicher, E. G.; Antunes, O. A. C. *Applied Catalysis A: General* **2007**, *317*, 154.

(171) Kirillov, A. M.; Kopylovich, M. N.; Kirillova, M. V.; Haukka, M.; da Silva, M. F. C. G.; Pombeiro, A. J. L. *Angewandte Chemie International Edition* **2005**, *44*, 4345.

(172) Kirillov, A. M.; Kopylovich, M. N.; Kirillova, M. V.; Karabach, E. Y.; Haukka, M.; da Silva, M. F. C. G.; Pombeiro, A. J. L. *Advanced Synthesis & Catalysis* **2006**, *348*, 159.

(173) Kirillova, M. V.; Kirillov, A. M.; Mandelli, D.; Carvalho, W. A.; Pombeiro, A. J. L.; Shul'pin, G. B. *J. Catal.* **2010**, *272*, 9.

(174) Kirillov, A. M.; Kirillova, M. V.; Pombeiro, A. J. L. *Coordination Chemistry Reviews* **2012**, *256*, 2741.

(175) Roy, P.; Manassero, M. *Dalton Transactions* **2010**, *39*, 1539.

(176) Fernandes, T. A.; Santos, C. I. M.; Andre, V.; Dias, S. S. P.; Kirillova, M. V.; Kirillov, A. M. *Catalysis Science & Technology* **2016**, *6*, 4584.

CHAPTER TWO

Utilisation of novel NiSNS complexes in paraffin oxidation

2.1 Summary

Two series of closely related SNS pincer ligands (**L1** and **L2**) were synthesised with the major structural variation on the nitrogen backbone containing either the methyl [**L1** = bis(Rthioethyl)methylamine: where R = Me (**a**), Et (**b**), Bu (**c**)] or the phenyl [**L2** = bis(Rthioethyl)phenylamine: where R = Me (**a**), Et (**b**), Cy (**d**)] functional group. When the ligands were complexed to Ni, **L1a-c** correspondingly yielded three new cationic dimeric $[L1Ni(\mu\text{-}Cl)_3NiL1]^+$ complexes (**1.1a-c**) whilst ligands **L2a-d** correspondingly yielded mononuclear ($L2NiBr_2$) complexes **1.2a-d**. All the new compounds were characterised by IR, HRMS, elemental analysis and single crystal X-ray diffraction for complexes **1.1c** and **1.2a-d**. X-ray structural data of **1.1c** revealed the unusual three chloro-bridged Ni dimer with the SNS ligand coordinated in a facial binding mode to the two pseudo-octahedral Ni centres. Molecular structures of complexes **1.2a**, **1.2b** and **1.2d** each displayed five-coordinate distorted trigonal bipyramidal geometry around the nickel(II) metal centres. When utilised as catalysts in the *tert*-butyl hydroperoxide oxidation of *n*-octane, all the complexes showed activity to mainly products of internal carbon activation (octanones and secondary octanols) with **1.2b** as the most active (10% total substrate to oxygenates yield), whereas **1.2a** was the least active, but most selective towards alcohols (alcohol/ketone = 2.13).

2.2 Introduction

The exploration of pincer compounds has become a dynamic area of research over the last few decades.[1-13] In addition to the greater stability brought about by the (tridentate) binding mode of a pincer ligand, control over the electronic and steric properties of their metal complexes is one of the desirable features that made this type of ligands so popular.[14-16] More specifically, sulfur and nitrogen based pincer ligands are considered hemilabile due to dissimilarity in the donor strengths of the two coordinating atoms i.e. the relatively soft sulfur donor combined with a hard nitrogen donor. This type of feature is especially advantageous in catalysis as it offers a balance between reactivity and stability of the metal complex.[17] Complexes bearing the SNS pincer moiety have found applications in catalytic reactions such as ethylene trimerization,[18-24] Suzuki coupling[25] and transfer hydrogenation[26], as well as in the medicinal field where SNS pincer complexes of radioactive metals have been found useful as brain imaging agents.[27-30]

In a previous work[31] novel CoSNS complexes were reported with two types of known SNS ligands;[22,32-35] the first series were characterised by a rigid backbone (with a central pyridine moiety as the N-donor atom), while the second series contained a more flexible backbone symmetrically built around an amine N-donor atom. In both series, simple alkyl groups (respectively methylene and ethylene) served as linkers to the S-donor atoms. The complexes were tested as catalysts in the oxidation of *n*-octane and the results showed that those with the more flexible backbone were more active as catalysts. This observation prompted the exploration into the relatively flexible variants of the SNS ligands, i.e. those constructed around a central amine N donor atom. For the current series of studies, additional functionalities (alkyl and aryl goups) were introduced on the central N-donor atom to allow for further modulation of its binding potentials to metals. A search of the literature revealed a paucity of reports (compounds **L1a** and **L2b**)[36-38] on the types of SNS ligands synthesised and reported in this work, hence many of the new compounds (**L1b**, **L1c**, **L2a** and **L2d**) are reported for the first time. Herein, we describe the synthetic protocols and characterisation of six SNS ligands and their coordination to nickel to yield a total of six novel complexes. A complete study on their structural properties and catalytic application in the oxidation of *n*-octane is also reported and discussed.

2.3 Experimental Section

2.3.1 General

All reactions and manipulations were performed using standard Schlenk techniques under nitrogen atmosphere. Solvents were dried according to established methods[39] and purged with high purity nitrogen gas prior to use. Diethyl ether (Et_2O) and tetrahydrofuran (THF) were dried over sodium wire and benzophenone, absolute ethanol (EtOH) and methanol (MeOH) were dried over magnesium turnings and iodine, and dichloromethane (DCM) was dried over phosphorous pentoxide. $Ni(DME)Cl_2$ was synthesized according to a procedure adapted from the literature[40], whilst $Ni(PPh_3)_2Br_2$ was purchased from Sigma. All other reagents were obtained commercially and used as received. All NMR spectra were recorded using a Bruker Avance III 400 MHz spectrometer at ambient temperature. The ^1H NMR data were reported as chemical shift (δ, ppm) and referenced to the solvent peak $CDCl_3$. The attached proton test (APT) ^{13}C NMR, which distinguishes between quaternary C, CH, CH_2 and CH_3 carbons, are listed as chemical shift (δ, ppm) and positive (pos) or negative (neg) with the corresponding carbons in parentheses and referenced to the solvent peak $CDCl_3$. The IR data were recorded on a Perkin Elmer Attenuated Total Reflectance (ATR) spectrophotometer and elemental analyses were performed on a Thermo-Scientific Flash 2000 CHNS/O elemental analyzer, the HRMS was recorded on a Waters Micromass LCT Premier TOF-MS, while the melting points were determined using a Stuart Scientific melting point apparatus.

2.3.2 Synthesis and characterisation of ligands and complexes

Bis(2-chloroethyl)methylamine. Into a 250 ml Schlenk flask containing 50 ml of DCM and

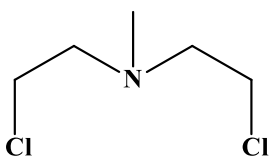

13.8 ml (120 mmol) of methyldiethanolamine, 26.0 ml (360 mmol) of $SOCl_2$ was added dropwise at 0 °C under vigorous stirring. The resultant solution was stirred at room temperature for 2 h, after which the solvent was removed *in vacuo* to yield a white solid which was dried under vacuum for several days. Yield: 98%. ^1H NMR (400 MHz, CD_3OD): δ 3.04 (s, 3H, C*H*$_3$-N), 3.69 (t, 4H, CH_2CH_2-N), 4.03 (t, 4H,

C*H*$_2$CH$_2$-N). ^{13}C APT NMR (400 MHz, CD$_3$OD): δ 38.14 (*C*H$_2$CH$_2$-N) pos, 41.44 (*C*H$_3$-N) neg, 58.22 (CH$_2$*C*H$_2$-N) pos. Melting point = 106-107 °C.

Bis(2-tosylethyl)phenylamine (Ph-Tos). In a 500 ml round bottom flask, phenyldiethanolamine

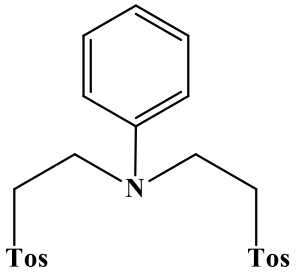

(10.54 g, 58.2 mmol) was dissolved in 100 ml of THF. In a separate beaker, 23.92 g (598 mmol) of NaOH was dissolved in 100 ml of double-distilled water and added to the THF solution. A solution of tosyl chloride (22.02 g, 116 mmol) in 100 ml of THF was added slowly to the resultant mixture at 0 °C which was then allowed to stir at that temperature for 30 min and thereafter at room temperature for a total time of 4 h. The mixture was then poured into 200 ml of double-distilled water and extracted with DCM (3 x 100 ml). The combined organic fractions were then washed with a saturated NaCl solution, dried with MgSO$_4$ and evacuated to yield a peach colored oil which, upon standing overnight, turned into a solid. After recrystallization from DCM and EtOH, a white crystalline product was obtained. Single crystals were grown from slow evaporation of a DCM solution of the product. Yield: 71%. ^{1}H NMR (400 MHz, CDCl$_3$): δ 2.44 (s, 6H, C*H*$_3$-tosyl), 3.56 (t, 4H, C*H*$_2$CH$_2$-N), 4.10 (t, 4H, CH$_2$C*H*$_2$-N), 6.44 (d, 2H, aromatic), 6.72 (t, 1H, aromatic), 7.14 (t, 2H, aromatic), 7.28 (d, 4H, aromatic), 7.72 (d, 4H, aromatic). ^{13}C APT NMR (400 MHz, CDCl$_3$): δ 21.65 (*C*H$_3$-tosyl) neg, 50.19 (CH$_2$*C*H$_2$-N) pos, 66.58 (*C*H$_2$CH$_2$-N) pos, 112.03 (aromatic) neg, 117.61 (aromatic) neg, 127.84 (aromatic) neg, 129.48 (aromatic) neg, 129.89 (aromatic) neg, 132.62 (aromatic) pos. Melting point = 88-89 °C.

Bis(methylthioethyl)methylamine (L1a). Sodium methanethiolate (3.38 g, 48.2 mmol) was

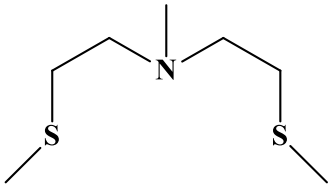

added to a solution of bis(2-chloroethyl)methylamine (2.64 g, 16.9 mmol) in EtOH (50 ml) and the resultant mixture was refluxed for 2 h. The solvent was removed *in vacuo* and the cream residue was purified by elution with 5% MeOH in DCM through a silica column to yield a pale yellow oil. Yield: 71%. ^{1}H NMR (400 MHz, CDCl$_3$): δ 2.10 (s, 6H, C*H*$_3$-S), 2.27 (s, 3H, C*H*$_3$-N), 2.59 (m, 8H, C*H*$_2$C*H*$_2$-N). ^{13}C APT NMR (400 MHz, CDCl$_3$): δ 15.83 (*C*H$_3$-S) neg, 31.78 (*C*H$_2$CH$_2$-N) pos, 42.03 (*C*H$_3$-N) neg, 56.95 (CH$_2$*C*H$_2$-N) pos. HRMS ESI (*m/z*) Calcd for: C$_7$H$_{18}$NS$_2$ = 180.0881. Found: 180.0879. IR ν_{max} (cm^{-1}): 2956 (m), 2915 (s), 2843 (m), 2788 (m), 1456 (m), 1437 (m), 1110 (s), 699 (m).

Bis(ethylthioethyl)methylamine (L1b). Sodium metal (1.101 g, 47.9 mmol) and ethanethiol (3.6 ml, 47.9 mmol) were stirred together in EtOH (50 ml) under inert atmosphere for 15 min in a 100 ml Schlenk flask. This mixture was then transferred to a solution of bis(2-chloroethyl)methylamine (2.49 g, 15.9 mmol) in EtOH (100 ml) via cannula and the resultant solution was refluxed for 2 h whilst monitoring by TLC. The solvent was then evacuated and the cream residue was purified analogously to **L1a** to obtain a pale yellow oil. Yield: 73%. ^{1}H NMR (400 MHz, $CDCl_3$): δ 1.24 (t, 6H, C*H*$_3$CH$_2$-S), 2.28 (s, 3H, C*H*$_3$-N), 2.53 (q, 4H, CH$_3$C*H*$_2$-S), 2.61 (m, 8H, C*H*$_2$C*H*$_2$-N). ^{13}C APT NMR (400 MHz, $CDCl_3$): δ 14.87 (*C*H$_3$CH$_2$-S) neg, 26.21 (CH$_3$*C*H$_2$-S) pos, 29.22 (*C*H$_2$CH$_2$-N) pos, 42.05 (*C*H$_3$-N) neg, 57.41 (CH$_2$*C*H$_2$-N) pos. HRMS ESI (*m/z*) Calcd for: $C_9H_{22}NS_2$ = 208.1194. Found: 209.1190. IR ν_{max} (cm^{-1}): 2961 (m), 2925 (s), 2871 (w), 2846 (w), 2790 (m), 1453 (s), 1109 (m), 733 (m).

Bis(butylthioethyl)methylamine (L1c). This ligand was synthesized and purified similarly to **L1b** with the following masses and volumes: 2.493 g (16.0 mmol) of bis(2-chloroethyl)methylamine, 1.102 g (47.9 mmol) of sodium metal and 5.1 ml (47.9 mmol) of butanethiol. The product was obtained as a yellow oil. Yield: 81%. ^{1}H NMR (400 MHz, $CDCl_3$): δ 0.90 (t, 6H, C*H*$_3$CH$_2$CH$_2$CH$_2$-S), 1.40 (m, 4H, CH$_3$C*H*$_2$CH$_2$CH$_2$-S), 1.56 (m, 4H, CH$_3$CH$_2$C*H*$_2$CH$_2$-S), 2.28 (s, 3H, C*H*$_3$-N), 2.52 (t, 4H, CH$_3$CH$_2$CH$_2$C*H*$_2$-S), 2.61 (br s, 8H, C*H*$_2$C*H*$_2$-N). ^{13}C APT NMR (400 MHz, $CDCl_3$): δ 13.69 (*C*H$_3$CH$_2$CH$_2$CH$_2$-S) neg, 22.00 (CH$_3$*C*H$_2$CH$_2$CH$_2$-S) pos, 29.67 (*C*H$_2$CH$_2$-N) pos, 31.87 (CH$_3$CH$_2$*C*H$_2$CH$_2$-S) pos, 32.11 (CH$_3$CH$_2$CH$_2$*C*H$_2$-S) pos, 42.17 (*C*H$_3$-N) neg 57.44 (CH$_2$*C*H$_2$-N) pos. HRMS ESI (*m/z*) Calcd for: $C_{13}H_{30}NS_2$ = 264.1820. Found: 264.1828. IR ν_{max} (cm^{-1}): 2956 (m), 2927 (m), 2872 (w), 2789 (w), 1458 (s), 1053 (m), 745 (m).

Bis(methylthioethyl)phenylamine (L2a). Sodium methanethiolate (0.601 g, 8.58 mmol) was added to a solution of bis(2-tosylethyl)phenylamine (1.389 g, 2.84 mmol) in THF (50 ml) and the resultant mixture was left to reflux for 24 h. The reaction mixture was filtered and the solvent was removed *in vacuo* to yield a pale yellow oil. Yield: 71%. ^{1}H NMR (400 MHz, $CDCl_3$): δ 2.10 (s, 6H, C*H*$_3$-S), 2.62 (t, 4H, C*H*$_2$CH$_2$-N), 3.48 (t, 4H, CH$_2$C*H*$_2$-N), 6.61 (m, 3H, Ph-N), 7.16 (t, 2H, Ph-N). ^{13}C APT NMR (400 MHz, $CDCl_3$): δ 15.80

(*C*H_3-S) neg, 31.36 (*C*$H_2$$CH_2$-N) pos, 51.06 ($CH_2$*C*$H_2$-N) pos, 111.83 (Ph-N) neg , 116.65 (Ph-N) neg , 129.43 (Ph-N) neg, 146.79 (Ph-N) pos. HRMS ESI (*m/z*) Calcd for: $C_{12}H_{20}NS_2$ = 242.1037. Found: 242.1031. IR ν_{max} (cm^{-1}): 3092 (w), 3034 (w), 2958 (w), 2914 (m), 1597 (s), 1501 (s), 1350 (m), 1186 (m), 745 (s), 691 (s).

Bis(ethylthioethyl)phenylamine (L2b). Sodium metal (0.194 g, 8.45 mmol) and ethanethiol (0.63 ml, 8.45 mmol) were stirred together in EtOH (100 ml) under inert atmosphere for 15 min in a 250 ml Schlenk flask. This mixture was then transferred to a solution of bis(2-tosylethyl)phenylamine (1.378 g, 2.82 mmol) in THF (80 ml) via cannula at 0 °C and the resultant solution was refluxed for 2 h whilst monitoring by TLC. The mixture was then poured into 100 ml of double distilled water and extracted three times with 50 ml portions of DCM. The organics were combined, washed with a brine solution and dried with $MgSO_4$. The product was obtained as a pale yellow oil upon evacuation of the solvent. Yield: 73%. ^{1}H NMR (400 MHz, $CDCl_3$): δ 1.29 (t, 6H, C*H*$_3$$CH_2$-S), 2.62 (q, 4H, CH_3C*H*$_2$-S), 2.73 (t, 4H, C*H*$_2$$CH_2$-N), 3.54 (t, 4H, CH_2C*H*$_2$-N), 6.68 (m, 3H, Ph-N), 7.24 (t, 2H, Ph-N). ^{13}C APT NMR (400 MHz, $CDCl_3$): δ 15.00 (*C*$H_3$$CH_2$-S) neg, 26.27 ($CH_3$*C*$H_2$-S) pos, 28.88 (*C*$H_2$$CH_2$-N) pos, 51.51 ($CH_2$*C*$H_2$-N) pos, 111.80 (Ph-N) neg , 116.58 (Ph-N) neg , 129.54 (Ph-N) neg, 146.77 (Ph-N) pos. HRMS ESI (*m/z*) Calcd for: $C_{14}H_{24}NS_2$ = 270.1350. Found: 270.1345. IR ν_{max} (cm^{-1}): 3025 (w), 2962 (w), 2924 (w), 2869 (w), 1597 (s), 1502 (s), 1349 (m), 1185 (m), 744 (s), 691 (s).

Bis(cyclohexylthioethyl)phenylamine (L2d). This ligand was synthesized using the same method as for **L2b** with the following masses and volumes: 3.085 g (6.31 mmol) of bis(2-tosylethyl)phenylamine, 0.432 g (18.92 mmol) of sodium and 2.32 ml (18.92 mmol) of cyclohexanethiol. The product was obtained as a waxy solid. Yield: 84%. ^{1}H NMR (400 MHz, $CDCl_3$): δ 1.27-1.35 (m, 12H, C_6H_{12}-S), 1.79 (m, 4H, C_6H_{12}-S), 1.97 (m, 4H, C_6H_{12}-S), 2.73 (t, 4H, C*H*$_2$$CH_2$-N, 3.51 (t, 4H, CH_2C*H*$_2$-N), 6.65 (d, 2H, Ph-N), 6.70 (t, 1H. Ph-N), 7.23 (t, 2H, Ph-N). ^{13}C APT NMR (400 MHz, $CDCl_3$): δ 25.80 (C_6H_{12}-S) pos, 26.12 (C_6H_{12}-S) pos, 27.28 (*C*$H_2$$CH_2$-N) pos, 33.90 ($C_6H_{12}$-S) pos, 43.81($C_6H_{12}$-S) neg, 51.85 ($CH_2$*C*$H_2$-N) pos, 111.83 (Ph-N) neg , 116.48 (Ph-N) neg, 129.51 (Ph-N) neg, 146.77 (Ph-N), pos. HRMS ESI (*m/z*) Calcd for:

$C_{22}H_{36}NS_2$ = 378.2289. Found: 378.2279. IR ν_{max} (cm^{-1}): 3087 (w), 3058 (w), 3022 (w), 2923 (s), 2849 (m), 1595 (m), 1503 (s), 745 (s).

Bis(bis(methylthioethyl)methylamine) dinickel(II) tris(μ-chloro) chloride (1.1a). An EtOH solution (3 ml) of ligand **L1a** (0.190 g, 1.06 mmol) was added to a 5 ml solution of Ni (DME)Cl_2 (0.201 g, 1.06 mmol) in EtOH. The resultant green solution was left to stir overnight at room temperature. The solvent was then evacuated and the green residue was stirred in 5 ml of Et_2O to obtain a green solid which was washed several time with Et_2O and collected by filtration. Yield: 45%. Melting point: 253-255 °C. HRMS ESI (*m/z*) Calcd for$[(C_7H_{17}NS_2)_2Ni_2Cl_3]^+$ = 580.9350. Found: 580.9438. IR ν_{max} (cm^{-1}): 2973 (w), 2922 (m), 2868 (m), 1463 (m), 1448 (m), 1420 (s), 1251 (m), 1018 (m), 739 (s). Anal. (%) calc. for $C_{14}H_{38}N_2S_4Cl_4Ni_2O_2$: C, 25.7; H, 5.9; N, 4.3; found: C, 25.5; H, 5.4; N, 4.0.

Bis(bis(ethylthioethyl)methylamine) dinickel(II) tris(μ-chloro) chloride (1.1b). Complex **1.1b** was synthesized according to the procedure described for **1.1a** with the following masses: 0.165 g (0.80 mmol) of **L1b** and 0.151 g (0.80 mmol) of Ni(DME)Cl_2. Yield: 74%. Melting point: 175-176 °C. HRMS ESI (*m/z*) Calcd for: $[(C_9H_{21}NS_2)_2Ni_2Cl_3]^+$ = 636.9970. Found: 636.9968. IR ν_{max} (cm^{-1}): 2964 (w), 2928 (m), 2872 (m), 1450 (s), 1428 (m), 1259 (m), 1040 (m), 738 (m). Anal. (%) calc. for $C_{18}H_{52}N_2S_4Cl_4Ni_2O_4$: C, 29.0; H, 6.8; N, 3.8; found: C, 28.5; H, 6.2; N, 3.3.

Bis(bis(butylthioethyl)methylamine) dinickel(II) tris(μ-chloro) chloride (1.1c). Complex **1.1c** was synthesized according to the procedure described for **1.1a** with the following masses: 0.086 g (0.39 mmol) of **L1c** and 0.074 g (0.39 mmol) of Ni(DME)Cl_2. Single crystals suitable for analysis were obtained from the crude green oil. Yield: 74%. Melting point: 89-91 °C. . HRMS ESI (*m/z*) Calcd for: $[(C_{13}H_{29}NS_2)_2Ni_2Cl_3]^+$ = 749.1230. Found: 749.1437. IR ν_{max} (cm^{-1}): 2958 (w), 2930 (m), 2871 (m), 1463 (s), 1426 (m), 1224 (m), 1043 (m), 736 (s). Anal. (%) calc. for $C_{26}H_{68}N_2S_4Cl_4Ni_2O_5$: C, 35.6; H, 7.8; N, 3.2; found: C, 35.5; H, 7.9; N, 2.8.

Bis(methylthioethyl)phenylamine nickel(II) bromide (1.2a). A THF solution (3 ml) of ligand

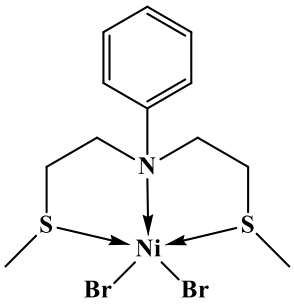

L2a (0.125 g, 0.519 mmol) was added to a 3 ml solution of $Ni(PPh_3)_2Br_2$ (0.383 g, 0.515 mmol) in THF. The resultant green solution was left to stir at room temperature over a period of four days. The solvent was then evacuated and the green residue was washed with several 5 ml portions of Et_2O. The product was then extract with 6 ml of DCM and upon evacuation of the solvent a brown solid was obtain, identified as the product. Single crystals were obtained from a DCM solution of **1.2a** layered with Et_2O. Yield: 26%. Decomposes > 200 °C. HRMS ESI (*m/z*) Calcd for: $C_{12}H_{19}NS_2BrNi$ = 377.9496. Found: 377.9503. IR ν_{max} (cm^{-1}): 3092 (w), 3024 (w), 2958 (w), 2914 (w), 1597 (m), 1501 (s), 1350 (m), 745 (s), 691 (s). Anal. (%) calc. for $C_{12}H_{19}NS_2NiBr_2$: C, 31.3; H, 4.2; N, 3.1; found: C, 31.4; H, 4.1; N, 2.9.

Bis(ethylthioethyl)phenylamine nickel(II) bromide (1.2b). This complex was synthesized

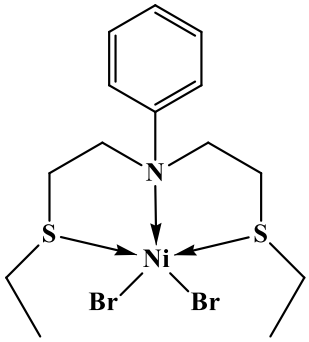

similarly to **1.2a** except that DCM was used as the solvent with the following masses: 0.146 g (0.543 mmol) of **L2b** and 0.394 g (0.530 mmol). The product was obtained as a maroon crystalline solid. Single crystals were grown from a DCM solution of **1.2b** layered with Et_2O. Yield: 30%. Melting point: 178-179 °C. HRMS ESI (*m/z*) Calcd for: $C_{14}H_{23}NS_2BrNi$ = 408.0661. IR ν_{max} (cm^{-1}): 3032 (w), 2963 (m), 2924 (m), 2863 (w), 1596 (m), 1588 (m), 1491 (s), 1458 (s), 1315 (m), 779 (s), 727 (s), 707 (s), 579 (s), 496 (s). Found: 407.9776. Anal. (%) calc. for $C_{14}H_{23}Br_2NNiS_2$: C, 34.5; H, 4.8; N, 2.9; found: C, 34.7; H, 4.8; N, 2.6.

Bis(cyclohexylthioethyl)phenylamine nickel(II) bromide (1.2d). This complex was synthesized

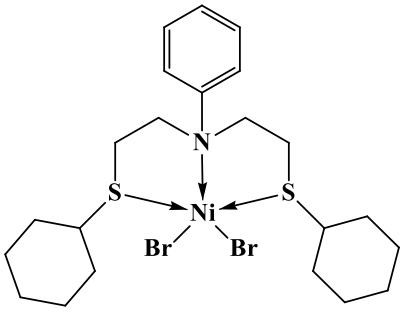

similarly to **1.2b** with the following masses: 0.103 g (0.273 mmol) of **L2d** and 0.192 g (0.258 mmol). The product was obtained as a purple crystalline solid. Single crystals were grown from a DCM solution of **1.2d** layered with Et_2O. Yield: 22%. Melting point: 190-191 °C. HRMS ESI (*m/z*) Calcd for: $C_{22}H_{35}NS_2BrNi$ = 516.2473. Found: 516.0714.IR ν_{max} (cm^{-1}): 2925 (m), 2851 (m), 1446 (s), 1265 (m), 998 (m), 745 (m), 693 (m). Found = 304.0253. Anal. (%) calc. for $C_{22}H_{35}NS_2NiBr_2$: C, 44.3; H, 5.9; N, 2.4; found: C, 44.3; H, 5.9; N, 2.6.

2.3.3 Crystallographic analyses

Single crystals for each complex were individually selected and glued onto the tip of a glass fiber, mounted in a stream of cold nitrogen and centered in the X-ray beam using a video camera. Single-crystal X-ray diffraction data were collected on a Bruker KAPPA APEX II DUO diffractometer using graphite-monochromated Mo-Kα radiation (χ = 0.71073 Å). Data collection was carried out at 100(2) or 173(2) K. Temperature was controlled by an Oxford Cryostream cooling system (Oxford Cryostat). Cell refinement and data reduction were performed using the program *SAINT*.[41] The data were scaled and absorption correction performed using *SADABS*.[42] The structures were solved by direct methods using *SHELXS*[42] and refined by full-matrix least-squares methods based on F^2 using *SHELXL*[42] and using the graphics interface program *X-Seed*[43,44]. All non-hydrogen atoms were refined anisotropically. All hydrogen atoms were placed in idealised positions and refined in riding models with U_{iso} assigned 1.2 or 1.5 times U_{eq} of their parent atoms and the bond distances were constrained to 0.98 or 0.99 Å. Selected crystallographic and structural refinement data are presented in Table 2.1.

2.3.4 Paraffin oxidation studies

The catalytic reactions were carried out in 25 ml two-neck pear shaped flasks fitted with a condenser and charged with acetonitrile as the solvent, cyclopentanone as the internal standard, *n*-octane as the paraffinic substrate and *t*-butyl hydroperoxide (TBHP) as the oxidant with the total volume of the reaction mixture equating to 5 ml. The catalyst was introduced in the form of a stock solution with the volumes varied so that the no. of moles of catalyst remained constant at 9.56 x 10^{-6} mol. The catalyst to substrate ratio was kept constant at 1:100 and the substrate to oxidant ratio was varied in order to determine the optimum. Noteworthy, the amounts used for the bimetallic catalysts **1.1** were adjusted according due to the presence of two 'active sites'. The reactions were stirred in an oil bath maintained at 50 °C for a period of 24 h after which a sample was removed, treated with an excess amount of PPh_3 (until the sample was saturated) and filtered through a Celite plug. Thereafter a 0.5 µl aliquot was injected into the GC for analysis and quantification of the products. The products were analysed using a PerkinElmer Auto System gas

chromatograph equipped with a flame ionisation detector (FID) which was set at 260 °C. A 50 m x 0.20 mm x 0.5µm Pona column was employed to efficiently separate the products with the injector temperature set at 240 °C. Yield was calculated based on the total moles of products formed divided by the initial moles of substrate added into the reaction mixture and was expressed as a percentage while the percentage selectivity was expressed as moles of each product divided by the total moles of all products in the stream.

Table 2.1: Selected crystallographic and structure refinement data for compounds **1.1c**, **1.2a**, **1.2b** and **1.2d**.

	1.1c	**1.2a**	**1.2b**	**1.2d**
Empirical formula	$C_{26}H_{58}Cl_3N_2Ni_2S_4$	$C_{11}HBr_2NNiS_2$	$C_{14}H_{23}Br_2NNi\ S_2$	$C_{22}H_{35}Br_2NNiS_2$
Formula weight	747.13	459.92	487.98	596.16
Temperature (K)	173(2)	100(2)	100(2)	100(2)
Crystal system	Triclinic	Monoclinic	Monoclinic	Monoclinic
Space group	*P*$\bar{1}$	$P2_1$	$P2_1$	$P2_1$
a (Å)	8.8883(6)	7.6710(2)	7.5226(2)	11.6435(5)
b (Å)	12.6986(7)	12.6361(3)	12.9514(4)	15.6123(6)
c (Å)	17.5591(11)	8.5913(2)	10.1018(3)	13.7664(6)
α (°)	86.7400(10)	90	90	90
β (°)	87.019(2)	101.201(2)	110.6820(10)	92.260(2)
γ (°)	83.6660(10)	90	90	90
Volume ($Å^3$)	1964.5(2)	820.01(3)	920.77(5)	2500.53(18)
Z	2	2	2	4
ρ_{calc} (g/cm^3)	1.450	2.028	1.760	1.584
μ (mm^{-1})	1.537	6.619	5.610	4.148
F(000)	906.0	476	488	1216
Crystal size (mm^3)	0.170 × 0.160 × 0.150	0.270 × 0.340 × 0.640	0.344 × 0.178 × 0.120	0.426 × 0.206 × 0.130
2Θ range for data collection (°)	2.326 to 56.694	2.41 to 25.47	2.668 to 25.496	1.750 to 27.257
Index ranges	-11≤ h ≤11, -16≤ k ≤16, -23≤ l ≤23	-9≤ h ≤9, -15≤ k ≤15, -9≤ l ≤10	-9≤ h ≤9, -15≤ k ≤15, -12≤ l ≤11	-14 ≤ h ≤ 14, -20 ≤ k ≤ 19, -17 ≤ l ≤ 16
Reflections collected	48931	7152	21020	95195
Independent reflections	9763 [R(int) = 0.0664]	2899 [R(int) = 0.0251]	3348 [R(int) = 0.0265]	10978 [R(int) = 0.0308]
Data / restraints / paramet	9763 / 0 / 376	2899 / 1 / 165	3348 / 1 / 184	10978 / 1 / 506
Goodness-of-fit on F^2	1.049	1.002	1.037	1.037
Final R indices [I >=2σ (I)]	R1 = 0.0486, wR2 = 0.1316	R1 = 0.0181, wR2 = 0.0460	R1 = 0.0127, wR2 = 0.0288	R1 = 0.0219, wR2 = 0.0434
Final R indices (all data)	R_1 = 0.0593, wR_2 = 0.1399	R1 = 0.0183, wR2 = 0.0461	R1 = 0.0132, wR2 = 0.0289	R1 = 0.0262, wR2 = 0.0445
Largest diff. peak and hole ($e.Å^{-3}$)	1.04 and -1.66	0.656 and -0.440	0.266 and -0.247	0.821 d -0.320

2.4 Results and discussion

2.4.1 Synthesis and characterization of ligands

This study reports on the synthesis and characterization of six pincer-type SNS ligands, (the majority of which are new) and the coordination chemistry of their Ni complexes. The SNS ligands prepared contained a flexible, straight chained amine backbone functionalised with a methyl or phenyl group as well as ethylene linkers to the S-donor atoms. The substituents bonded to the S-donor atoms were varied to investigate steric and electronic effects on the complexes. The synthetic route followed for the preparation of the ligands and complexes was developed and optimised to obtain the best yield and purity of the compounds.

Ligands **L1** and **L2** (Scheme 2.1) were synthesised by the reaction of bis(2-chloroethyl)methylamine or bis(2-tosylethyl)phenylamine with the respective thiol, which was activated by stirring with sodium metal in ethanol, to form the products as oils (with the exception of **L2d**) in 71–84% yields. The ligands were purified on a silica gel column and characterised by NMR, IR and HRMS.

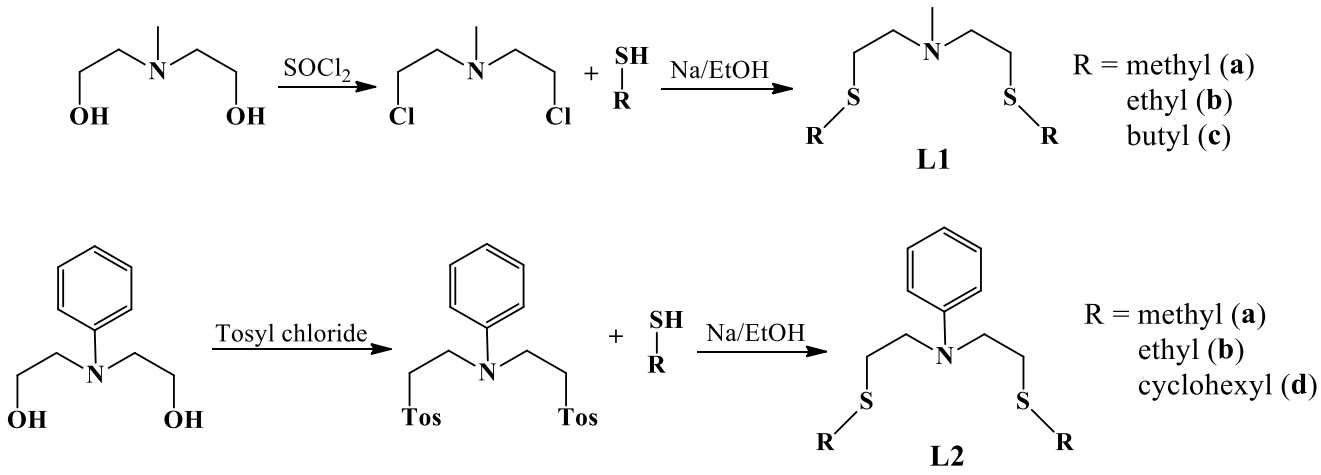

Scheme 2.1: Synthetic route for the preparation of ligands **L1a-c** and **L2a-d**.

^{1}H and ^{13}C APT NMR experiments were employed to elucidate the structures of the ligands prepared, since these are reliable and efficient techniques that provide important characterisation data. Spectra obtained for each ligand showed clean signals which integrated to the correct number of protons with no signs of impurity peaks present. An analysis of the results revealed that the methyl group bonded to the central N-donor atom on the ligand backbone appeared as a singlet in the region of 2.27-2.28 ppm for **L1a-c**. The two symmetric ethylene linker groups gave rise to a multiplet or a broad signal between 2.59 and 2.61 ppm which integrated to the expected eight protons (for **L1a-c**). In contrast, two triplets of four protons each were observed for the ethylene spacers of the phenyl substituted ligands **L2a-d**.

An HSQC NMR experiment (Fig. 2.1) was undertaken to highlight the correlation between the broad signal of **L1b** and the related carbon atoms. It showed that all the associated eight protons are equivalent to each other and are in the same environment, hence the overlapping signals.

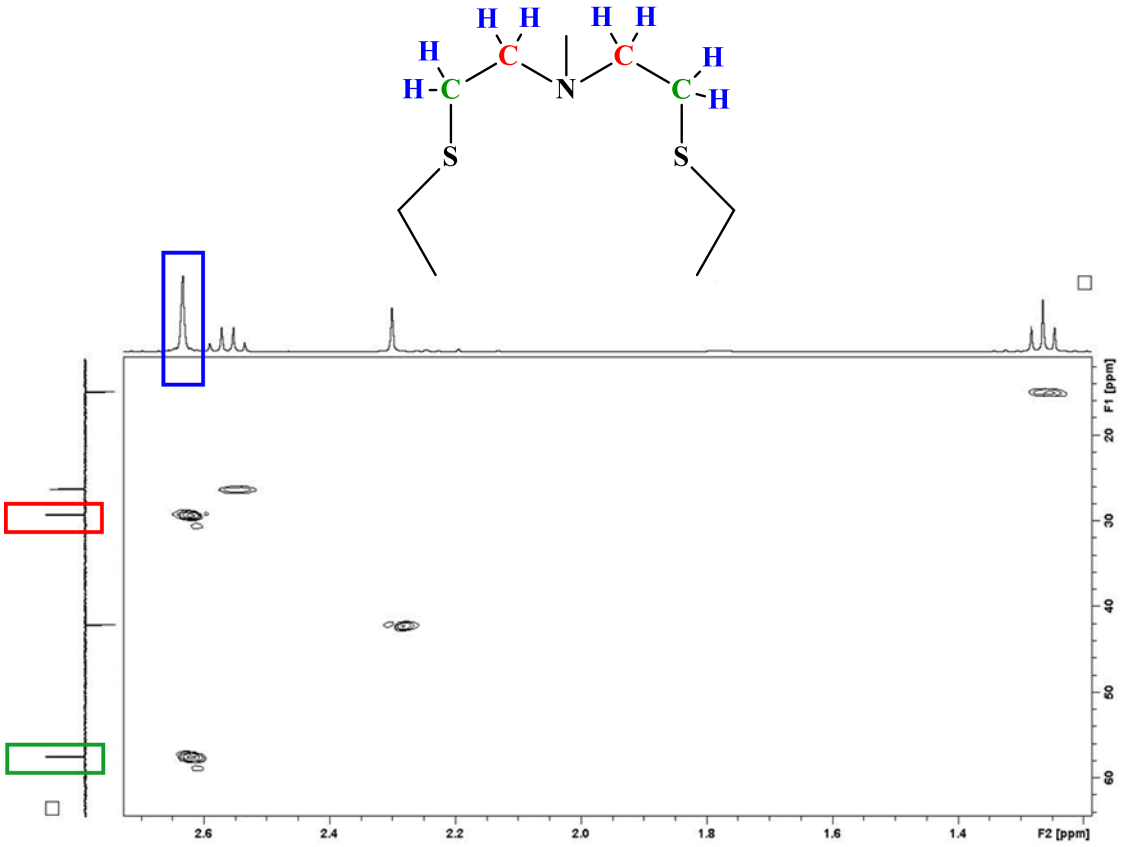

Figure 2.1: HSQC NMR spectrum of **L1b** showing the correlation between the proton and carbon signals of the ethylene group.

For the second series of ligands functionalised by the N-backbone phenyl group (**L2a-d)**, the aromatic protons were all observed as expected further downfield in the region of 6.61- 7.24 ppm.

The data obtained from IR and HRMS analyses are all as expected for each of the prepared ligands.

2.4.2 Structural analysis of ligand and metal precursors by single crystal X-ray crystallography

Single crystals of the ligand precursor bis(2-tosylethyl)phenylamine (**Ph-Tos**, Fig. 2.2) were obtained from slow evaporation of a concentrated solution in DCM. This structure has not been previously reported. **Ph-Tos** crystallises as a centrosymmetric molecule in the $P2_1$ space group of the monoclinic crystal system. The aromatic substituents of the tosyl moiety are twisted such that the planes defined by [C(9)-(C15)] and [C(18)-C(24)] intersect at an acute angle of 66.38°. Furthermore the phenyl group on the N-donor atom lies in a plane [C(1)-C(6)] that runs parallel to that of the [C(9)-(C15)] atoms.

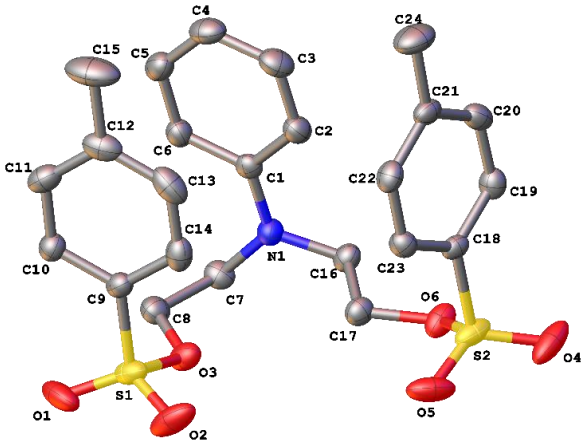

Figure 2.2: Molecular structure of ligand precursor **Ph-Tos** with hydrogens omitted for clarity and thermal ellipsoids drawn at the 50% probability.

Single crystals of $Ni(PPh_3)_2Br_2$ were obtained from a DCM solution layered with Et_2O from which a polymorph of an earlier reported structure[45] was obtained. The molecule also crystallises in the

monoclinic crystal system in the *P*2/*c* space group, whereas, in comparison, the earlier reported molecule belongs to the *P*2/*n* space group.

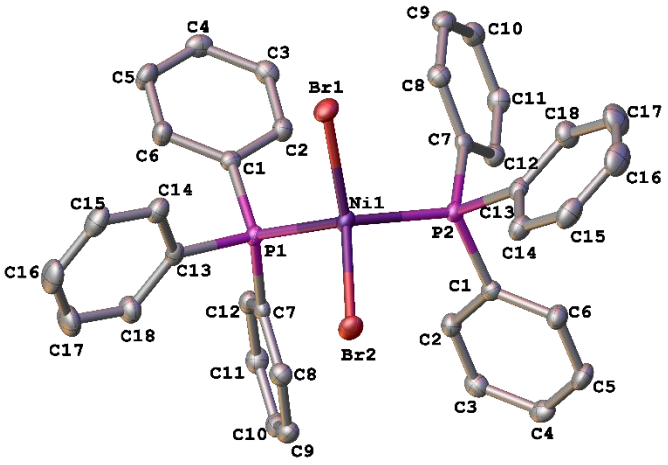

Figure 2.3: Molecular structure of $Ni(PPh_3)_2Br_2$ with hydrogens omitted for clarity and thermal ellipsoids drawn at the 50% probability.

Table 2.2: Selected bond lengths and bond angles for the reported[45] and new structures of the complex precursor $Ni(PPh_3)_2Br_2$.

Bond lengths (Å)	**Reported**	**This report**
Br(1)−Ni(1)	2.346(3)	2.3380(2)
Br(2)−Ni(1)	2.329(3)	2.3380(2)
P(1)−Ni(1)	2.323(5)	2.3220(4)
P(2)−Ni(1)	2.343(5)	2.3221(4)
Bond angles (°)	**Reported**	**This report**
Br(1)−Ni(1)−Br(2)	126.3(1)	125.801(16)
Br(1)−Ni(1)−P(1)	106.5(1)	104.675(11)
Br(1)−Ni(1)−P(2)	108.3(2)	104.470(11)
Br(2)−Ni(1)−P(1)	101.8(2)	104.469(11)
Br(2)−Ni(1)−P(2)	103.1(2)	104.674(11)
P(1)−Ni(1)−P(2)	110.4(2)	112.95(2)

From the structure depicted in Fig. 2.3, it is evident that the geometry around the Ni(II) centre is a distorted tetrahedron with the Br and PPh_3 groups situated in a pseudo-trans configuration to minimize steric interactions.

Data representing a comparison of its selected bond lengths and angles to those of its earlier reported polymorph are presented in Table 2.2. Although the differences are marginal, it is evident that in comparison, the bond angles show the most variability between the two $Ni(PPh_3)_2Br_2$ polymorphic solids.

2.4.3 Synthesis and characterisation of complexes

The combination of a solution of the respective SNS ligand bis(Rthioethyl)methylamine [R= methyl, **L1a**; ethyl, **L1b** and butyl, **L1c**] and bis(Rthioethyl)phenylamine [R= methyl, **L2a**; ethyl, **L2b**; and cyclohexyl, **L2d**] with a solution of the respective metal salts ($Ni(DME)Cl_2$ or $Ni(PPh_3)_2Br_2$) resulted in the formation of the new cationic dimeric $[L1Ni(\mu\text{-}Cl)_3NiL1]^+$ (**1.1a-1.1c**) and neutral mononuclear ($L2NiBr_2$) (**1.2a-1.2d**) complexes (Fig. 2.4). An immediate colour change observed at the start of these reactions served as the initial sign of successful Ni complexation to the ligand. Unresolved NMR signals are attributed to the paramagnetic nature of nickel in the +2 state, therefore other characterisation techniques were relied on (IR, MS, elemental analysis and single crystal XRD diffraction for selected complexes) to analyse and unambiguously confirm the structural composition and purity of the new Ni complexes.

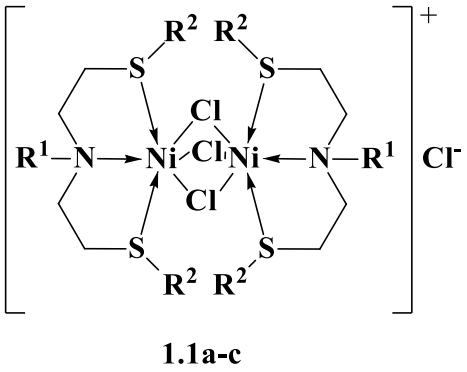

1.1a-c

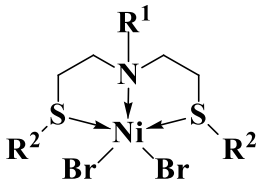

1.2a-d

1.1a: R^1 = Me, R^2 = Me
1.1b: R^1 = Me, R^2 = Et
1.1c: R^1 = Me, R^2 = Bu

1.2a: R^1 = Ph, R^2 = Me
1.2b: R^1 = Ph, R^2 = Et
1.2d: R^1 = Ph, R^2 = Cy

Figure 2.4: General representation of the NiSNS complexes **1.1** and **1.2**.

2.4.4 Characterisation of metal complexes by IR spectrophotoscopy

The prepared NiSNS complexes are hygroscopic and, hence, absorbed moisture upon exposure to air. This was evident from the broad band observed in the O−H stretching region of the IR spectra. Nevertheless, upon complexation, significant shifts in the frequencies of bands associated with the SNS ligands were noted and interpreted as indicators of successful coordination of the isolated SNS ligands to the Ni(II) centres. From the selected data listed in Table 2.3 for complex series **1.1a**-**1.1c**, it is clear that enhanced dπ-pπ overlap between the nickel metal centre and the N-donor atom of the SNS moiety occurred upon coordination, with the consequence that the ligand C−N bond weakened while the alkyl C−H stretch strengthened, as shown by the IR results.

Table 2.3: Selected IR data for ligands and the corresponding nickel complexes **1.1a-c**.

Compound	IR ν_{max}/cm^{-1}		
	C−H stretch[a]	C−H bend[a]	C−N stretch[b]
L1a	2915	1456	1056
1.1a	2922	1464	1048
L1b	2925	1453	1050
1.1b	2930	1449	1040
L1c	2927	1458	1053
1.1c	2930	1464	1043

[a] Strong. [b] Medium

2.4.5 Characterisation of metal complexes by MS and EA

ESI-MS data for the two metal complex series (**1.1** and **1.2)** displayed the $[NiSNSX]^+$ ion (where X = Cl or Br) as the predominant species and the specific isotopic patterns found were consistent and in line with what is expected for halogenated complexes. Furthermore, for complex series **1.1** bearing the methyl N-substituent, a mass corresponding to a dimer linked by three chlorides was observed. This suggests that these complexes possibly dimerise via three bridging chloro groups. The observation was later confirmed by X-ray crystallographic data of **1.1c**. However, this pattern was not observed with complex series **1.2** bearing the phenyl N-substituent. The CHN analyses

obtained for complexes **1.1b-1.1c** revealed the presence of varying amounts of water in the sample which was expected due to the hygroscopic nature of these complexes. The data acquired for complex series **1.2** were within the acceptable range which is indicative of their high purity.

2.4.6 Single crystal X-ray structural analysis of complexes 1.1c and 1.2a-d

Green single crystals were grown for complex **1.1c** from the crude green oil and for complexes **1.2a-d** from DCM solutions layered with diethyl ether to yield dark brown to purple crystals. Complex **1.1c** was isolated as a bimetallic dimer with octahedral geometry around each Ni(II) centre (Fig. 2.5), while complexes **1.2a**, **1.2b** and **1.2d** (Figs. 2.6 and 2.7) crystallised as monomeric five coordinate complexes that are characterised by trigonal bipyramidal geometry around the metal. Selected bond lengths and angles are listed in Table 2.4.

Table 2.4: Selected bond lengths (Å) and angles (°) for **1.1c**, **1.2a**, **1.2b** and **1.2d**.

Bond lengths (Å)	**1.1c**	**1.2a**	**1.2b**	**1.2d**
N(1)−Ni(1)	2.139(3)	2.106(2)	2.107(2)	2.114(3)
S(1)−Ni(1)	2.3860(9)	2.4319(8)	2.4329(8)	2.4283(9)
S(2)−Ni(1)	2.4167(8)	2.3981(8)	2.4310(7)	2.4291(10)
X(1)−Ni(1)	2.4600(8)	2.4481(4)	2.4313(4)	2.4461(5)
X(2)−Ni(1)	2.4068(8)	2.4147(4)	2.4221(4)	2.4293(5)
X(3)−Ni(1)	2.4195(8)	N/A	N/A	N/A
Bond angles (°)	**1.1c**	**1.2a**	**1.2b**	**1.2d**
S(1)−Ni(1)−S(2)	97.97(3)	170.13(3)	166.49(3)	158.93(3)
N(1)−Ni(1)−S(1)	87.41(8)	85.07(7)	83.27(7)	84.09(8)
N(1)−Ni(1)−S(2)	85.48(7)	85.06(7)	84.87(7)	82.97(8)
N(1)−Ni(1)−X(1)	97.10(7)	100.30(6)	101.02(6)	97.44(7)
N(1)−Ni(1)−X(2)	176.50(7)	143.78(6)	143.59(6)	148.72(8)
N(1)−Ni(1)−X(3)	94.07(8)	N/A	N/A	N/A

X = Cl or Br

Complex **1.1c** crystallised in the triclinic *P*ī space group as a cationic dimeric species containing distorted octahedrally bonded Ni(II) centres (I in Fig. 2.5) bridged via three chloride substituents, with a chloride as the counter ion. Related NiSNS complexes with halogen bridging have been reported in the literature.[46,47] The tridentate SNS ligand chelates in a facial binding mode to the metal centre such that the S-donor atoms, Cl(1) and Cl(3) lie in the same equatorial plane while the N-donor atoms and Cl(2) occupy axial positions of the octahedron. The coordination environment around Ni(2) is identical to that of Ni(1).

I **II**

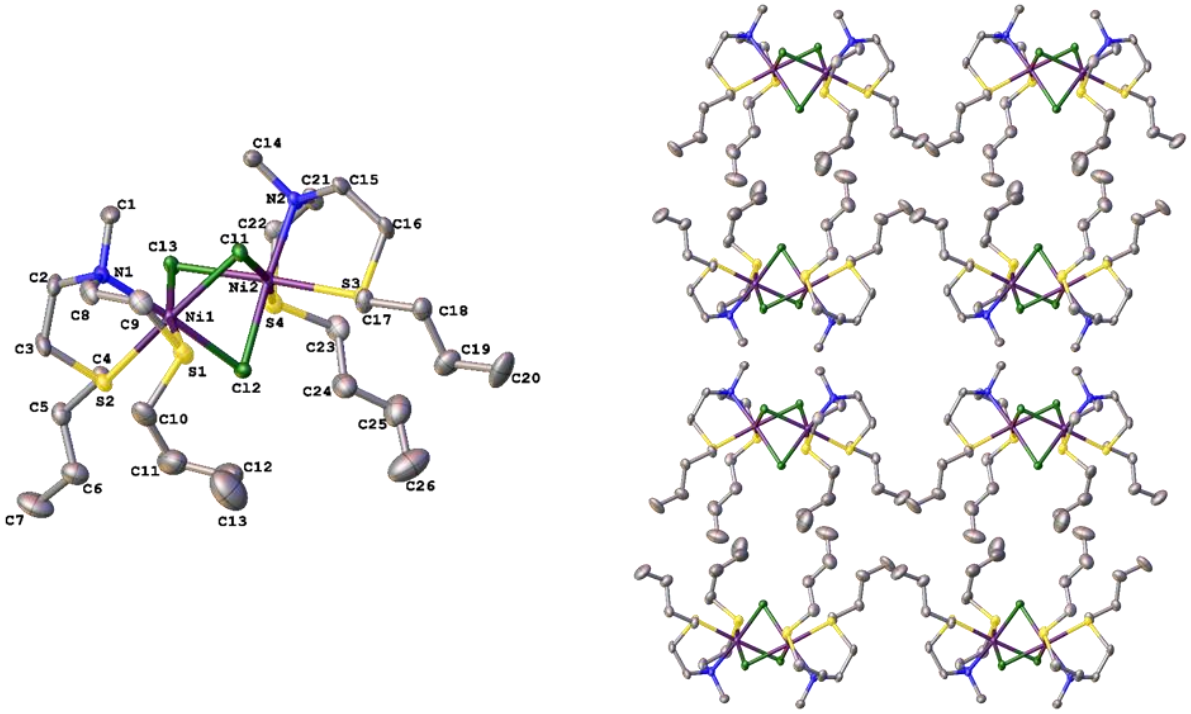

Figure 2.5: Cationic fragment (I) and crystal packing viewed along the *a*-axis (100) (II) of **1.1c** with hydrogens and Cl^- counter ion omitted for clarity. Thermal ellipsoids are drawn at the 50% probability level.

The two octahedral metal centres are separated by a Ni···Ni distance of 3.018 Å which is shorter than the sum of the van der Waals radii for two nickel atoms (3.260 Å). Therefore, it can be regarded as a relatively strong interaction, specifically in comparison to the previously reported

CoSNS complex[31] which displayed a Co···Co distance of 3.684 Å and a related tetradentate Ni complex containing an asymmetric pyrazolate ligand with a Ni···Ni distance of 3.823 Å.[35] Although it is quite rare to find Ni complexes that are bridged via three chlorides, there are a few reports on related complexes.[48-50] One of these, is reported by Wikstrom *et al.*, contains a tridentate NNN ligand.[50] A Ni···Ni distance of 3.086 Å was calculated for this complex, which is still slightly longer than what is observed for **1.1c**. In the crystal of **1.1c**, if the Me-N substituent is regarded as the head of each molecule and the butyl S-substituent as the tail, then the packing arrangement may be described as alternating units in a tail-to-tail and head-to-head configuration between successive layers (II in Fig. 2.5).

Complexes **1.2a**, **1.2b** (labelled as I and II respectively in Fig 2.6) and **1.2d** (I in Fig. 2.7) all crystallised in the $P2_1$ space group of the monoclinic crystal system. Only **1.2d** crystallised with two identical but independent molecules in the asymmetric unit cell as shown in Fig. 2.7. All three complexes exhibit a five coordinate, distorted trigonal bipyramidal geometry around the metal with the S-donor atoms occupying axial positions and the equatorial sites taken up by the N-donor and the two bromide substituents.

The phenyl ring, N(1), Ni(1), Br(1) and Br(2) reside in the same plane for complexes **1.2a** and **1.2b** (Fig. 2.6) with this also serving as a plane of symmetry in **1.2a**. However, for **1.2d**, the phenyl ring deviates from the [N(1), Ni(1), Br(1), Br(2)] plane by 0.026 – 0.500 Å. The general trend observed is that as the flexibility of the substituents on the S-donor atoms increased, the degree of asymmetry of the entire complex also increased. Furthermore, the 'bite angle' defined by the S(1)−Ni(1)−S(2) chelation gradually became more acute as the substituents on the S-donor atoms increased in steric complexity [methyl = 170.13(3), ethyl = 166.49(3) and cyclohexyl = 158.93(3)°]. This can be attributed to an increased steric crowding around the metal centre resulting in a decreased 'bite angle'.

Complexes **1.2a-d** pack in a similar ordered arrangement of alternating units forming parallel sheets of independent molecules. Each vertical layer of molecular sheets is related to the subsequent layer through an inversion axes. The cyclohexyl groups present in **1.2d** neatly fitted into the interlayer spaces between the parallel sheets resulting in a more efficiently packed crystal lattice (II in Fig. 2.7) as compared to **1.2a** and **1.2b** (Fig. 2.6).

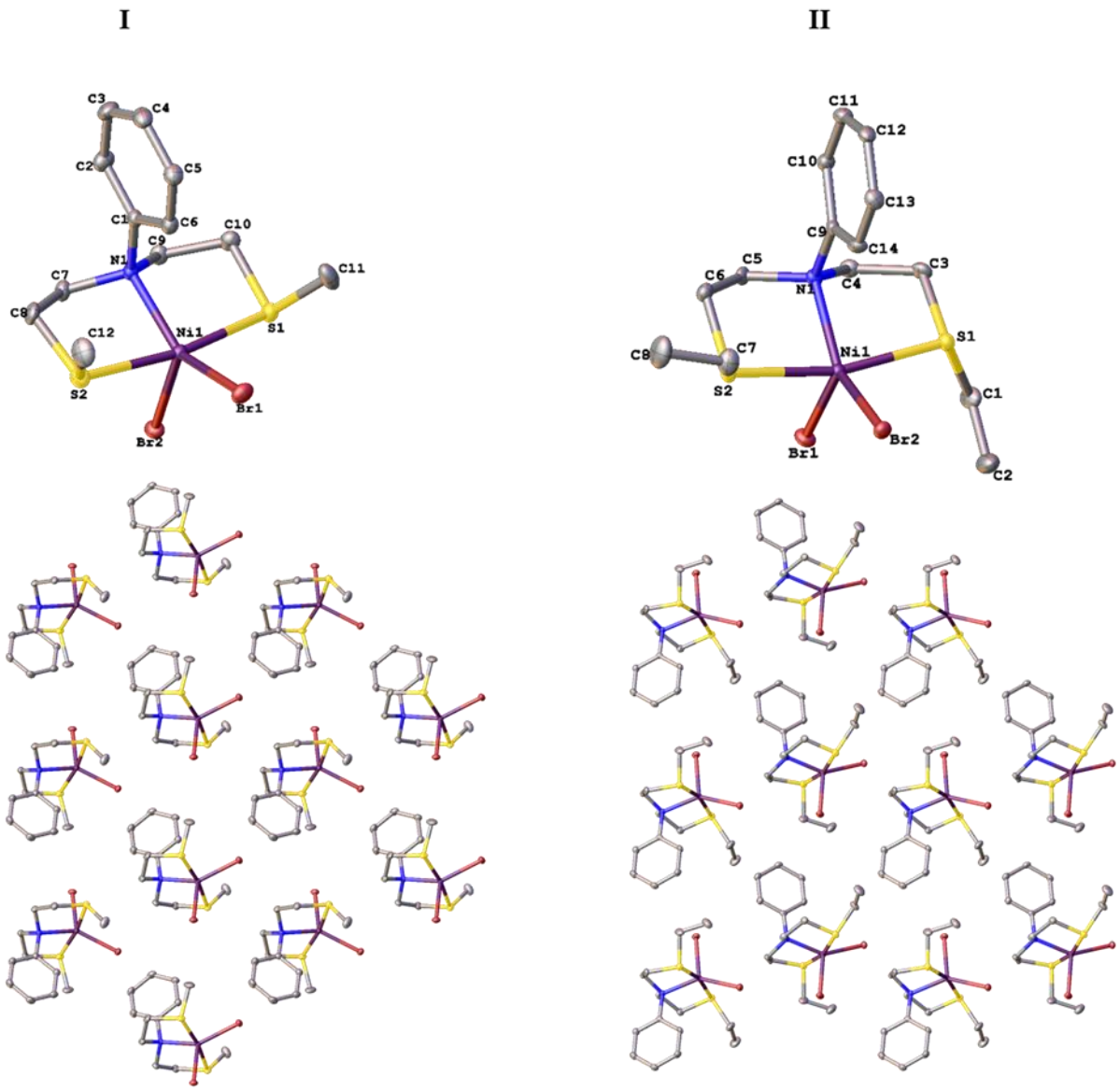

Figure 2.6: Molecular structures and crystal packing viewed along the *a*-axis (100) of **1.2a** (I) and **1.2b** (II) with the hydrogens omitted for clarity and thermal ellipsoids shown at the 50% probability level.

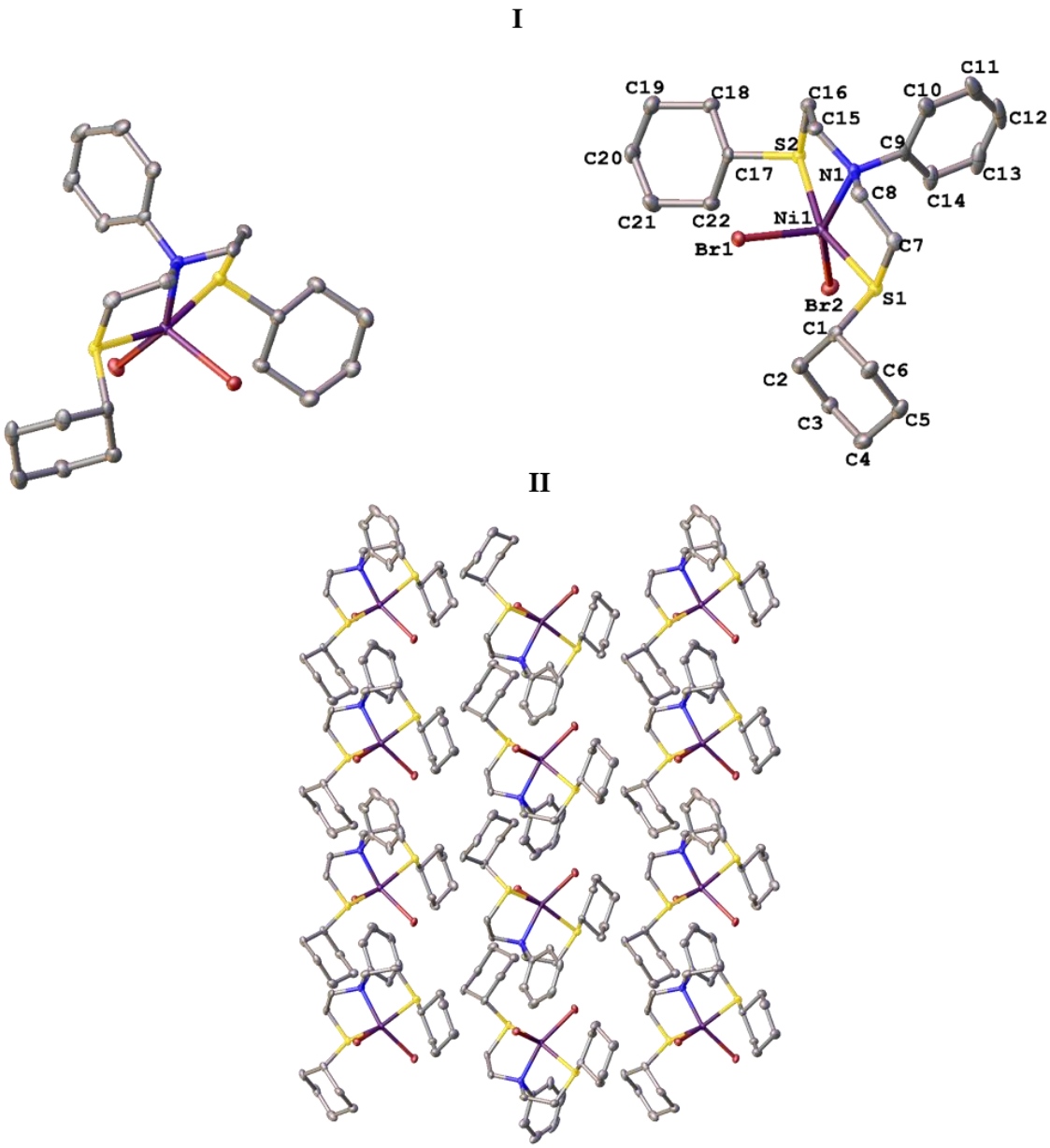

Figure 2.7: Molecular structure of **1.2d** showing two crystallographically independent molecules in the asymmetric unit cell (I) and the crystal packing viewed along the a-axis (100) (II) with the hydrogens omitted for clarity and thermal ellipsoids shown at the 50% probability level.

2.4.7 Application of the NiSNS complexes in paraffin oxidation

The prepared nickel complexes were applied as catalysts in the oxidation of *n*-octane with either H_2O_2 or TBHP as the source of oxygen in acetonitrile medium. Tests using H_2O_2 as the oxidant gave yields equivalent to that of the blank reaction over 24 h (1-2%), which indicate that the catalysts were inactive for C-H functionalisation with this particular oxidant. Therefore, TBHP was investigated further since it is a milder oxidant in comparison to H_2O_2.

Preliminary studies established the optimum conditions for the oxidation reaction as 50 °C, at a catalyst to octane to TBHP ratio of 1:100:1200 and a reaction time of 48 h (data was also recorded at 24 h). The cost and efficiency of utilising the oxidant is critical in the successful adoption of any oxidation catalyst system, hence the octane to TBHP ratio was thoroughly investigated (1:3, 1:6, 1:9, 1:12, 1:15 and 1:18), however, the best balance between conversion and product selectivity was observed at 1:12 substrate to oxidant ratio. The reactions were performed in air since no effect was observed when inert conditions were implemented. A blank reaction gave a yield of 2% in 48 h, while reactions with the simple salts ($NiCl_2$ and $NiBr_2$) gave yields of 3 and 5% respectively. Catalytic data highlighting yields to total oxidation products for **1.1** and **1.2**, is presented in Figs. 2.8 and 2.9 respectively.

The yields were calculated after treatment of the reaction aliquot with PPh_3, in order to reduce any octyl hydroperoxides present in the sample. This is a standard and largely accepted procedure for paraffin oxidation reactions first developed and reported by the Shul'pin group.[51]

For catalyst series **1.1**, bearing the sterically smaller N-substituent, (Fig. 2.8), it is clear that the yields are substantially higher than that over the metal precursor ($NiCl_2$). This suggests that the ligands influenced the enhanced activities of the catalysts. Furthermore, a slight increase in yield was observed on extending the time of reaction from 24 to 48 h, with **1.1a** producing the highest yield of 9% in 48 h. The ligand of this catalyst contains the smallest R-substituent bonded to the S-donor atoms ($-CH_3$) which resulted in the least sterically hindered metal centre. The metal centre is the active site to which the substrate binds, hence in theory, a least sterically crowded metal centre should render higher activity. The yield then drops to 7% for **1.1b**, presumably because of an increase in the steric environment around the metal centre caused by increasing the S-donor

substituent to an ethyl group. However, the slight increase to 8% for catalyst **1.1c** can be attributed to an electronic effect caused by the electron pushing long chain butyl groups.

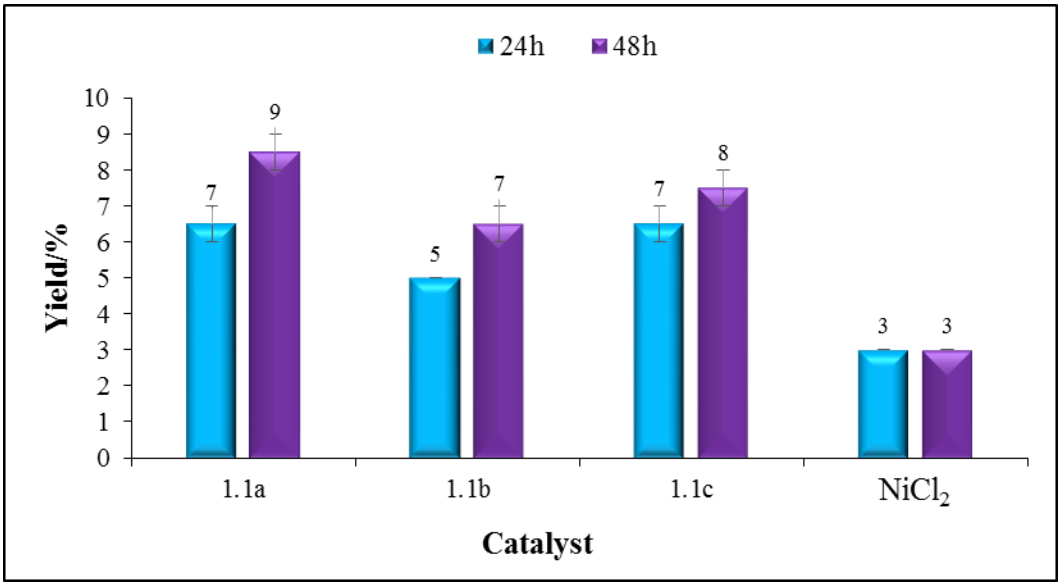

Figure 2.8: Product yields obtained for catalyst series **1.1** at an octane to TBHP ratio of 1:12 at 50 °C for 24 and 48 h.

The catalytic activities of the more rigid phenyl N-substituted catalysts **1.2** (Fig. 2.9) showed a different trend to that of **1.1**. Catalyst **1.2a**, containing the methyl substituents on the S-donor atoms was the least active giving a yield only marginally higher than that of the metal precursor in 48 h. However, **1.2b**, substituted with the ethyl groups on the S-donor atoms, gave a significantly higher yield of 10% in 48 h. This suggests that electronic effects and increased hydrophobicity influence the catalytic activity, since the ethyl groups are better electron donors and more hydrophobic than the methyl substituents. Although catalyst **1.2d** is electronically the richest in the series due to the cyclohexyl S-substituents, in comparison to **1.2b**, a lower yield was recorded indicating that both electronic and steric effects contribute to the catalytic activity. The cyclohexyl rings contributed to a degree of steric crowding around the active site which slightly decreased its activity.

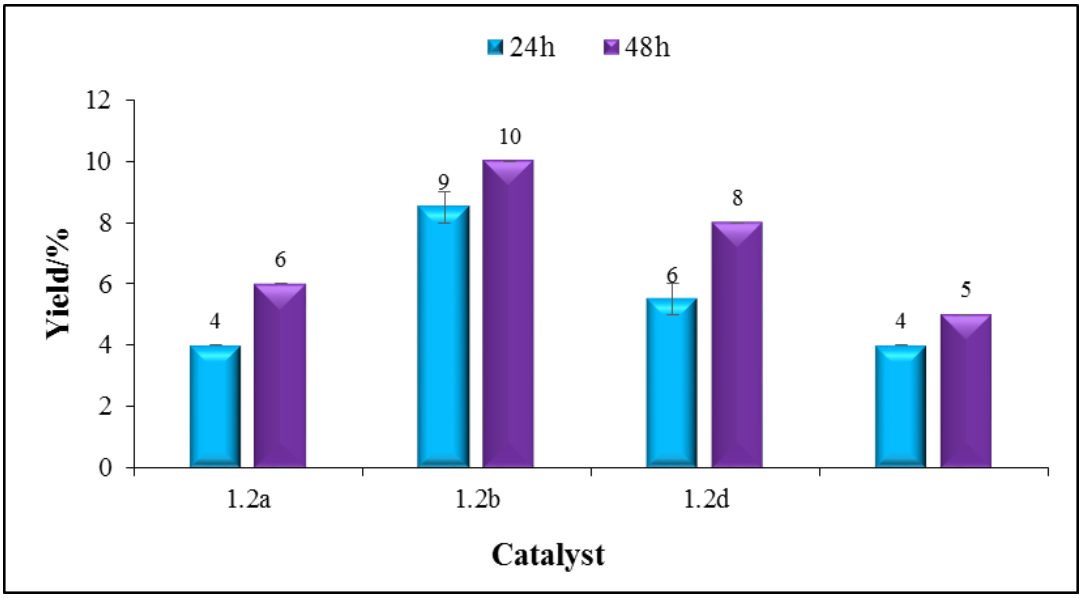

Figure 2.9: Product yields obtained for catalyst series **1.2** at an octane to TBHP ratio of 1:12 at 50 °C for 24 and 48 h.

Product selectivity is an important aspect in determining the efficiency of a catalytic system. Obtaining a single product would be ideal but also unrealistic, especially in the oxidation of *n*-octane. Considering the product distribution obtained for both catalyst series, a mixture of octanols and octanones oxygenated at carbon positions 2, 3 and 4 (C-2, C-3 and C-4) of the octane C-8 backbone was observed. No terminal carbon (C(1)) activation was observed for any of the systems in this study. The combined alcohol and ketone selectivities for **1.1a** are displayed in Fig. 2.10, from which the following points are observed:

- Octanones represent the majority product class at both 24 and 48 h reaction periods.
- Accumulation of the ketones seems to be a secondary reaction of alcohol over-oxidation. This is clear from the increased ketone selectivity at 48 h which is matched by decreased alcohol selectivity.

It is also important to note that a similar trend is observed for the rest of the catalysts, indicating that they all followed a similar reaction pathway.

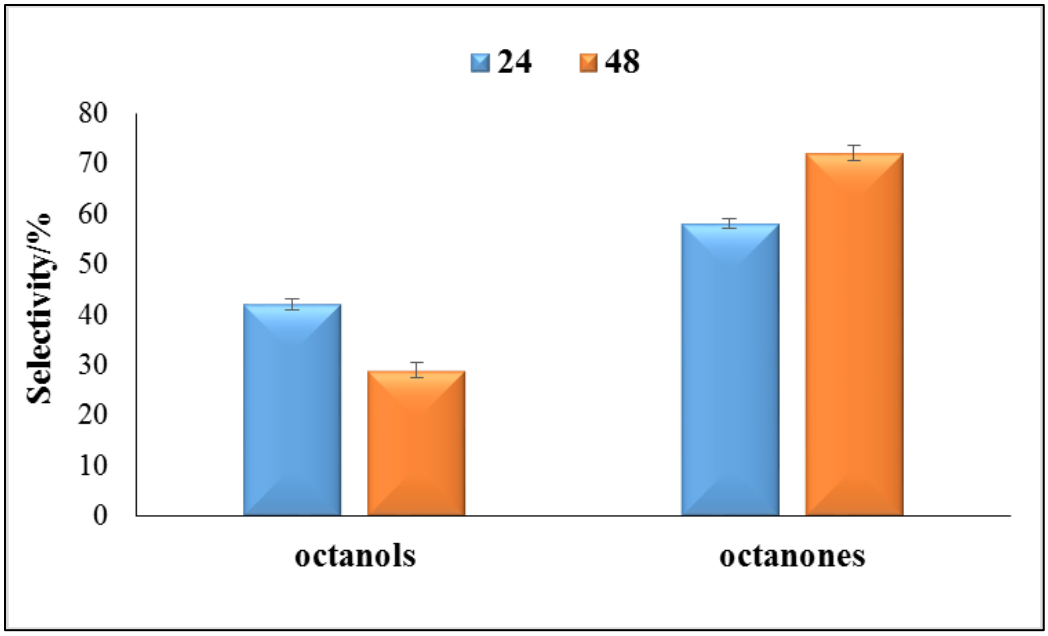

Figure 2.10: Selectivities to combined alcohol and ketone products for catalyst **1.1a** at an octane to TBHP ratio of 1:12 at 50 °C for 24 and 48 h.

The product distribution pattern, which displays the individual product selectivities as well as the regioselectivity parameters at each carbon, i.e. C(2):C(3):C(4) is presented in Table 2.5. Amongst the methyl N-substituted catalysts, **1.1a** and **1.1c** showed higher selectivity to the ketone products with low alcohol/ketone (*A*/*K*) ratios of 0.28 and 0.30 respectively. Overall, catalyst **1.2a** was the most selective to the alcohols with the highest *A*/*K* ratio of 2.13, presumably because of its comparatively lower activity. Hence, its ability to further oxidize the initial alcohol products to ketones was also low, meaning that at the end of the reaction period, more of the alcohol products remain. A low *A*/*K* ratio of 0.35 was observed for **1.2b** and this can be attributed to the higher activity it displayed, which further emphasizes the belief that over-oxidation, driven by a very active catalyst, is responsible for the prevalence of ketone products in this systems. In line with literature reports, the total regioselectivity indicated that the internal hydrogens on the C(2) position of the octane chain was the most active.[52-54]

Table 2.5: Product selectivities and regioselectivity parameters in the oxidation of *n*-octane.[a]

Catalyst	Product selectivities/%						C(2):C(3):C(4)[b]	*A*/*K*[c]
	2-ol	3-ol	4-ol	2-one	3-one	4-one		
1.1a	10	6	6	28	24	26	1.3:1:1.1	0.28
1.1b	26	12	12	18	15	17	1.5:1:1	1.00
1.1c	11	6	6	29	22	26	1.5:1:1.2	0.30
1.2a	34	17	17	10	10	12	1.7:1:1.1	2.13
1.2b	13	7	6	28	21	25	1.4:1:1.1	0.35
1.2d	18	9	9	23	18	23	1.6:1:1.2	0.56
$NiCl_2$	31	14	13	14	13	15	1.7:1:1	1.38
$NiBr_2$	23	10	10	20	17	20	1.6:1:1.1	0.75

[a] Reaction conditions: catalyst (9.56×10^{-6} mol, 1.91×10^{-3} M), *n*-octane (9.56×10^{-4} mol, 0.155 ml), TBHP (70% in H_2O, 0.0164 mol), 50 °C, 48 h, MeCN added as a solvent to give a total reaction volume of 5 ml.

[b] Total regioselectivity parameter takes into consideration both alcohol and ketone products at each carbon position and these values are normalized, i.e. taking into account the number of hydrogen atoms, 3 for the terminal carbon (CH_3) and 2 for each of the unique internal carbon (CH_2) positions.

[c] The *A*/*K* ratio gives the relative selectivity irrespective of carbon position of all alcohol/all ketone products, i.e. total moles of octanols divided by total moles of octanones.

Results obtained in this study are comparable to those reported by Pombeiro and co-workers using a Mn(salen) catalyst with TBHP.[52] They had also observed no C(1) activation and reported similar regioselectivities for the oxidation of *n*-octane.

In order to gain an insight into the mechanistic pathway, a reaction was conducted under our standard conditions with catalyst 11 in the presence of a radical inhibitor, TEMPO. No products were detected in this reaction, thus indicating that the mechanism follows a radical pathway as described in numerous literature reports.[51,52,55,56]

2.5 Conclusions

In this work, a total of six pincer-type SNS ligands were prepared, characterised and coordinated to Ni(II) to yield novel complexes which have also been fully characterised. The Ni complex **1.1c**, with butyl substituents on the S-donor atoms, crystallised as an unusual three chloro-bridged homo bimetallic dimer. The NiSNS complexes, characterised by a phenyl functionality on the N-donor atom, crystallised as monomeric species with the SNS ligand coordinated in a tridentate fashion around each trigonal bipyramidal Ni(II) centre.

All the complexes were utilised as catalysts in the oxidation of *n*-octane with TBHP as the oxidant. No products of terminal or C(1) carbon activation was observed for any of the catalysts studied. Furthermore, no cracking of the octane chain was detected and only C-8 products were observed. Overall, catalyst **1.2b** was the most active with a total product yield of 10%, whilst **1.2a** was the least active and most selective to alcohol products. The highest selectivity to the ketone products was seen for **1.1a**. The regioselectivity parameter revealed that the C(2) position on the *n*-octane chain was the most prominent position of attack for all the catalytic systems studied in this work.

2.6 References

(1) Moulton, C. J.; Shaw, B. L. *J. Chem. Soc., Dalton Trans.* **1976**, 1020.

(2) Singleton, J. T. *Tetrahedron* **2003**, *59*, 1837.

(3) Morales-Morales, D. *Rev. Soc. Quim. Mex* **2004**, *48*, 338.

(4) Harkins, S. B.; Peters, J. C. *Organometallics* **2002**, *21*, 1753.

(5) Gunanathan, C.; Milstein, D. *Chem. Rev,* **2014**, *114*, 12024.

(6) Selander, N.; J. Szabó, K. l. n. *Chem. Rev,* **2010**, *111*, 2048.

(7) Spasyuk, D. M.; Gorelsky, S. I.; van der Est, A.; Zargarian, D. *Inorg. Chem.* **2011**, *50*, 2661.

(8) Baber, R. A.; Bedford, R. B.; Betham, M.; Blake, M. E.; Coles, S. J.; Haddow, M. F.; Hursthouse, M. B.; Orpen, A. G.; Pilarski, L. T.; Pringle, P. G.; Wingad, R. L. *Chem. Commun.* **2006**, *0*, 3880.

(9) Gelman, D.; Musa, S. *ACS Catalysis* **2012**, *2*, 2456.

(10) Tang, Z.; Otten, E.; Reek, J. N. H.; van der Vlugt, J. I.; de Bruin, B. *Chem. Eur. J.* **2015**, *21*, 12529.

(11) Pascualini, M. E.; Di Russo, N. V.; Quintero, P. A.; Thuijs, A. E.; Pinkowicz, D.; Abboud, K. A.; Dunbar, K. R.; Christou, G.; Meisel, M. W.; Veige, A. S. *Inorg. Chem.* **2014**, *53*, 13078.

(12) Zhang, B.-S.; Wang, W.; Shao, D.-D.; Hao, X.-Q.; Gong, J.-F.; Song, M.-P. *Organometallics* **2010**, *29*, 2579.

(13) Yang, M.-J.; Liu, Y.-J.; Gong, J.-F.; Song, M.-P. *Organometallics* **2011**, *30*, 3793.

(14) van der Vlugt, J. I.; Reek, J. N. H. *Angew. Chem. Int. Ed.* **2009**, *48*, 8832.

(15) Milstein, D. *Topics in Catalysis* **2010**, *53*, 915.

(16) Jia, W.-G.; Li, D.-D.; Zhang, H.; Dai, Y.-C.; Sheng, E.-H. *J. Coord. Chem.* **2014**, *68*, 220.

(17) Klerman, Y.; Ben-Ari, E.; Diskin-Posner, Y.; Leitus, G.; Shimon, L. J. W.; Ben-David, Y.; Milstein, D. *Dalton Trans.* **2008**, 3226.

(18) McGuinness, D. S.; Brown, D. B.; Tooze, R. P.; Hess, F. M.; Dixon, J. T.; Slawin, A. M. Z. *Organometallics* **2006**, *25*, 3605.

(19) McGuinness, D. S.; Wasserscheid, P.; Morgan, D. H.; Dixon, J. T. *Organometallics* **2005**, *24*, 552.

(20) McGuinness, D. S.; Wasserscheid, P.; Keim, W.; Morgan, D.; Dixon, J. T.; Bollmann, A.; Maumela, H.; Hess, F.; Englert, U. *J. Am. Chem. Soc.* **2003**, *125*, 5272.

(21) Albahily, K.; Shaikh, Y.; Ahmed, Z.; Korobkov, I.; Gambarotta, S.; Duchateau, R. *Organometallics* **2011**, *30*, 4159.

(22) Temple, C. N.; Gambarotta, S.; Korobkov, I.; Duchateau, R. *Organometallics* **2007**, *26*, 4598.

(23) Temple, C.; Jabri, A.; Crewdson, P.; Gambarotta, S.; Korobkov, I.; Duchateau, R. *Angew. Chem.* **2006**, *118*, 7208.

(24) Jabri, A.; Temple, C.; Crewdson, P.; Gambarotta, S.; Korobkov, I.; Duchateau, R. *J. Am. Chem. Soc.* **2006**, *128*, 9238.

(25) Bai, S.-Q.; Hor, T. S. A. *Chem. Comm.***2008**, 3172.

(26) Page, M. J.; Wagler, J.; Messerle, B. A. *Organometallics* **2010**, *29*, 3790.

(27) Mastrostamatis, S. G.; Papadopoulos, M. S.; Pirmettis, I. C.; Paschali, E.; Varvarigou, A. D.; Stassinopoulou, C. I.; Raptopoulou, C. P.; Terzis, A.; Chiotellis, E. *J. Med. Chem.* **1994**, *37*, 3212.

(28) Papadopoulos, M. S.; Pirmettis, I. C.; Pelecanou, M.; Raptopoulou, C. P.; Terzis, A.; Stassinopoulou, C. I.; E., C. *Inorg. Chem.* **1996**, *35*, 7377.

(29) Chen, X.; Femia, F. J.; Babich, J. W.; Zubieta, J. *Inorg. Chim. Acta* **2000**, *307*, 88.

(30) Nock, B. A.; Maina, T.; Yannoukakos, D.; Pirmettis, I. C.; Papadopoulos, M. S.; Chiotellis, E. *J. Med. Chem.* **1999**, *42*, 1066.

(31) Soobramoney, L.; Bala, M. D.; Friedrich, H. B. *Dalton Trans.* **2014**, *43*, 15968.

(32) Teixidor, F.; Escriche, L.; Casabo, J.; Molins, E.; Miravitlles, C. *Inorg. Chem.* **1986**, *25*, 4060.

(33) Canovese, L.; Chessa, G.; Marangoni, G.; Pitteri, B.; Uguagliati, P.; Visentin, F. *Inorg. Chim. Acta* **1991**, *186*, 79.

(34) Teixidor, F.; Sanchez-Castello, G.; Lucena, N.; Escriche, L.; Kivekas, R.; Sundberg, M.; Casabo, J. *Inorg. Chem.* **1991**, *30*, 4931.

(35) Konrad, M.; Meyer, F.; Heinze, K.; Zsolnai, L. *J. Chem. Soc., Dalton Trans.* **1998**, 199.

(36) Spasyuk, D.; Smith, S.; Gusev, D. G. *Angew. Chem. Int. Ed.* **2013**, *52*, 2538.

(37) Golding, B. T.; Kebbell, M. J.; Lockhart, I. M. *J. Chem. Soc., Perkin Trans. 2* **1987**, 705.

(38) Park, C. S.; Lee, J. Y.; Kang, E.-J.; Lee, J.-E.; Lee, S. S. *Tetrahedron Lett.* **2009**, *50*, 671.

(39) Furniss, B. S.; Hannaford, A. J.; Smith, P. W. G.; Tatchell, A. R. *Vogel's textbook of practical organic chemistry*; 5th ed.; J. Wiley and sons: New York, 1989.

(40) Tyree, S. Y. In *Inorg. Synth.*; John Wiley & Sons, Inc.: 1953; Vol. 4, p 104.

(41) SAINT Version 7.60a, Bruker AXS Inc., Madison, WI, USA, 2006.

(42) G. M. Sheldrick, SHELXS-97, SHELXL-2014 and SADABS version 2.05, University of Göttingen, Germany, 1997.

(43) Barbour, L. J. *Supramol. Chem.* **2001**, *1*, 189.

(44) Atwood, J. L. and Barbour, L. J. *Cryst. Growth Des.* **2003**, *3*, 3.

(45) Jarvis, J. A. J.; Mais, R. H. B.; Owston, P. G. *J. Chem. Soc. A***1968**, 1473.

(46) Basauri-Molina, M.; Hernández-Ortega, S.; Morales-Morales, D. *Eur. J. Inorg. Chem.* **2014**, *2014*, 4619.

(47) Márquez, V. E.; Anacona, J. R.; Hurtado, R. J.; Díaz de Delgado, G.; Roque, E. M. *Polyhedron* **1999**, *18*, 1903.

(48) Blake, A. J.; Halcrow, M. A.; Schroder, M. *Acta Crystallogr., Sect. C* **1992**, *48*, 1844.

(49) Baker, M. V.; Brown, D. H.; Skelton, B. W.; White, A. H. *Aust. J. Chem.* **2002**, *55*, 655.

(50) Wikstrom, J. P.; Filatov, A. S.; Staples, R. J.; Guifarro, C. R.; Rybak-Akimova, E. V. *Inorg. Chim. Acta* **2010**, *363*, 884.

(51) Shul'pin, G. B. *Mini-Rev. Org. Chem.* **2009**, *6*, 95.

(52) Mac Leod, T. C. O.; Kirillova, M. V.; Pombeiro, A. J. L.; Schiavon, M. A.; Assis, M. D. *Appl. Catal., A* **2010**, *372*, 191.

(53) Kirillova, M. V.; Kirillov, A. M.; Mandelli, D.; Carvalho, W. A.; Pombeiro, A. J. L.; Shul'pin, G. B. *J. Catal.* **2010**, *272*, 9.

(54) Naicker, D.; Friedrich, H. B.; Omondi, B. *RSC Adv.* **2015**, *5*, 63123.

(55) Förster, S.; Rieker, A.; Maruyama, K.; Murata, K.; Nishinaga, A. *J. Org. Chem.* **1996**, *61*, 3320.

(56) Fokin, A. A.; Schreiner, P. R. *Chem. Rev.* **2002**, *102*, 1551.

CHAPTER THREE

Flexible pincer backbone revisited: the case of CuSNS complexes as efficient catalysts in paraffin oxidation

3.1 Summary

New SNS ligands based on a flexible, straight chain amine backbone have been prepared and coordinated to copper to yield new SNS pincer-type complexes. The complexes were fully characterised by IR, HRMS, elemental analysis and single crystal X-ray diffraction. These are Cu[bis(Rthioethyl)methylamine]Cl_2 (**2.1)** and Cu[bis(Rthioethyl)phenylamine]Cl_2 (**2.2**) where R = methyl, **a**; ethyl, **b**; butyl, **c**; cyclohexyl, **d** and *t*-butyl, **e**. Crystal structures of these complexes exhibited a five-coordinate geometry around each Cu(II) centre with the exception of **2.2b**, which crystallised as a dimer bridged through a cuprate anion. All ten copper complexes were applied as catalysts in the oxidation of *n*-octane using TBHP and H_2O_2 as oxidants. A product yield of ca. 15% C-8 oxygenates was obtained for all the catalysts tested using TBHP, which was equivalent to that obtained for uncomplexed $CuCl_2$ as the catalyst. However, the H_2O_2 systems with catalysts in series **2.2** gave significantly higher yields in comparison to the simple copper salt, with **2.2d** producing the highest yield of 57% in 1 h. Additionally, high turnover numbers (2270-3180) were obtained for the **2.2**/H_2O_2 system with substantial selectivity of 22-27% to the terminal (C(1)) products. The high activity of catalyst series **2.2** was attributed to a reactive copper-peroxo intermediate.

3.2 Introduction

The oxidation of saturated alkanes is an important yet challenging field of scientific research. These compounds are relatively inert but are abundantly present as by-products of petroleum and oil refining industries.[1,2] The immense amount of effort invested in the transformation of these unreactive substrates into more reactive and/or valuable products over the last few decades has indeed been remarkable.[3-21] However, the development of economically viable catalysts which are capable of functioning under mild reaction conditions, with exceptional activities and selectivities, remains a difficult task.

Inspiration for this project has been drawn from biological catalysts, such as the monooxygenases, which possess extraordinary activity in the mild oxidation of alkane substrates.[22-26] More specifically, copper containing enzymes have displayed interesting catalytic activity[27] and this has been one of the sources of motivation to explore homogeneous copper catalysts for alkane oxidation.

This work has expounded upon previous studies in which SNS pincer ligands were incorporated with other relatively cheap metals for the oxidation of *n*-octane which achieved promising results.[28] The SNS ligand system was specifically chosen because of its hemilable, chelating and flexible properties, all of which are key features for developing new effective catalysts.
In this study, the synthesis, characterisation and coordination chemistry of ten new CuSNS complexes (Fig. 3.1) is reported. Also reported, is their application in the oxidation of *n*-octane using *t*-butyl hydroperoxide (TBHP) and H_2O_2 as oxidants.

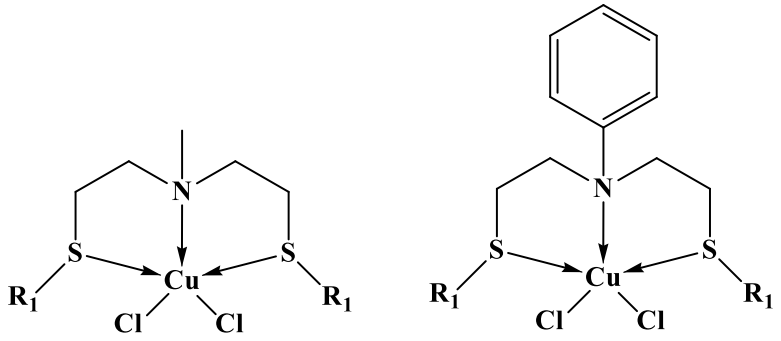

2.1 **2.2**

Figure 3.1: General representation of the two series of CuSNS complexes **2.1** and **2.2** where R_1 = methyl (**a**), ethyl (**b**), butyl (**c**), cyclohexyl (**d**) and *t*-butyl (**e**).

3.3 Experimental Section

3.3.1 General

An inert nitrogen atmosphere was employed for the synthesis of the ligands and complexes. All solvents were dried according to reported methods[29] and dissolved oxygen was expelled by purging with high purity nitrogen gas prior to use. Diethyl ether (Et_2O) and tetrahydrofuran (THF) were dried over sodium wire and benzophenone, absolute ethanol (EtOH) and methanol (MeOH) were dried over magnesium turnings and iodine, and dichloromethane (DCM) was dried over phosphorous pentoxide. All other reagents were purchased commercially and used as received. All NMR spectra were recorded using a Bruker Avance III 400 MHz spectrometer at ambient temperature. The ^{1}H NMR data are reported as chemical shift (δ, ppm) and referenced to the solvent peak $CDCl_3$. The proton decoupled ^{13}C NMR data are presented as chemical shift (δ, ppm) and referenced to the solvent peak $CDCl_3$ with the specific carbon indicated in parentheses. The ^{13}C APT NMR data, which distinguishes between quaternary C, CH, CH_2 and CH_3 carbons, are listed as chemical shift (δ, ppm) and positive (pos) or negative (neg) with the corresponding carbons in parentheses. The IR spectra were recorded on a Perkin Elmer Attenuated Total Reflectance (ATR) spectrophotometer and elemental analyses were performed on a Thermo-Scientific Flash 2000 CHNS/O elemental analyzer, the HRMS was recorded on a Waters Micromass LCT Premier TOF-MS, while the melting points were determined using a Stuart Scientific melting point apparatus. Ligands **L1** (**a**-**c**) and **L2** (**a**, **b**, **d**) were synthesized according to the protocols described in Chapter 2, Section 2.3.2.

3.3.2 Synthesis and characterisation of ligands and complexes

bis(Cyclohexylthioethyl)methylamine (L1d). This ligand was synthesized similarly to **L1b** (Chapter 2, Section 2.3.2), with the following masses and volumes: bis(2-chloroethyl)methylamine (3.454 g, 22.1 mmol), sodium metal (1.527 g, 66.4 mmol) and cyclohexanethiol (8.1 ml, 66.4 mmol). The cream residue obtained after evacuation of the solvent was purified on a silica column, first with hexane to remove to excess starting material and then

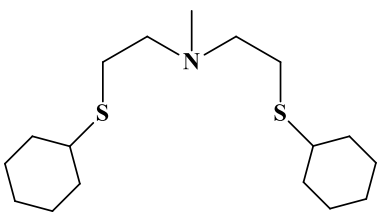

with 5% MeOH in DCM to elute the product, which was isolated as a pale yellow oil. Yield: 84%. ^{1}H NMR (400 MHz, $CDCl_3$): δ 1.19-1.31 (m, 12H, C_6H_{12}-S), 1.73 (m, 4H, C_6H_{12}-S), 1.93 (m, 4H, C_6H_{12}-S), 2.25 (s, 3H, C*H*$_3$-N), 2.55-2.63 (m, 10H, C_6H_{12}-S, C*H*$_2$C*H*$_2$-N). ^{13}C APT NMR (400 MHz, $CDCl_3$): δ 25.83 (C_6H_{12}-S) pos, 26.09 (C_6H_{12}-S) pos, 27.68 (*C*H$_2$CH$_2$-N) pos, 33.78 (C_6H_{12}-S) pos, 42.09 (C_6H_{12}-S) neg, 43.72 (*C*H$_3$-N) neg, 57.76 (CH$_2$*C*H$_2$-N) pos. HRMS ESI (*m/z*) Calcd for: $C_{17}H_{33}NS_2Na$ = 338.1952. Found: 338.1949. IR ν_{max} (cm^{-1}): 2924 (s), 2850 (m), 2788 (w), 1447 (s), 999 (m), 745 (w).

bis(*t*-Butylthioethyl)methylamine (L1e). This ligand was synthesized and purified similarly to

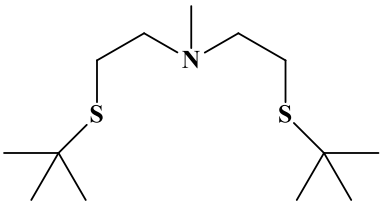

L1b (Chapter 2, Section 2.3.2), with the following masses and volumes: bis(2-chloroethyl)methylamine (1.163 g, 7.5 mmol), sodium metal (0.539 g, 23.4 mmol) and *tert*-butylthiol, (2.6 ml, 23.4 mmol). The product was isolated as an orange oil. Yield: 80%. ^{1}H NMR (400 MHz, $CDCl_3$): δ 1.33 (s, 18H, C_4H_9-S), 2.32 (s, 3H, C*H*$_3$-N), 2.63 (m, 8H, C*H*$_2$C*H*$_2$-N). ^{13}C APT NMR (400 MHz, $CDCl_3$): δ 26.00 (*C*H$_2$CH$_2$-N) pos, 31.01 (*C*$_4$H$_9$-S) neg, 41.97 (*C*$_4$H$_9$-S) pos, 42.07 (*C*H$_3$-N) neg, 57.53 (CH$_2$*C*H$_2$-N) pos. HRMS ESI (*m/z*) Calcd for: $C_{13}H_{29}NS_2Na$ = 286.1639. Found: 286.1637. IR ν_{max} (cm^{-1}): 2959 (s), 2899 (w), 2862 (w), 2790 (w), 1458 (s), 1363 (s), 1162 (s), 1055 (m), 750 (w).

bis(Butylthioethyl)phenylamine (L2c). This ligand was synthesized analogously to **L2b**

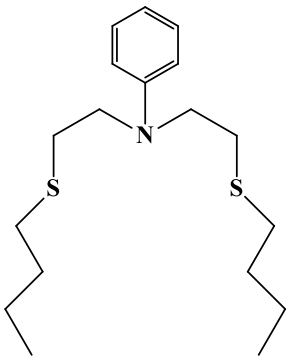

(Chapter 2, Section 2.3.2), with the following masses and volumes: bis(2-tosylethyl)phenylamine (1.559 g, 3.19 mmol), sodium metal (0.230 g, 9.56 mmol) and butanethiol (1.0 ml, 9.56 mmol). The crude oil was purified on a silica gel column similarly to **L1d** to elute the product as a yellow oil. Yield: 96%. ^{1}H NMR (400 MHz, $CDCl_3$): δ 0.96 (t, 6H, C*H*$_3$CH$_2$CH$_2$CH$_2$-S), 1.45 (m, 4H, CH$_3$C*H*$_2$CH$_2$CH$_2$-S), 1.62 (m, 4H, CH$_3$CH$_2$C*H*$_2$CH$_2$-S), 2.61 (t, 4H, CH$_3$CH$_2$CH$_2$C*H*$_2$-S), 2.73 (t, 4H, C*H*$_2$CH$_2$-N), 3.56 (t, 4H, CH$_2$C*H*$_2$-N), 6.69 (d, 2H, Ph-N), 6.73 (t, 1H, Ph-N), 7.26 (t, 2H, Ph-N). ^{13}C APT NMR (400 MHz, $CDCl_3$): δ 13.71 (*C*H$_3$CH$_2$CH$_2$CH$_2$-S) neg, 22.00 (CH$_3$*C*H$_2$CH$_2$CH$_2$-S) pos, 29.28 (*C*H$_2$CH$_2$-N) pos, 31.98 (CH$_3$CH$_2$*C*H$_2$CH$_2$-S) pos, 32.12 (CH$_3$CH$_2$CH$_2$*C*H$_2$-S) pos, 51.55 (CH$_2$*C*H$_2$-N) pos, 111.80 (Ph-N) neg , 116.56 (Ph-N) neg , 129.54 (Ph-N) neg, 146.80 (Ph-N) pos. HRMS ESI (*m/z*) Calcd for: $C_{18}H_{32}NS_2$ = 326.1976. Found: 326.1971. IR ν_{max} (cm^{-1}): 2956 (m), 2927 (m), 2872 (w), 2789 (w), 1458 (s), 1053 (m), 745 (m).

bis(*t*-Butylthioethyl)phenylamine (L2e). This ligand was synthesized using the same procedure as for **L2b** (Chapter 2, Section 2.3.2), with the following masses and volumes: bis(2-tosylethyl)phenylamine (2.984 g, 6.10 mmol), sodium (0.420 g, 18.30 mmol) and *t*-butanethiol (2.06 ml, 18.30 mmol). The product was obtained as a yellow oil. Yield: 83%. ^{1}H NMR (400 MHz, $CDCl_3$): δ 1.37 (s, 18H, C_4H_9-S), 2.76 (t, 4H, CH_2CH_2-N), 3.52 (t, 4H, CH_2CH_2-N), 6.71 (m, 3H, Ph-N), 7.27 (t, 2H, Ph-N). ^{13}C APT NMR (400 MHz, $CDCl_3$): δ 25.71 (CH_2CH_2-N) pos, 31.31 (C_4H_9-S) neg, 42.30 (C_4H_9-S) pos, 51.63 (CH_2CH_2-N) pos, 111.76 (Ph-N) neg, 116.32 (Ph-N) neg, 129.59 (Ph-N) neg. HRMS ESI (*m/z*) Calcd for: $C_{18}H_{32}NS_2$ = 326.1976. Found: 326.1983. IR ν_{max} (cm^{-1}): 2959 (s), 2862 (w), 1598 (s), 1503 (s), 1458 (m), 1363 (m), 1160 (m), 745 (s), 691 (s).

Cu[bis(methylthioethyl)methylamine] (2.1a). A solution of **L1a** (0.1759 g, 0.98 mmol) in 4 ml of MeOH was added to a light green MeOH solution (4 ml) of $CuCl_2.2H_2O$ (0.1672 g, 0.98 mmol). Immediately a colour change from light to dark green was observed and a green precipitate began to form. The reaction mixture was allowed to stir at room temperature for 2 h, after which the volume was reduced to ~2 ml and filtered via cannula. The precipitate was washed several times with 3 ml portions of Et_2O and dried to yield a green microcrystalline solid. Single crystals suitable for X-ray diffraction were grown from the mother liquor. Yield: 71%. Melting point: 133-134 °C. HRMS ESI (*m/z*) Calcd for: $C_7H_{17}NS_2Cu$ = 242.0098. Found = 242.0094. IR ν_{max} (cm^{-1}): 2991 (w), 2963 (w), 2916 (m), 2857 (w), 2808 (w), 1472 (m), 1441 (s), 1424 (s), 1231 (m), 1085 (m), 741 (s). Anal. (%) calc. for $C_7H_{17}NS_2CuCl_2$: C, 26.8; H, 5.5; N, 4.5; found: C, 26.8; H, 5.6; N, 4.5.

Cu[bis(ethylthioethyl)methylamine] (2.1b). This complex was synthesized analogously to **2.1a** with the following masses: **L1b** (0.142 g, 0.69 mmol) and $CuCl_2.2H_2O$ (0.1167 g, 0.69 mmol). A colour change from light to dark green was observed, however, no precipitate formed, and therefore the reaction was left to stir overnight at room temperature. The solution was concentrated and Et_2O was added, giving a green oil. After decanting the liquid, the oil was extracted with DCM and hexane. Upon, a dark green crystalline solid was obtained. Single crystals suitable for analysis were grown by slow diffusion of Et_2O into a

concentrated MeOH solution of **2.1b**. Yield: 64%. Melting point: 118-119 °C. HRMS ESI (*m/z*) Calcd for: $C_9H_{21}NS_2Cu$ = 270.0411. Found = 269.9984. IR ν_{max} (cm^{-1}): 2961 (w), 2924 (w), 2866 (m), 1472 (w), 1446 (s), 1423 (m), 1380 (m), 1231 (m), 1086 (m), 735 (s). Anal. (%) calc. for $C_9H_{21}NS_2CuCl_2$: C, 31.6; H, 6.2; N, 4.1; found: C, 31.6; H, 6.3; N, 4.1.

Cu[bis(butylthioethyl)methylamine] (2.1c). A similar procedure as for **2.1b** was followed to obtain **2.1c** with the following masses: **L1c** (0.232 g, 0.88 mmol) and $CuCl_2.2H_2O$ (0.147 g, 0.86 mmol). A similar colour change as the previous reactions was observed and the reaction solution was evacuated to dryness after stirring overnight. The resultant green residue was washed with Et_2O, taken up in 3 ml of DCM and the product precipitated as a green powder upon the addition of 2 ml of Et_2O. The filtrate was removed by cannula and the solid was washed several times with Et_2O and dried under vacuum to afford a bright green powder. Single crystals suitable for analysis were grown from a solution of **2.1c** in DCM layered with Et_2O. Yield: 81%. Melting point: 101-103 °C. HRMS ESI (*m/z*) Calcd for: $C_{13}H_{29}NS_2Cu$ = 326.1037. Found = 326.0524. IR ν_{max} (cm^{-1}): 2958 (w), 2930 (m), 2871 (m), 1463 (s), 1426 (m), 1224 (m), 1043 (m), 736 (s). Anal. (%) calc. for $C_{13}H_{29}NS_2CuCl_2$: C, 39.2; H, 7.4; N, 3.5; found: C, 39.2; H, 7.6; N, 3.6.

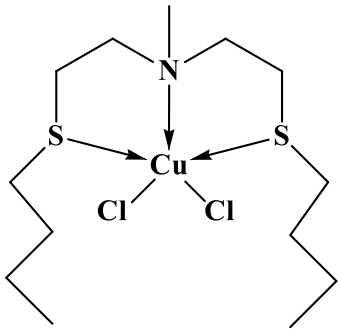

Cu[bis(cyclohexylthioethyl)methylamine] (2.1d). A similar procedure as for complex **2.1b** was adapted to synthesize complex **2.1d** with the following masses: **L1d** (0.210 g, 0.67 mmol) and $CuCl_2.2H_2O$ (0.112 g, 0.66 mmol). The solution was concentrated to 1 ml and stirred in 10 ml of Et_2O overnight. A dark green solid was obtained, which was washed with several portions of Et_2O and dried *in vacuo*. Single crystals were grown from a MeOH solution layered with heptane. Yield: 92%. Melting point: 120-121 °C. HRMS ESI (*m/z*) Calcd for: $C_{17}H_{33}NS_2Cu$ = 378.1350. Found = 378.0914. IR ν_{max} (cm^{-1}): 2922 (s), 2850 (m), 1447 (s), 1265 (m), 1042 (w), 732 (m). Anal. (%) calc. for $C_{17}H_{33}NS_2CuCl_2$: C, 45.4; H, 7.4; N, 3.1; found: C, 45.4; H, 7.3; N, 2.8.

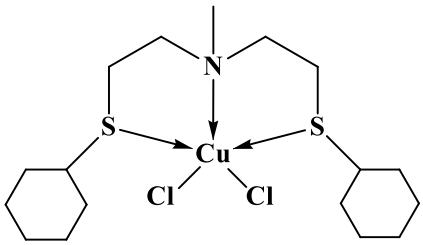

Cu[bis(*t*-butylthioethyl)methylamine] (2.1e). A similar procedure as for **2.1a** was adapted to synthesize **2.1e** with the following masses: **L1e** (0.140 g, 0.53 mmol) and $CuCl_2.2H_2O$ (0.090 g, 0.53 mmol). A precipitate formed within a few minutes, however, the reaction mixture was allowed to stir at room temperature for a further 2 h, after which the mixture was concentrated to ~3 ml and filtered via cannula. The precipitate was washed several times with 3 ml portions of Et_2O and dried to yield a lime green powder. Single crystals suitable for X-ray diffraction were grown from a DCM solution of **2.1e** layered with Et_2O. Yield: 73%. Melting point: 118-119 °C. HRMS ESI (*m/z*) Calcd for: $C_{13}H_{29}NS_2Cu$ = 326.1037. Found = 326.1037. IR ν_{max} (cm^{-1}): 2956 (w), 2862 (m), 1461 (m), 1363 (m), 1209 (m), 1163 (s), 998 (m), 745 (m). Anal. (%) calc. for $C_{13}H_{29}NS_2CuCl_2$: C, 39.2; H, 7.4; N, 3.5; found: C, 39.0; H, 7.3; N, 3.2.

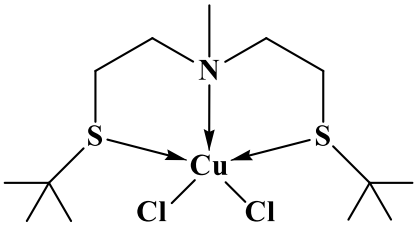

Cu[bis(methylthioethyl)phenylamine] (2.2a). A solution of **L2a** (0.142 g, 0.589 mmol) in 5 ml of EtOH was added to a light green EtOH solution (5 ml) of $CuCl_2.2H_2O$ (0.100 g, 0.587 mmol). Immediately a colour change from light to dark green was observed and a green precipitate began to form. The reaction mixture was allowed to stir at room temperature for 2 h, after which the volume was reduced to ~2 ml and filtered via cannula. The precipitate was washed several times with 3 ml portions of Et_2O and dried to yield a green solid. Single crystals suitable for X-ray diffraction were grown from a DCM solution of **2.2a** layered with Et_2O. Yield: 74%. Melting point: 102-103 °C. HRMS ESI (*m/z*) Calcd for: $C_{12}H_{19}NS_2Cu$ = 304.0255. Found = 304.0253. IR ν_{max} (cm^{-1}): 3049 (w), 3028 (w), 2985 (w), 2921 (w), 1597 (m), 1497 (s), 1462 (s), 1348 (m), 956 (s), 741 (s). Anal. (%) calc. for $C_{12}H_{19}NS_2CuCl_2$: C, 38.4; H, 5.1; N, 3.7; found: C, 38.2; H, 5.1; N, 3.6.

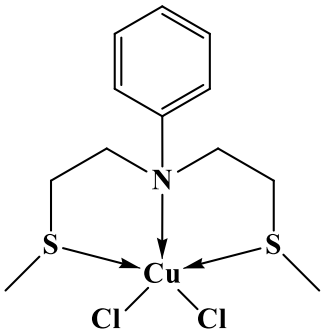

Cu[bis(ethylthioethyl)phenylamine] (2.2b). This complex was synthesized similarly to **2.2a** with the following masses: **L2b** (0.102 g, 0.379 mmol) and $CuCl_2.2H_2O$ (0.063 g, 0.370 mmol). The resultant dark green solution was allowed to stir overnight, after which the solvent was reduced to ~1 ml and upon the addition of 10 ml of Et_2O a green solid precipitated. This solid was recrystallized from DCM and Et_2O and single crystals were also obtained using the same solvent system. Yield: 73%. Melting point: 80-82 °C. HRMS ESI (*m/z*) Calcd for: $C_{14}H_{22}NS_2Cu$ = 332.0568. Found = 332.0560. IR ν_{max} (cm^{-1}): 3045 (w), 3023 (w), 2967 (w), 2928 (w), 2869 (w), 1594 (s), 1496 (s), 1450 (s), 1343 (m), 980 (m), 762 (s), 728 (m) 697 (s). Anal. (%) calc. for $C_{14}H_{23}NS_2CuCl_2$: C, 41.6; H, 5.7; N, 3.5; found: C, 41.7; H, 5.6; N, 3.0.

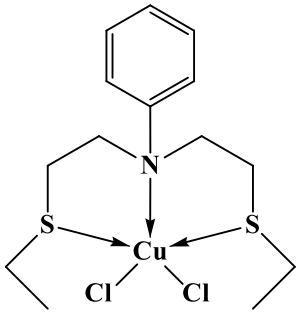

Cu[bis(butylthioethyl)phenylamine] (2.2c). This complex was synthesized using the same protocol as for complex **2.2a** with the following masses: **L2c** (0.141 g, 0.433 mmol) and $CuCl_2.2H_2O$ (0.073 g, 0.428 mmol). Single crystals were obtained from a DCM solution layered with Et_2O. Yield: 31%. Melting point: 77-78 °C. HRMS ESI (*m/z*) Calcd for: $C_{18}H_{31}NS_2Cu$ = 388.1194. Found = 388.1190. IR ν_{max} (cm^{-1}): 3032 (w), 2959 (m), 2934 (m), 2869 (m), 1593 (m), 1491 (s), 1459 (s), 1215 (m), 784 (s), 704 (s). Anal. (%) calc. for $C_{18}H_{31}NS_2CuCl_2$: C, 47.0; H, 6.8; N, 3.0; found: C, 46.8; H, 6.7; N, 2.8.

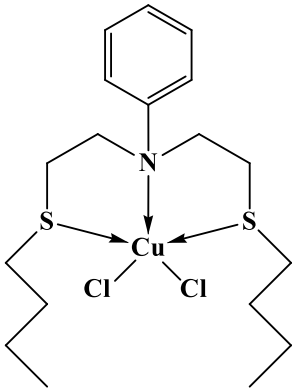

Cu[bis(cyclohexylthioethyl)phenylamine] (2.2d). This complex was synthesized similarly to **2.2a** with the following masses: **L2d** (0.126 g, 0.334 mmol) and $CuCl_2.2H_2O$ (0.057 g, 0.333 mmol). Single crystals were obtained by slow evaporation of a DCM solution layered with Et_2O. Yield: 68%. Melting point: 118-119 °C. HRMS ESI (*m/z*) Calcd for: $C_{22}H_{35}NS_2Cu$ = 440.1507. Found = 440.1501. IR ν_{max} (cm^{-1}): 3066 (w), 3041 (w), 2994 (w), 2921 (s), 2848 (m), 1595 (m), 1490 (s), 1463 (m), 1446 (s), 991 (s), 696 (s). Anal. (%) calc. for $C_{22}H_{35}NS_2CuCl_2$: C, 51.6; H, 6.9; N, 2.7; found: C, 51.6; H, 6.9; N, 2.4.

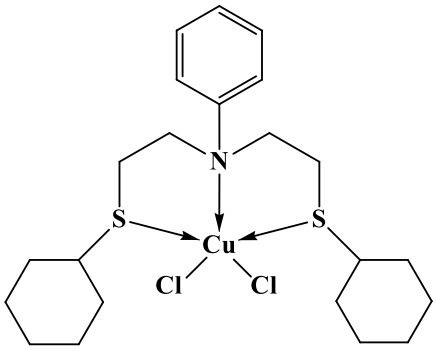

Cu[bis(*t*-butylthioethyl)phenylamine] (2.2e). A solution of **L2e** (0.124 g, 0.381 mmol) in 3 ml of DCM was added to a suspension of $CuCl_2.2H_2O$ (0.063 g, 0.370 mmol) in DCM to yield an orange-brown solution, which was allowed to stir at room temperature overnight. Thereafter the solvent was evacuated and the residue was stirred in 10 ml of Et_2O. The solid that formed was collected by cannula filtration and washed with Et_2O to isolate the product as a pale olive green powder. Yield: 68%. Decomposes > 126 °C. HRMS ESI (*m/z*) Calcd for: $C_{18}H_{31}NS_2Cu$ = 388.1194. Found = 388.1188. IR ν_{max} (cm^{-1}): 3053 (w), 2962 (w), 2644 (w), 2502 (w), 2426 (w), 1597 (m), 1495 (m), 1487 (s), 1455 (s), 1368 (s), 758 (s), 695 (s). Anal. (%) calc. for $C_{18}H_{31}NS_2CuCl_2$: C, 47.0; H, 6.8; N, 3.0; found: C, 46.8; H, 6.7; N, 2.8.

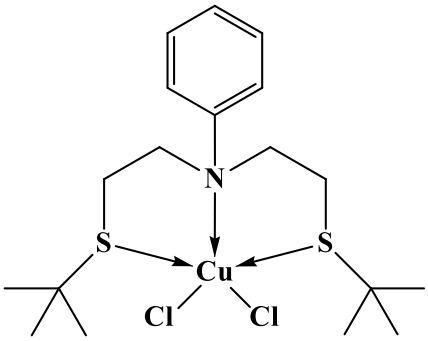

3.3.3 Crystallographic analyses

Single crystals for each complex were individually selected and glued onto the tip of a glass fiber, mounted in a stream of cold nitrogen and centered in the X-ray beam by using a video camera. Single-crystal X-ray diffraction data were collected on a Bruker KAPPA APEX II DUO diffractometer using graphite-monochromated Mo-Kα radiation (χ = 0.71073 Å). Data collection was carried out at 173(2) or 100(2) K. Temperature was controlled by an Oxford Cryostream cooling system (Oxford Cryostat). Cell refinement and data reduction were performed using the program *SAINT*.[30] The data were scaled and absorption correction performed using *SADABS*.[31] The structure was solved by direct methods using *SHELXS*[31] and refined by full-matrix least-squares methods based on F^2 using *SHELXL*[31] and using the graphics interface program *X-Seed*[32,33]. All non-hydrogen atoms were refined anisotropically. All hydrogen atoms were placed in idealised positions and refined in riding models with U_{iso} assigned 1.2 or 1.5 times U_{eq} of their parent atoms and the bond distances were constrained to 0.98 or 0.99 Å. Selected crystallographic and structural refinement data are presented in Tables 3.1 and 3.2.

Table 3.1: Selected crystallographic and structure refinement data for complexes and **2.1a-2.1e**.

	2.1a	**2.1b**	**2.1c**	**2.1d**	**2.1e**
Empirical formula	$C_7H_{17}Cl_2CuNS_2$	$C_9H_{21}Cl_2CuNS_2$	$C_{13}H_{29}Cl_2CuNS_2$	$C_{17}H_{33}Cl_2CuNS_2$	$C_{13}H_{27}Cl_2CuNS_2$
Formula weight	313.78	341.85	397.96	449.86	395.92
Temperature (K)	100(2)	173(2)	100(2)	100(2)	100(2)
Crystal system	Monoclinic	Monoclinic	Triclinic	Orthorhombic	Monoclinic
Space group	$P2_1/n$	$P2_1/n$	$P\bar{1}$	$Pbca$	$P2_1/c$
a (Å)	7.7103(4)	12.8374(4)	8.58240(10)	12.1895(6)	13.573(19)
b (Å)	12.1139(7)	14.2641(5)	14.5582(2)	21.8132(10)	9.761(14)
c (Å)	13.6506(8)	16.1896(3)	15.4678(2)	31.6331(14)	15.10(2)
α (°)	90	90	105.5750(10)	90	90
β (°)	101.201(2)	91.293(2)	98.6340(10)	90	110.564(14)
γ (°)	90	90	96.7680(10)	90	90
Volume ($Å^3$)	1250.70(12)	2963.79(15)	1814.99(4)	8411.0(7)	1874.(7)
Z	4	4	4	16	4
ρ_{calc} (g/cm^3)	1.666	1.532	1.353	1.4209	1.415
μ (mm^{-1})	2.466	2.088	1.712	1.491	1.676
F(000)	644	1416.0	724.0	3803.9	828
Crystal size (mm^3)	0.270 x 0.340 x 0.640	0.210 × 0.140 × 0.090	0.203 × 0.175 × 0.100	0.844 × 0.656 × 0.42	0.078 x 0.092 x 0.246
2Θ range for data collection (°)	2.27 to 28.40	7.616 to 55.758	4.6 to 57.22	2.58 to 50.74	2.54 to 28.38
Index ranges	$-10\leq h\leq10$, $-16\leq k\leq15$, $-17\leq l\leq18$	$-16\leq h\leq16$, $-18\leq k\leq18$, $-21\leq l\leq21$	$-11\leq h\leq11$, $-19\leq k\leq19$, $-20\leq l\leq20$	$-14\leq h\leq14$, $-26\leq k\leq26$, $-37\leq l\leq38$	$-20\leq h\leq19$, $-12\leq k\leq13$, $-17\leq l\leq17$
Reflections collected	28014	164198	34856	170453	29195
Independent reflections	3117 [R(int) = 0.0237]	7054 [R(int) = 0.0604]	9199 [R(int) = 0.0181]	7720 [R(int) = 0.0808]	4604 [R(int) = 0.0271]
Data / restraints parameters	3117 / 0 / 121	7054 / 0 / 277	9199 / 0 / 349	7720 / 0 / 432	4604 / 0 / 179
Goodness-of-fit on F^2	1.226	1.108	1.071	1.069	1.077
Final R indices [$I>=2\sigma(I)$]	R1 = 0.0199, wR2 = 0.0568	R1 = 0.0289, wR2 = 0.0575	R1 = 0.0335, wR2 = 0.1291	R1 = 0.0408, wR2 = 0.0856	R1 = 0.0292, wR2 = 0.0714
Final R indices (all data)	R1 = 0.0203, wR2 = 0.0570	R1 = 0.0450, wR2 = 0.0638	R1 = 0.0366, wR2 = 0.1351	R1 = 0.0642, wR2 = 0.0989	R1 = 0.0335, wR2 = 0.0734
Largest diff. peak and hole ($e.Å^{-3}$)	0.409 and -0.771	0.54 and -0.38	3.05 and -1.16	0.82 and -0.62	2.064 and -0.412

Table 3.2: Selected crystallographic and structure refinement data for ligand **L1e** and complexes and **2.2a-2.2d**.

	L1e	**2.2a**	**2.2b**	**2.2c**	**2.2d**
Empirical formula	$C_{13}H_{30}BrNS_2$	$C_{16}H_{20}Cl_2CuNS_2$	$C_{28}H_{46}Cl_6Cu_3NS_4$	$C_{18}H_{31}Cl_2CuNS_2$	$C_{22}H_{35}Cl_2CuNS_2$
Formula weight	344.41	424.89	942.26	460.00	512.07
Temperature (K)	100(2)	100(2)	100(2)	100(2)	100(2)
Crystal system	Orthorhombic	Monoclinic	Triclinic	Orthorhombic	Monoclinic
Space group	$P2_12_12$	$P2_1/n$	$P\bar{1}$	$P2_12_12_1$	$P2_1/c$
a (Å)	10.1665(15)	7.63300(10)	9.4138(3)	9.9707(3)	12.1308(2)
b (Å)	27.674(4)	12.5026(2)	14.6457(5)	13.7074(4)	13.1137(2)
c (Å)	6.3937(9)	8.27820(10)	15.5502(5)	15.5277(4)	15.9077(3)
α (°)	90	90	67.032(2)	90	90
β (°)	90	100.0090(10)	78.754(2)	90	110.5430(10)
γ (°)	90	90	89.949(2)	90	90
Volume (Å^3)	1798.9(4)	777.984(19)	1929.34(11)	2122.21(10)	2369.67(7)
Z	4	2	2	4	4
ρ_{calc} (g/cm^3)	1.272	1.814	1.622	1.440	1.435
μ (mm^{-1})	2.502	2.009	2.294	1.479	1.333
F(000)	728	436	962	964	1076
Crystal size (mm^3)	0.290 × 0.180 × 0.140	0.222 x 0.383 x 0.410	0.279 x 0.220 x 0.070	0.150 x 0.130 x 0.090	0.357 x 0.187 x 0.143
2Θ range for data collection (°)	2.134 to 28.289	2.71 to 28.41	1.515 to 28.402	1.982 to 28.315	1.793 to 28.512
Index ranges	-11 ≤ h ≤ 13, -18 ≤ k ≤ 36, -8 ≤ l ≤ 5	-10<=h<=10, -16<=k<=16, -11<=l<=11	-12<=h<=12, -19<=k<=19, -20<=l<=20	-11<=h<=13, -18<=k<=17, -20<=l<=18	-16<=h<=15, -17<=k<=17, -20<=l<=17
Reflections collected	8366	14230	59437	17385	34017
Independent reflections	3932 [R(int) = 0.0240]	3687 [R(int) = 0.0532]	9531 [R(int) = 0.0348]	4944 [R(int) = 0.0375]	5903 [R(int) = 0.0153]
Data / restraints parameters	3932 / 0 / 155	3687 / 1 / 165	9531 / 0 / 388	4944 / 0 / 220	5903 / 0 / 253
Goodness-of-fit on F^2	1.049	1.003	1.173	1.014	1.064
Final R indices [I >=2σ (I)]	R1 = 0.0273, wR2 = 0.0532	R1 = 0.0127, wR2 = 0.0295	R1 = 0.0418, wR2 = 0.1005	R1 = 0.0303, wR2 = 0.0593	R1 = 0.0187, wR2 = 0.0487
Final R indices (all data)	R1 = 0.0317, wR2 = 0.0549	R1 = 0.0488, wR2 = 0.0300	R1 = 0.0510, wR2 = 0.1039	R1 = 0.0381, wR2 = 0.0614	R1 = 0.0203, wR2 = 0.0495
Largest diff. peak and hole (e.Å^{-3})	0.427 and -0.685	0.250 and -0.191	1.907 and -0.546	0.542 and -0.346	0.391 d -0.267

3.3.4 Alkane oxidation studies

A PerkinElmer Auto System gas chromatograph was utilised to analyse the products which was equipped with a flame ionisation detector (FID) set at 260 °C. A Pona column (50 m x 0.20 mm x 0.5µm) was employed for the separation the products with the injector temperature set at 240 °C. All catalytic reactions were carried out in duplicate in 25 ml two-neck pear shaped flasks into which the reaction components were added and connected to a reflux condenser. Acetonitrile was employed as the solvent, while cyclopentanone and *n*-octane was used as the internal standard and paraffin substrate respectively.

Two different oxidants were investigated i.e. *t*-butyl hydroperoxide (TBHP) and H_2O_2. Furthermore, the total volume of the reaction mixture was kept constant at 5 ml. The catalyst was introduced in the form of a stock solution so that the no. of moles of catalyst remained constant at 9.56×10^{-6} mol. A catalyst to substrate ratio of 1:100 was utilised, whilst the substrate to oxidant ratio was varied in order to determine the optimum ratio. The optimum reaction times were different for the two oxidant systems. The reaction mixture was stirred in an oil bath maintained at 50 °C, after which an aliquot was removed, treated with an excess amount of PPh_3 and filtered through a silica plug prior to injecting 0.5 µl into the GC for analysis and quantification of the products.

The yield was calculated based on the total moles of product formed divided by the initial moles of substrate added into the reaction mixture and was expressed as a percentage, while the percentage selectivity was expressed as moles of each product divided by the total moles of all products.

3.4 Results and discussion

3.4.1 Synthesis and characterization of complexes

This study reports on the synthesis and characterization of four new SNS ligands and these, along with six previously reported ligands (Chapter 2), were coordinated to copper resulting in the isolation of ten new pincer-type SNS complexes. The two series are separated based on the variation of the ligand backbone i.e. a methyl and phenyl substituent on the central N-donor atom. The general synthetic procedure for the preparation of these complexes involved addition of a solution of the ligand in MeOH to a methanolic solution of $CuCl_2.2H_2O$. The observance of an instantaneous colour change was interpreted as the initial sign of successful complexation to Cu(II). These complexes were characterised by IR, MS, elemental analysis, melting point determination and single crystal XRD.

3.4.2 X-ray crystal structure analyses

It is interesting to note that most of the SNS ligands presented in this study are oils, but an attempted complexation of ligand **L1e** to $Ni(PPh_3)_2Br_2$ in EtOH yielded single crystals that were found to be those of a salt of the 'oily' ligand. The crystals were grown from a solution of the supposed 'Ni complex' in DCM layered with Et_2O. The reason for the formation of this salt may be due to the use of a protic EtOH solvent, which led to the protonation and quarternisation of the ternary N-donor atom of the SNS ligand.

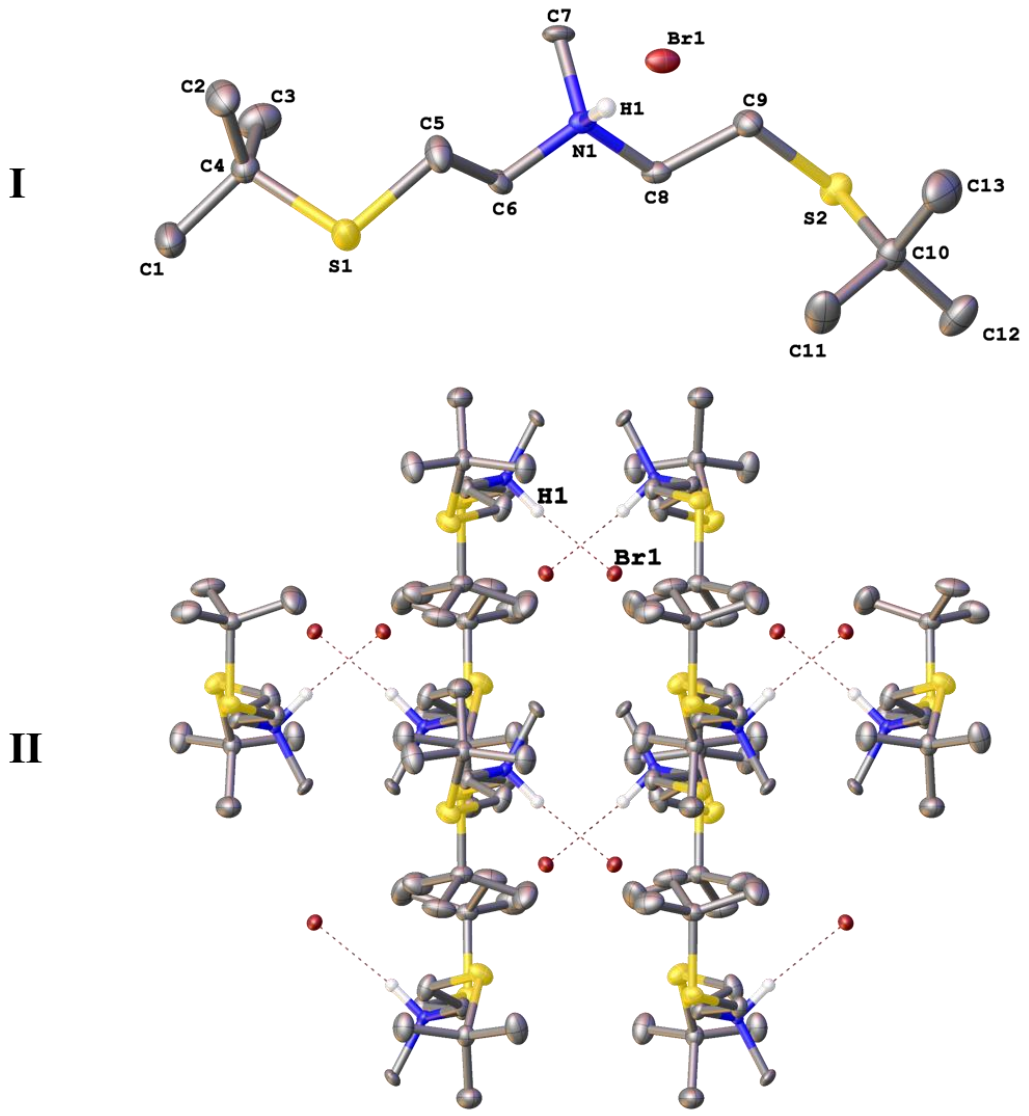

Figure 3.2: Molecular structure (I) and crystal packing viewed along 010 (II) of ligand **L1e** with most hydrogens omitted for clarity and thermal ellipsoids drawn at 50% probability.

From the molecular structure of **L1e** presented in Fig. 3.2, it can be seen that the ethylene linkers [C(5), C(6)] and [C(8), C(9)], and the central atoms defined by [C(7), N(1), H(1) Br(1)] reside in two different planes that are nearly perpendicularly at an angle of 88.5°. The [C(7), N(1), H(1), Br(1)] plane can also be considered as a C_2 rotation axis for the SNS skeletal backbone. Molecules of **L1e** exhibited non-classical hydrogen bonding (N–H···Br) separated by 2.191 Å, which is a relatively strong interaction in comparison to literature reports.[34,35] Furthermore, the N–H···Br

bond angle at 173° is slightly distorted from the ideal 180°. Hence, the crystal packing, (II, Fig. 3.2) viewed along the *b*-axis, shows the intermolecular interactions in which two adjacent molecules are hydrogen bonded (N−H···Br) in an almost perpendicular pattern or array. Selected bond angles and lengths are presented in Appendix A3.

Single crystals of **2.1a** were grown from solution in MeOH, while concentrated solutions of **2.1b**-**2.1e** and **2.2a**-**2.2d** in MeOH or DCM layered with diethyl ether or heptane, yielded dark green crystals. All of the complexes crystallised with a five coordinate, trigonal bipyramidal geometry around the Cu(II) centres with the exception of **2.2b**, which was isolated as a dimer bridged via a $[CuCl_4]^{2-}$ anion. Selected bond lengths and bond angles are listed in Tables 3.3 and 3.4 for complexes in series **2.1** and **2.2** respectively.

ORTEP diagrams of the molecular structures of complexes **2.1a**, **2.1c** and **2.1e**, presented in Fig. 3.3, shows the SNS ligand coordinated in the expected tridentate fashion around each Cu(II) centre. The complexes crystallised in the monoclinic $P2_1/n$, triclinic $P\bar{1}$ and monoclinic $P2_1/c$ space groups. The N-donor and Cl(1) occupy the axial positions, while the three equatorial positions are taken up by the two S-donor atoms and Cl(2). The 'bite angle', which is defined by S(1)−Cu(1)−S(2), is more acute at 109.594(14)° for **2.1a**, whilst opening up for **2.1c** and **2.1e** (112.938(17) and 123.036(17)° respectively).

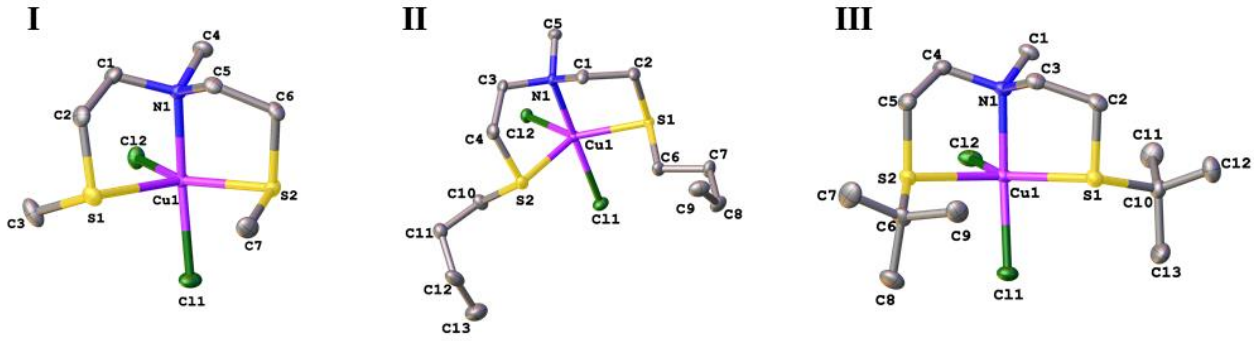

Figure 3.3: Molecular structure of **2.1a** (I), **2.1c** (II) and **2.1e** (III) with hydrogens omitted for clarity. Thermal ellipsoids are drawn at 50% probability level.

The general trend observed is that as the steric nature of the S-donor substituents increased from methyl through to *t*-butyl, the bite angle also increased. This type of steric influence on the bite angle is also evident in related compounds found in the literature.[36-38] The bond lengths corresponding to N(1)−Cu(1), S(1)−Cu(1) and S(2)−Cu(1) are comparable for **2.1a** and **2.1c**, however, for complex **2.1e** the S(1)−Cu(1) bond is slightly shorter at 2.5178(5) Å, whilst a longer S(2)−Cu(1) bond is noted at 2.4027(5) Å. Overall, the S(1)−Cu(1) bond for all three complexes is significantly longer than what has been reported in the literature.[38] Noteworthy, the bond distances for **L1e** and **2.1e** are virtually the same. This indicates that coordination to $CuCl_2$ does not alter the ligand in any significant way

Table 3.3: Selected bond lengths (Å) and bond angles (°) for **2.1a**, **2.1c** and **2.1e**.

Bond lengths (Å)	**2.1a**	**2.1c**	**2.1e**
N(1)−Cu(1)	2.0741(12)	2.0808(16)	2.0781(15)
S(1)−Cu(1)	2.5632(4)	2.5552(5)	2.5178(5)
S(2)−Cu(1)	2.3495(4)	2.3474(5)	2.4027(5)
Cl(1)−Cu(1)	2.2623(4)	2.2637(5)	2.2736(5)
Cl(2)−Cu(1)	2.2968(4)	2.2981(5)	2.2964(5)
Bond angles (°)	**2.1a**	**2.1c**	**2.1e**
S(1)−Cu(1)−S(2)	109.594(14)	112.938(17)	123.036(17)
N(1)−Cu(1)−S(1)	83.99(3)	86.31(4)	85.33(4)
N(1)−Cu(1)−S(2)	86.40(4)	83.31(5)	83.73(4)
N(1)−Cu(1)−Cl(1)	172.19(4)	170.61(5)	170.77(4)
N(1)−Cu(1)−Cl(2)	93.52(3)	92.41(5)	92.54(4)

Complex **2.1b** crystallises with two crystallographically independent molecules in the asymmetric unit cell, labelled A and B in Fig. 3.4. Although both fragments share similar bond parameters, a slightly wider bite angle of 110.54(2)° is observed for fragment A in comparison to fragment B, with a S(1)−Cu(1)−S(2) angle of 107.66(2)°. Similar to the other complexes discussed, the two S-donor atoms, along with Cl(2), occupy the equatorial positions with the N-donor atom and Cl(1) in the axial positions, which defined the trigonal bipyramidal configuration for both fragments. Furthermore, the axial ([N(1), Cu(1), Cl(1)]) and the equatorial ([S(1), Cu(1), S(2), Cl(2)]) planes

intersect at an average angle of 85.05° for the two fragments and this contributes to the distorted geometry observed around the metal centres.

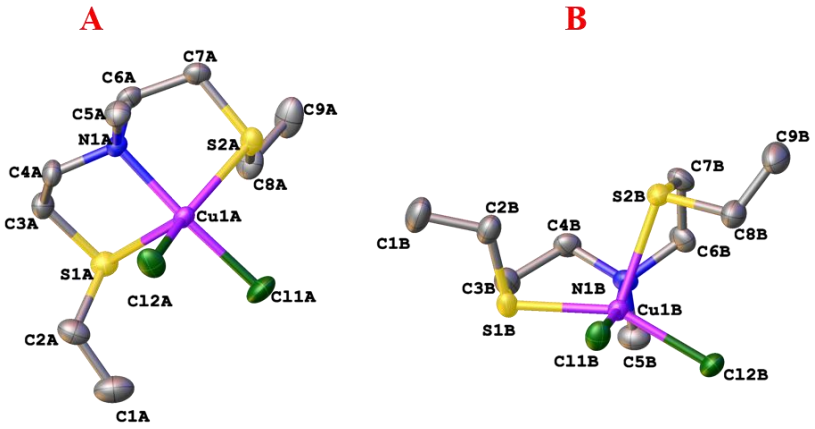

Figure 3.4: Molecular structure of **2.1b** showing two independent molecules (A and B) in the asymmetric unit cell with hydrogens omitted for clarity. Thermal ellipsoids are drawn at 50% probability level.

Complex **2.1d** also crystallised with two crystallographically independent molecules (A and B in Fig. 3.5) in the asymmetric unit cell. Unlike the monoclinic crystal systems of **2.1a** and **2.1b**, complex **2.1d** crystallized in the orthorhombic *Pbca* space group. There are a few prominent features that make these fragments different from each another. Firstly, in each fragment, the geometry around the metal centre is unique. A distorted square pyramidal geometry is observed for fragment A in which the basal positions are occupied by N(1A), S(1A), S(2A) and Cl(2A), while Cl(1A) takes up the apical position.

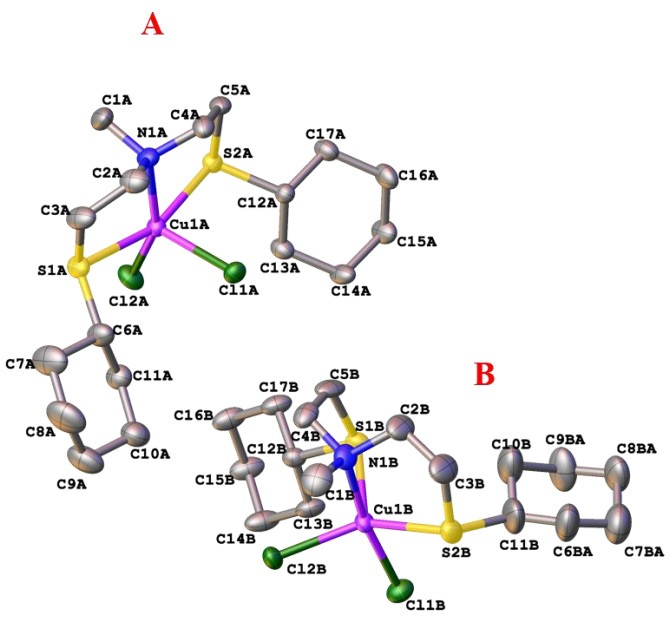

Figure 3.5: Molecular structure of **2.1d** showing two independent molecules (A and B) in the asymmetric unit cell, with one conformation of the disordered cyclohexyl group displayed. All hydrogens are omitted for clarity and thermal ellipsoids are drawn at 50% probability level.

This is comparable in conformation to a similar CuSNS complex reported in the literature, containing bromide instead of chloride ligands and a secondary amine backbone, however, the reported bite angle was more obtuse at 170.58(2)° vs 161.36(4)° for fragment A.[39] In fragment B, a distorted trigonal bipyramidal geometry is displayed, where N(1B) and Cl(1B) occupy the axial positions forming an angle of 171.02(9)°, while S(1B), S(2B) and Cl(2B) reside in the equatorial plane. Furthermore, disorder within the cyclohexyl ring C(6B) – C(11B) was observed in fragment B with one of the two positions occupied by the ring depicted in Fig. 3.5. The disorder may be responsible for the conformational differences between the two fragments. A plane of symmetry is identified in fragment A, defined by [C(1A), N(1A), Cu(1A), Cl(1A), Cl(2A)], whereas in fragment B, C(1B) deviates from the [N(1B), Cu(1B), Cl(1B), Cl(2B)] plane by 1.115 Å. Furthermore, the cyclohexyl substituents bonded to the S-donor atoms assumed the chair configuration in both fragments. In comparison to **2.1a**, **2.1b** and **2.1c**, a notably wider bite angle is observed for **2.1d** and this can be attributed to the bulkiness of the cyclohexyl substituents.

Table 3.4: Selected bond lengths (Å) and bond angles (°) for fragments A and B of complexes **2.1b** and **2.1d**.

Bond lengths (Å)	**2.1b**		**2.1d**	
	A	**B**	**A**	**B**
N(1)−Cu(1)	2.0604(15)	2.0830(16)	2.076(3)	2.084(3)
S(1)−Cu(1)	2.6525(6)	2.6020(6)	2.3688(10)	2.5432(11)
S(2)−Cu(1)	2.3620(5)	2.3529(6)	2.3733(10)	2.3852(11)
Cl(1)−Cu(1)	2.2988(5)	2.2868(5)	2.4699(10)	2.2798(10)
Cl(2)−Cu(1)	2.2531(6)	2.2676(6)	2.2493(10)	2.2928(10)
Bond angles (°)	**2.1a**		**2.1d**	
	A	**B**	**A**	**B**
S(1)−Cu(1)−S(2)	110.542(19	107.656(19)	161.36(4)	118.37(4)
N(1)−Cu(1)−S(1)	82.44(4)	85.94(5)	85.00(9)	83.66(10)
N(1)−Cu(1)−S(2)	86.41(5)	82.76(5)	84.47(9)	84.27(9)
N(1)−Cu(1)−Cl(1)	171.89(5)	172.77(5)	94.27(9)	171.02(9)
N(1)−Cu(1)−Cl(2)	93.36(5)	93.98(5)	152.38(9)	92.59(9)

All the series **2.2** complexes (Figs. 3.6-3.9) crystallised as five coordinate monomers that displayed trigonal bipyramidal geometries around each copper(II) centre with the exception of **2.2b**, which crystallised as an unusual dimer bridged through a tetrachlorocuprate ($[CuCl_4^{2-}]$) anion. With respect to the five coordinate complexes, the S-donor atoms occupy the axial positions, whilst N(1), Cl(1) and Cl(2) reside in the equatorial plane. Due to this arrangement of the SNS ligand, in which the S-donor atoms are axially bound to Cu, a plane of symmetry passing through the equatorial plane [N(1), Cu, Cl(1), Cl(2)] is the key feature of these set of complexes, leading to an essentially open 'bite angle'. This is best illustrated by **2.2a**, bearing relatively small methyl S-substituents, with a bite angle of 171.5°. The Cu(1)−S(1) and Cu(1)−S(2) bond lengths are similar for all complexes and in line with related reports.[40,41] However, for complex **2.2d**, longer bonds of 2.4423(3) and 2.4171(3) Å were observed.

Table 3.5: Selected bond lengths (Å) and bond angles (°) for **2.2a-2.2d**.

Bond lengths (Å)	**2.2a**	**2.2b**	**2.2c**	**2.2d**
N(1)−Cu(1)	2.0999(10)	2.061(3)	2.091(3)	2.0837(9)
S(1)−Cu(1)	2.3461(3)	2.3466(10)	2.3902(9)	2.4423(3)
S(2)−Cu(1)	2.3779(3)	2.3775(9)	2.3807(9)	2.4171(3)
Cl(1)−Cu(1)	2.2526(3)	2.2310(9)	2.2570(9)	2.4079(3)
Cl(2)−Cu(1)	2.4254(4)	2.6131(10)	2.4482(9)	2.2357(3)
Bond angles (°)	**2.2a**	**2.2b**	**2.2c**	**2.2d**
S(1)−Cu(1)−S(2)	171.458(12)	169.97(4)	161.37(3)	161.683(11)
N(1)−Cu(1)−S(1)	85.71(3)	85.40(8)	84.46(8)	84.11(3)
N(1)−Cu(1)−S(2)	85.74(3)	85.26(8)	84.64(8)	84.15(3)
N(1)−Cu(1)−Cl(1)	144.22(3)	156.73(9)	151.30(8)	153.15(3)
N(1)−Cu(1)−Cl(2)	101.18(3)	103.46(9)	96.41(8)	97.71(2)

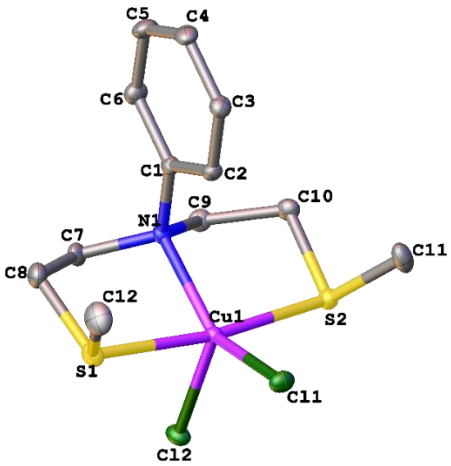

Figure 3.6: Molecular structure of **2.2a** with hydrogens omitted for clarity. Thermal ellipsoids are drawn at 50% probability level.

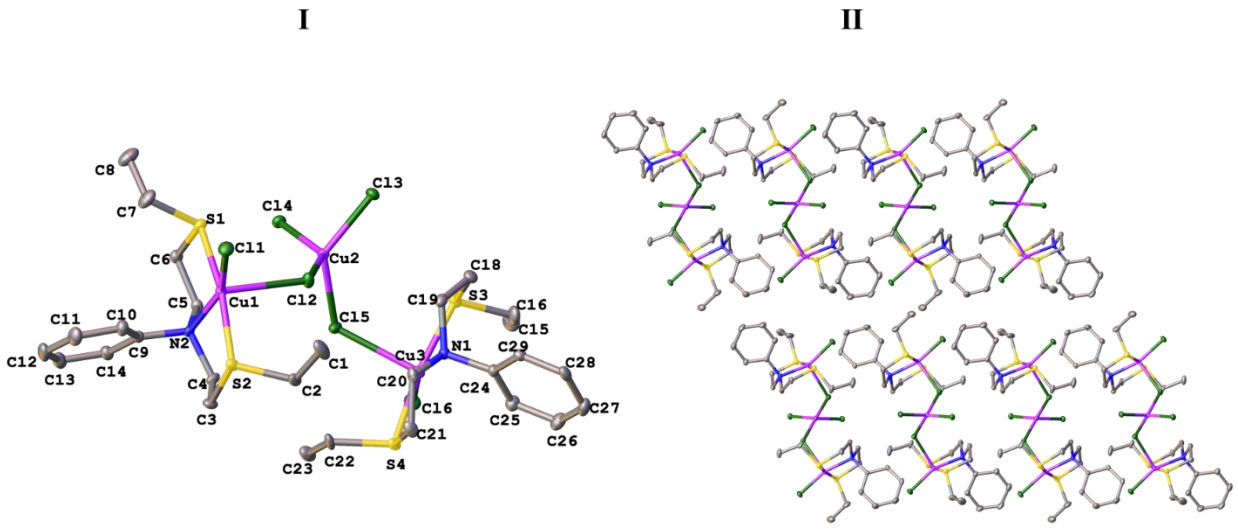

Figure 3.7: Molecular structure (I) and crystal packing (II) of **2.2b** with hydrogens omitted for clarity. Thermal ellipsoids are drawn at 50% probability level.

Complex **2.2b**, presented by the molecular structure in Fig. 3.7, belongs to the triclinic crystal system in the *P*ī space group. The key feature of this complex is the bridging, tetrahedrally bound cuprate anion. This links two SNS-Cu complexes forming a supermolecular dimer. Although the coordination mode is unique and unusual, related reports found in literature portray a similar dimerization with tridentate ligand moieties.[42-44] The central copper atom displays a distorted tetrahedral geometry, whereas a distorted square pyramidal geometry is observed around Cu(1) and Cu(3). The basal positions are occupied by the N-donor and two S-donor atoms from the ligand, as well as by the terminal chloride, while the bridging chloride is found in the apical position of the square pyramid. Unlike the previously discussed molecular structures in this complex series, **2.2b** does not exhibit a plane of symmetry. A representation of the molecular packing viewed along the *a*-axis (100) is illustrated in Fig. 3.7, labelled (II). The molecules are organised to limit steric interference between neighbouring molecules, with a *trans* arrangement of the SNS ligands around the central $(CuCl_4)^{2-}$ anions. Furthermore, short contacts are formed between hydrogens in the vicinity of the terminal chloride groups of the central Cu atom.

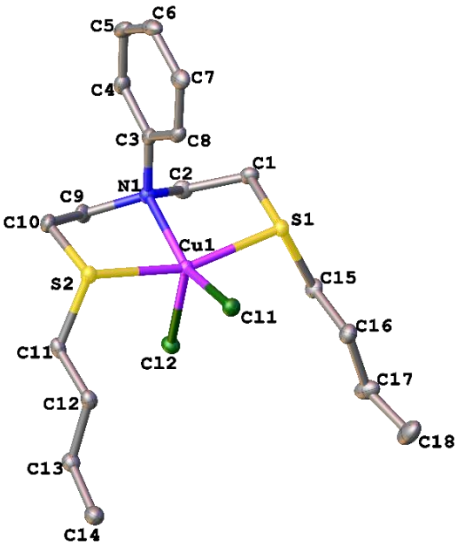

Figure 3.8: Molecular structure of **2.2c** with hydrogens omitted for clarity. Thermal ellipsoids are drawn at 50% probability level.

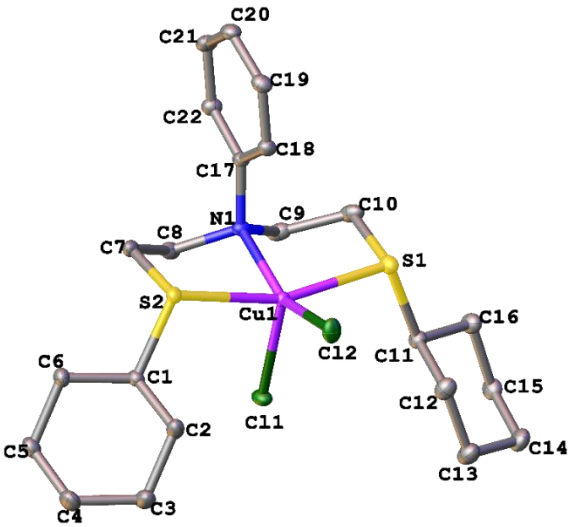

Figure 3.9: Molecular structure of **2.2d** with hydrogens omitted for clarity. Thermal ellipsoids are drawn at 50% probability level.

3.4.3 Oxidation of *n*-octane

All the complexes of series **2.1** and **2.2** were applied as catalysts in the oxidation of *n*-octane using either TBHP or H_2O_2 as the oxidant. All reactions were conducted in air at atmospheric pressure and a reaction temperature of 50 °C. Various octane to oxidant ratios were tested in order to determine the optimum amount of oxidant required. Ratios of 1:12 and 1:9 for octane:TBHP and octane:H_2O_2, respectively, were experimentally found to be optimum for the best balance between product yield and selectivity. Blank reactions in the absence of the catalyst produced yields of ca. 1% in 24 h for the system with TBHP as the oxidant, whilst no conversion was observed at the optimum reaction time for the H_2O_2 system (1 h). The conversion and product distribution of the catalytic systems were compared to those of the simple $CuCl_2$ salt in order to determine the influence of SNS complexation to Cu in the oxidation of *n*-octane.

3.4.3.1 TBHP

For the **2.1** and **2.2**/TBHP systems, both the conversion and product distribution, presented in Figs. 3.10 and 3.11 respectively, were comparable to those of the $CuCl_2$ precursor. This result implies that the ligand dissociates upon the addition of TBHP, leaving the $CuCl_2$ moiety from the complex as the active catalyst. Despite the absence of any ligand effect with TBHP as the source of oxidant, a reasonable total yield of ~15% C-8 oxygenates was recorded, which is higher than some of the results reported in the literature.[45,46] A closer analysis of the distribution of products indicates that within the 24 h reaction time, the ketones (octanones) represent the major products. Furthermore, it was found that the reaction does not proceed in the presence of TEMPO, a common radical inhibitor, thus suggesting that the oxidation reaction followed a radical initiated pathway.

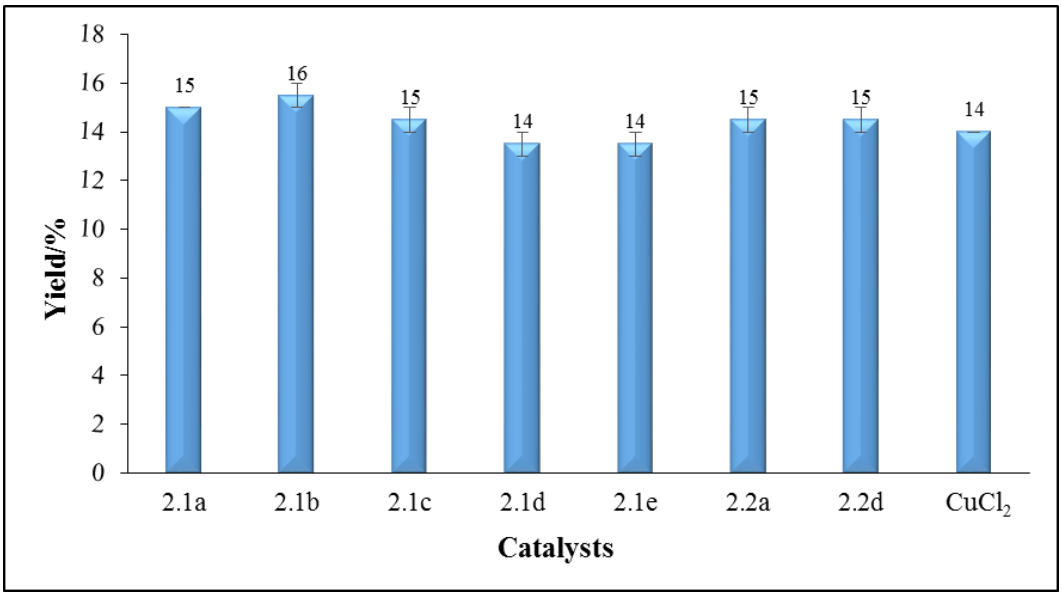

Figure 3.10: Product yields for the oxidation of *n*-octane with catalyst series **2.1** and **2.2**. Conditions: 24 h, 50 °C and an octane to TBHP ratio of 1:12.

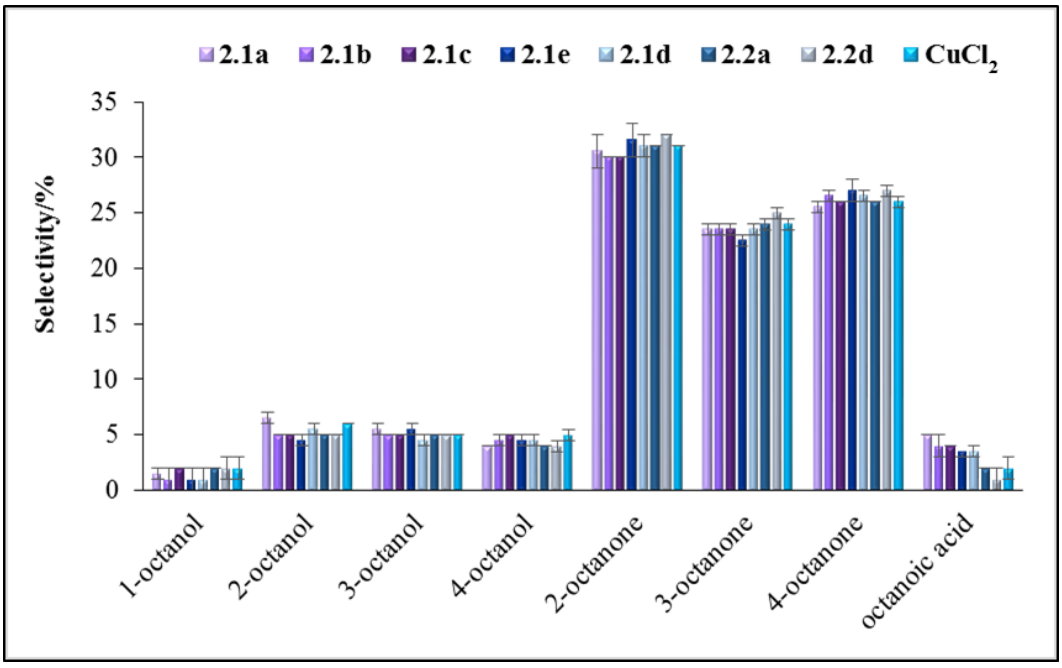

Figure 3.11: A comparison of the product distribution in the TBHP oxidation of *n*-octane for catalyst series **2.1** and **2.2**. Conditions: 24 h, 50 °C and an octane to TBHP ratio of 1:12.

3.4.3.2 H_2O_2

The results obtained for the **2.1** and **2.2**/H_2O_2 systems are much different to the reactions with TBHP as the oxidant. Initially, the precursor salt, $CuCl_2$, was tested at varying octane to H_2O_2 ratios and compared to **2.2a** as the representative catalyst. An optimum substrate to oxidant ratio of 1:9 was established for both systems. Progression of the catalytic reactions were also monitored over a 4 h time period and the results are presented in Fig. 3.12.

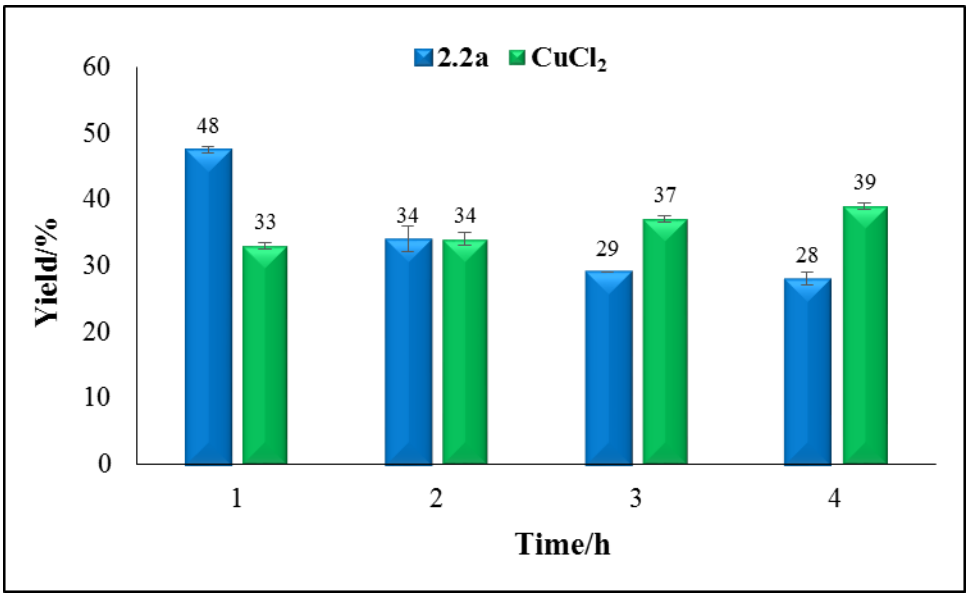

Figure 3.12: Product yields for **2.2a** and $CuCl_2$ monitored over 4 h at an octane to H_2O_2 ratio of 1:9 and 50 °C.

Within the first hour, the yield obtained for catalyst **2.2a** was much higher compared to the simple $CuCl_2$ salt, reaching a maximum of 48% against of 33% for $CuCl_2$ (after the addition of PPh_3). Thereafter, the yield declined with time for catalyst **2.2a**, but gradually increased for $CuCl_2$. Since the yield is based on the total moles of products detected with respect to the initial moles of octane, the C-8 oxygenate yield can only decrease if the products were consumed and further reacted. This, therefore, suggests that possibly over time, catalyst **2.2a** promoted secondary reactions or decomposition pathways involving the major products to produce other, unidentified, by-products. However, this is not seen with the simple $CuCl_2$ metal salt, thus implying a significant ligand effect

in retaining the integrity of **2.2a**. It is well known that the major products in alkane oxidation reactions are the alkyl hydroperoxides (ROOH), which are often reduced with PPh_3 to the corresponding alcohol (ROH) and ketone (R=O) products, thus boosting the overall efficiency of the catalytic reactions.[14,15,17] It is presumed that during the course of the reaction, the octyl hydroperoxides dimerise to produce C(16) products which, due to their high boiling points, are not detected under the conditions of the current GC method. This most probably accounts for the decline in product yield over time with catalyst **2.2a**.

In order to test the hypothesis of a secondary time-dependent reaction involving alkyl hydroperoxides, a study using **2.2a** was conducted. In the study, the total moles of products detected was monitored over a six hour period, before and after the addition of PPh_3. The total moles of octyl hydroperoxides (ROOH) in the system is the difference between the total moles of products, before and after PPh_3 addition.

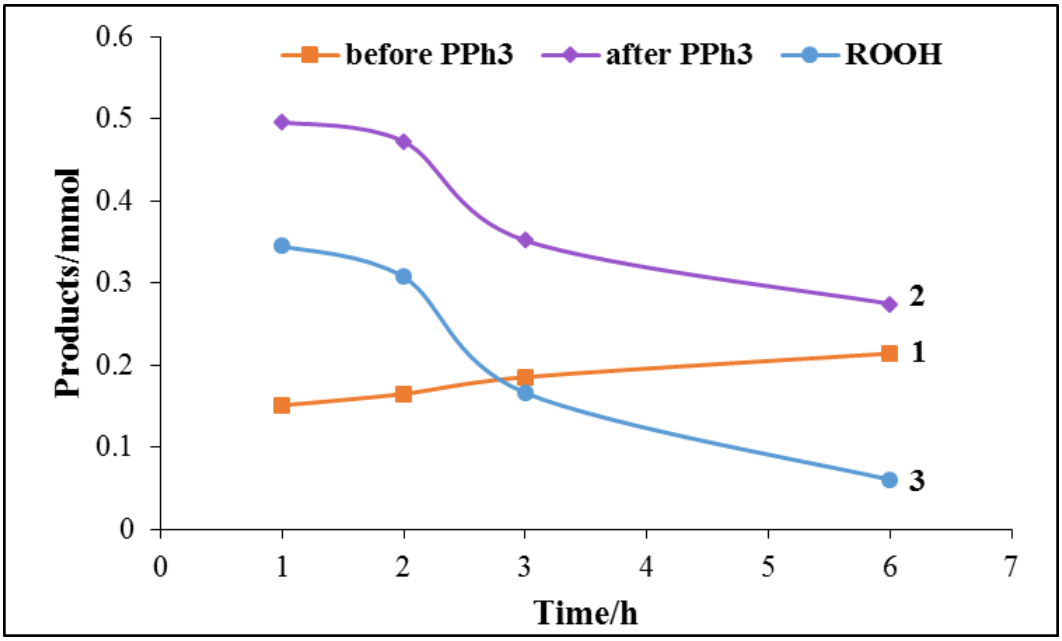

Figure 3.13: Effects of reduction with PPh_3 with catalyst **2.2a** at optimum reaction conditions.

The data, presented in Fig. 3.13, shows that over six hours, there is a slow but steady increase in the amount of detectable products before the addition of PPh_3 (curve 1), whereas after the addition of PPh_3 there is an overall significant increase in the amounts of detectable products (curve 2) (due

to the effects of PPh_3 reduction of ROOH to ROH and R=O). But over the six hour period, instead of accumulating, the total amount of C-8 oxygenate products showed a gradual decline, indicating that they are being consumed by the system. Furthermore, the estimated amount of ROOH (curve 3, which is the difference between curves 2 and 1) also declines with time, proving that it is indeed the ROOH products which further reacted or possibly decomposed after the initial one hour spike, causing a decrease in the overall C-8 oxygenate yield with time.

Since the oxidation reaction spiked at 1 h, the 0-1 h time frame was further investigated at 15 min intervals, however, the yield of C-8 oxygenates steadily increased up until the one hour period. Therefore, further reactions were terminated after 1 h for all the catalysts tested. The catalytic activity of catalyst series **2.1** and **2.2** is presented in Fig. 3.14. From the examination of these results, it is evident that series **2.1** was less active than **2.2**. In fact, their activities were similar or lower, in some cases, than uncomplexed $CuCl_2$, ranging from 23–35%. This result suggests that the complexes are not stable under the oxidising environment, probably due to ligand dissociation, much like what was observed with the TBHP systems. Furthermore, the X-ray crystal structural data of complex series **2.1** showed some degree of asymmetry and/or disorder, brought about by the flexible backbone, which may be one of the contributing factors to the instability of the complexes to oxidation by H_2O_2.

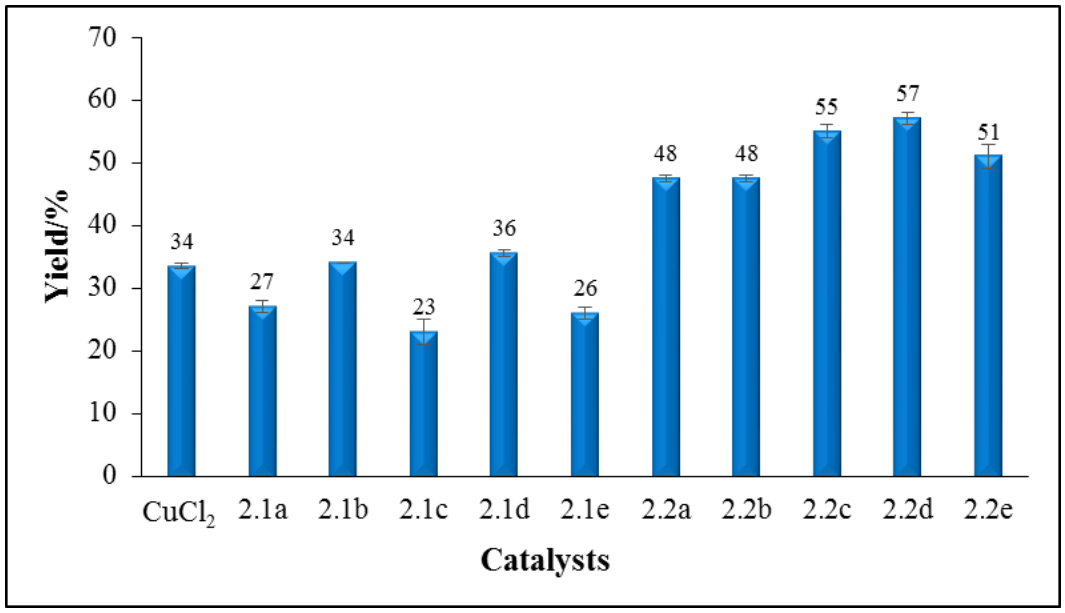

Figure 3.14: Product yields for the oxidation of *n*-octane with catalyst series **2.1** and **2.2**. Conditions: 1 h, 50 °C and an octane to H_2O_2 ratio of 1:9.

In general, the catalyst series **2.2** produced significantly higher product yields (48-57%) in comparison to series **2.1**, suggesting that the activity of the catalyst is influenced by the substituent bonded to the N-donor atom. The phenyl substituent (series **2.2)** is a bulkier and more rigid group, in addition to being more electron donating, when compared to the methyl functionality (series **2.1**) and hence imparts added stability to the complex. Moreover, the crystal structures of the complexes in the **2.2** series revealed a more symmetric and ordered configuration, which may add to the stability and consequently, enhance the life time of the catalyst and possibly the catalytic activity.

Furthermore, the general trend observed for catalysts **2.2** is that the activity increased as the substituents on the S-donor atoms became more electron donating which correlates to a stronger coordination to the metal centre. This implies a dominance of ligand electronic effects on catalytic activity of the complex, with the maximum product yield of 57% achieved by complex **2.2d**, a catalyst bearing the electron-rich cyclohexyl side groups. However, a steric variation from a butyl to a *t*-butyl side group resulted in a slight decrease in the yield from 55 to 51% for **2.2c** and **2.2e** respectively, thus suggesting a possible minor steric influence.

The product distribution profiles (Fig. 3.15) shows combined selectivity to the internal (ketone and alcohol) products, oxygenated at C(2) to C(4) in comparison to the C(1) (1-ol and acid) products. It is evident that the profiles are comparable for series **2.1** and $CuCl_2$, however, the catalysts of the **2.2** series displayed significantly different selectivities, further supporting a strong ligand effect with this series. The difference in the product distribution with a variation in S-donor substituents is negligible, which implies that product selectivity is not influenced by the electronic or steric nature of the S-donor atoms on the ligand. However, high selectivities toward the octanols were noted, contrary to prior reports where the octanones were the main products after reduction with PPh_3.[46,47] Individual product selectivities are presented in Appendix A3 for each catalyst in series **2.2**.

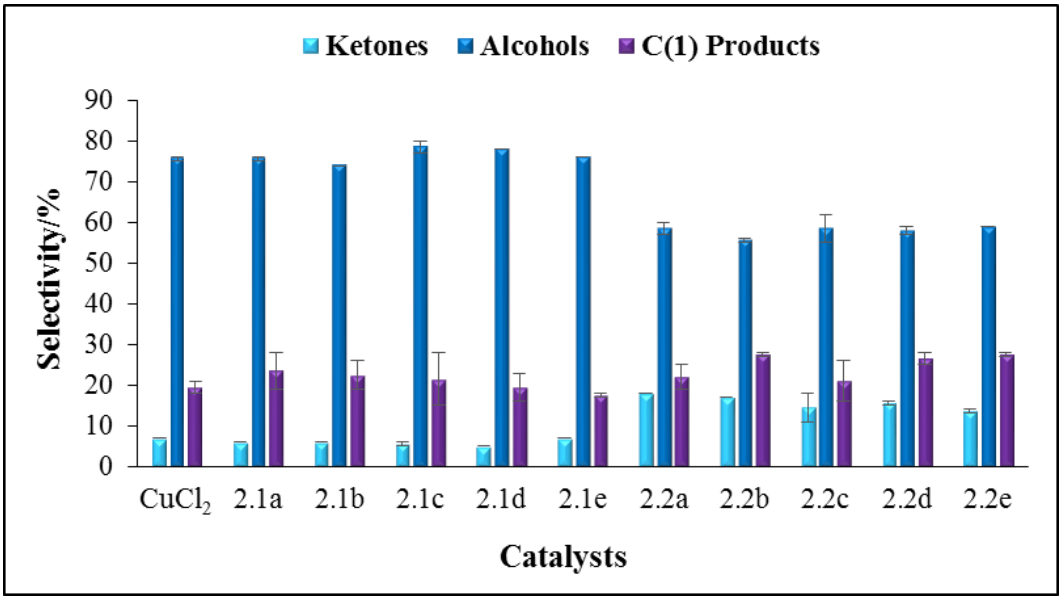

Figure 3.15: A comparison of the product distribution in the H_2O_2 oxidation of *n*-octane for catalyst series **2.1** and **2.2**. Conditions: 1 h, 50 °C and an octane to H_2O_2 ratio of 1:9.

A relatively high selectivity to the terminal products (22-27%) was observed for all the catalysts tested. This is further reflected by the total regioselectivity parameters presented in Table 3.6, which illustrates the reactivity of the hydrogens at each unique carbon position on the *n*-octane backbone. Usually, the terminal or C(1) position on the alkane chain is the most difficult to activate because of the relatively high C−H bond strengths. In comparison, previous catalytic systems have either exhibited poor terminal selectivity, or were completely unable to functionalise the terminal carbon positions of linear alkanes.[10,20,47,48]

From Table 3.6, it is clear that the product distribution (regioselectivity parameter) for catalysts in series **2.2** is relatively similar for all carbon positions, implying that the terminal (CH_3) and internal (CH_2) carbons were almost equally active (e.g. for **2.2e** regioselectivity parameter = 1:1.1:1.5:1.2). However, for octanol regioselectivity, because 1-octanol was selectively over-oxidised to the corresponding acid, the regioselectivity parameter is bias towards the internal carbon positions (e.g. for **2.2e** regioselectivity parameter = 1:2.8:4:2.9).

Table 3.6: Regioselectivity parameters for series **2.2** in the oxidation of *n*-octane.[a]

Catalyst	**Octanol** C(1):C(2):C(3):C(4)	**Octanone** C(2):C(3):C(4)	**Total**[b] C(1):C(2):C(3):C(4)
2.2a	1:5.4:7.2:5.7	1:1:1	1:1.7:2.1:1.8
2.2b	1:4.8:7.2:5.5	1.1:1:1.2	1:1.1:1.5:1.3
2.2c	1:4.7:6.7:5	1:1:1.1	1:1.3:1.7:1.3
2.2d	1:3:4.3:3.2	1:1:1.2	1:1.3:1.8:1.4
2.2e	1:2.8:4:2.9	1:1:1.3	1:1.1:1.5:1.2

[a] Reaction conditions: catalyst (9.56×10^{-6} mol, 1.91×10^{-3} M), *n*-octane (9.56×10^{-4} mol, 0.155 ml), H_2O_2 (23% in H_2O, 0.0374 mol), 50 °C, 1 h, MeCN added as a solvent to give a total reaction volume of 5 ml.

[b] Total regioselectivity parameter takes into consideration all products (alcohols, ketones, and acid) at each carbon position and these values are normalized by accounting for the hydrogens at each carbon position.

With these types of alkane oxidation, it is not uncommon for 1-octanol to be further oxidised to octanoic acid. However, when the peak corresponding to the acid was analysed my GC-MS it was confirmed to be peroxyoctanoic acid, which has similar properties to octanoic acid and therefore, eluted in the same region. The peroxyoctanoic acid could have easily been formed by the reaction of octanoic acid with excess H_2O_2 in the system. Biocatalysts, such as lipase, are known to catalyse the generation of peroxyoctanoic acid from octanoic acid and hydrogen peroxide.[49-53] However, to the best of our knowledge, this is the first report of a chemical catalyst for this transformation. The copper-based catalysts in this work seem to catalyse this reaction via the following sequence:

1-octanol ⟶ octanoic acid ⟶ peroxyoctanoic acid

This sequence was confirmed by carrying out an experiment with 1-octanol as the substrate and th results were in line with the trend observed.

In order to determine the scope and limitations of the series **2.2** catalysts in terms of turnovers and efficiency, reactions were carried out with a lower amount of catalyst (0.01 mol%) over a 24 h period. The results presented in Fig. 3.16 show that significantly high TONs of 2270-3180 were obtainable for the **2.2**/H_2O_2 system within a 24 h reaction time, whilst maintaining relatively high yields of 23-32%. Other reports on the use of copper-based catalysts and H_2O_2 in the oxidation of cyclohexane only gave TONs of 11-19[54] and up to 380,[55] which are substantially lower than what was obtained in this study, indicating the high efficiency of these new catalytic systems. The selectivity profile did not change significantly when the catalyst concentration was decreased from 1 to 0.01 mol%. Furthermore, the trend observed with regards to the yield across the catalyst series were similar to that observed for the higher catalyst loading of 1 mol%.

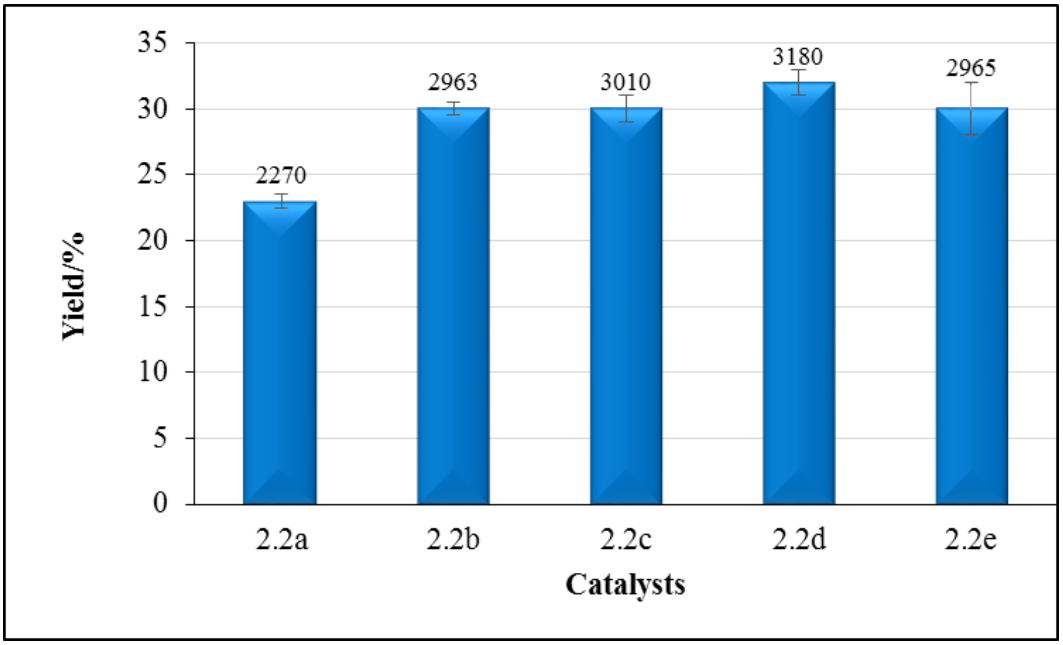

Figure 3.16: Product yields for the oxidation of *n*-octane with catalyst series **2.2**, with the corresponding TON displayed above each bar. Conditions: 24 h, 50 °C, catalyst loading of 0.01 mol% and an octane to H_2O_2 ratio of 1:9.

Numerous reports have emphasised the use of acids as co-catalysts in the oxidation of alkanes, with many even demonstrating that the catalytic reaction does not proceed in the absence of an acid.[18,19,56,57] Therefore, to determine the effect of an acid additive on the CuSNS/H_2O_2 system,

reactions were carried out using **2.2d** as the representative catalyst, in the presence of acetic acid and hydrochloric acid. However, no positive effect or improvement in yields were observed, thus demonstrating that these systems are self-initiating and work independently of acid co-catalysts.

Mechanistic considerations

It is important to note that for catalyst series **2.2**, distinct colour changes were observed upon the addition of H_2O_2, which was a strong indicator that catalytic intermediates were formed early in the reaction. Initially, the reaction mixture appeared green in colour before the addition of an oxidant, but changed to purple within 5 min after the addition of H_2O_2, which persisted for about 10-15 min. Finally, the reaction mixture gradually changed to, and remained, orange with a fine orange suspension for the remainder of the reaction time. Noteworthy, the purple colour change was not observed for $CuCl_2$ or series **2.1** catalysts, rather the reaction changed directly to the orange colour with a fine suspension immediately after addition of the oxidant.

To gain some insight into to the mechanistic aspects of the oxidation catalysis, UV analysis of a representative catalytic reaction based on catalyst **2.2a** was conducted (Fig. 3.17). The UV spectrum of **2.2a** in acetonitrile showed absorption bands at 306 and 406 nm with a shoulder at 440-480 nm (green spectrum, t = 0 min). Immediately after the addition of H_2O_2, the band at 306 nm disappeared and the intensity of the 406 nm band decreased, with a slight shift to 404 nm (yellow spectrum, t = 1 min). After ca. 10 min, the solution turned to purple and the UV spectrum showed a band in the region of 530 nm (purple spectrum), which has been recognised as the active copper-peroxo species.

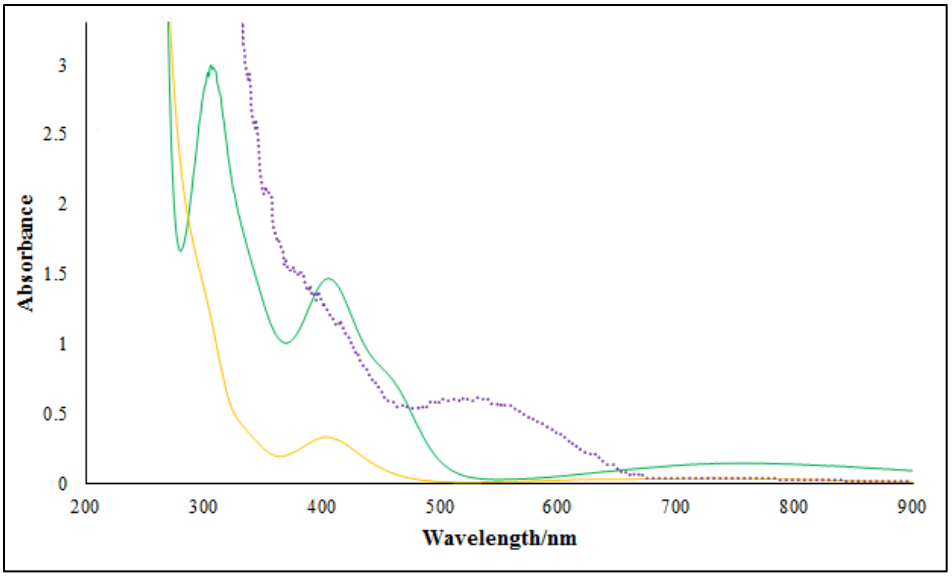

Figure 3.17: UV-vis spectrum of **2.2a**. Green spectrum (no H_2O_2, t = 0 min); yellow (H_2O_2 added, t = 1 min) and purple (H_2O_2 added, t = 10 min).

This band is within the region of reported wavelengths for copper complexes containing peroxo ligands.[58-63]

To determine the pathway of the current catalytic reactions, a reaction was conducted using the most active catalyst, **2.2d**, in combination with a common radical inhibitor, TEMPO. The result showed a significant decrease in product yield from 57 to 5% for a 1:1 octane to TEMPO ratio. Furthermore, no products were detected with an octane to TEMPO ratio of 1:4, suggesting that a radical mechanism is most likely the pathway in these oxidation reactions. Similar results were seen in the literature using this type of radical inhibitor.[64]

In summary, based on the data obtained in this entire study, a possible radical mechanism is proposed for the CuSNS/H_2O_2 system in the oxidation of linear alkanes (RH), as shown in Scheme 3.1. Similar pathways have been reported in the literature for the oxidation of cycloalkanes with H_2O_2, using copper-based catalysts.[20,64] The first step of the reaction mechanism involves formation of copper-peroxo ($SNSCu^{II}(OOH)$) species by the reaction of the $Cu^{II}SNS$ complex with H_2O_2 (eq. 1).[65] This species is correlated to the purple colour observed upon addition of H_2O_2 to the complex which tallies with the UV spectrum (λ_{max} = 560 nm). The reactive copper-peroxo intermediate then reduces another $SNSCu^{II}$ complex to yield two $SNSCu^{I}$ species (eq. 2).[20] A hydroxyl radical ($HO^{\bullet}$) is then generated by the reaction between the $SNSCu^{I}$ intermediate and a

molecule of H_2O_2 (eq. 3) which then proceeds to abstract a proton from the alkane (RH) to form the alkyl radical ($R^{\bullet}$) (eq. 4). The first three steps will be influenced by the nature of the ligands in that the more electron rich substituents will lead to a stronger coordination between the ligand and the metal centre thus limiting ligand dissociation. The alkylperoxyl radical ($ROO^{\bullet}$) is then formed from the combination of $R^{\bullet}$ and the earlier generated oxygen (eq. 5), which is then reduced by $SNSCu^{I}$ to form the anion and consequently the alkyl hydroperoxide as the major product (eqs. 6 and 7). Formation of the alcohol products occur from ROOH via the $SNSCu^{I}$ assisted generation of the alkoxyl radical ($RO^{\bullet}$) (eq. 8), which then reacts with the alkane (eq. 9). It is also possible for the alkylperoxyl radical to undergo dismutation to yield the alcohol and ketone products (eq. 10). However, from the results obtained in this study, most of the alcohols and ketones were obtained from decomposition of the alkyl hydroperoxides with PPh_3 (eq. 11).

$$SNSCu^{II} + H_2O_2 \longrightarrow SNSCu^{II}[(OOH)]^- + H^+ \quad (1)$$

$$SNSCu^{II}[(OOH)]^- + SNSCu^{II} \longrightarrow 2SNSCu^{I} + O_2 + H^+ \quad (2)$$

$$SNSCu^{I} + H_2O_2 \longrightarrow SNSCu^{II} + HO^{\bullet} + OH^- \quad (3)$$

$$RH + HO^{\bullet} \longrightarrow R^{\bullet} + H_2O \quad (4)$$

$$R^{\bullet} + O_2 \longrightarrow ROO^{\bullet} \quad (5)$$

$$ROO^{\bullet} + SNSCu^{I} \longrightarrow ROO^- + SNSCu^{II} \quad (6)$$

$$ROO^- + H^+ \longrightarrow ROOH \quad (7)$$

$$ROOH + SNSCu^{I} \longrightarrow RO^{\bullet} + SNSCu^{II} + OH^- \quad (8)$$

$$RO^{\bullet} + RH \longrightarrow ROH + R^{\bullet} \quad (9)$$

$$2ROO^{\bullet} \longrightarrow ROH + R'{=}O + O_2 \quad (10)$$

$$ROOH + PPh_3 \longrightarrow ROH + R'{=}O + OPPh_3 \quad (11)$$

Scheme 3.1: Proposed general mechanism for the oxidation of alkanes (RH) to alkyl hydroperoxides (ROOH), alcohols (ROH) and ketones (R′=O) catalyzed by CuSNS complexes using H_2O_2 as the oxidant.

3.5 Conclusions

In this work, four new pincer-type SNS ligands and ten new SNS complexes of copper were successfully synthesized using simple synthetic methods. A variation in the ligand backbone, utilising a methyl and a phenyl substituent, distinguished the two series of complexes as **2.1** and **2.2** respectively. Characterisation by various techniques confirmed the structural composition and bulk purity of all the prepared complexes. All the complexes existed as monomers characterised by a trigonal bipyramidal geometry around each Cu(II) centre. The exception to this was **2.2b**, which crystallised in an unusual dimeric fashion, bridged through a cuprate anion. Molecular structures of **2.1** were less ordered due to the flexibility of the backbone, whereas those of **2.2** were highly symmetric and ordered due to the rigidity of the phenyl substituent on the N-donor.

All these complexes were applied as catalysts for the oxidation of *n*-octane using TBHP and H_2O_2 as oxidants. It is interesting to recall that similar product yields and profiles were obtained for **2.1**/TBHP, **2.2**/TBHP and $CuCl_2$/TBHP. This suggests that the ligand most likely dissociated from the metal centre upon the addition of TBHP, releasing the Cu^{2+} ion as the active catalytic species. The **2.1**/H_2O_2 system produced C-8 oxygenate yields of 23-35%, which were either similar or lower than those obtained using $CuCl_2$/H_2O_2, in addition to possessing similar selectivity profiles as the salt. On the other hand, the **2.2**/H_2O_2 system of catalysts were very active, producing C-8 oxygenate yields of up to 57%, with the major products being the alcohols (ca. 59%). This system also proved to be very efficient with high TONs of 2270-3180 obtained. The high activity is attributed to the formation of copper-peroxo species. Furthermore, peroxyoctanoic acid was also detected as a product presumably from the over-oxidation of octanoic acid.

In conclusion, this study serves to extend our understanding on the critical role of a flexible SNS backbone on catalytic activity in *n*-octane oxidation.[28] Hence, in combination with Cu(II), one of the most active *n*-octane oxidation catalysts ever reported has been developed from a relatively flexible SNS ligand. The degree of flexibility was modulated by a rigid, electron-rich phenyl N-substituent. However, the unhindered and highly flexible methyl N-substituted analogues only showed modest activity and were unstable under the catalytic oxidising environment.

3.6 References

(1) Labinger, J. A.; Bercaw, J. E. *Nature* **2002**, *417*, 507.

(2) Janowicz, A. H.; Bergman, R. G. *J. Am. Chem. Soc.* **1982**, *104*, 352.

(3) Crabtree, R. H. *J. Chem. Soc., Dalton Trans.* **2001**, 2437.

(4) Crabtree, R. H. *J. Organomet. Chem.* **2004**, *689*, 4083.

(5) Shilov, A. E.; Shteinman, A. A. *Coord. Chem. Rev.* **1977**, *24*, 97.

(6) Shilov, A. E. e.; Shul'pin, G. B. *Russ. Chem. Rev.* **1987**, *56*, 442.

(7) Shilov, A. E.; Shul'pin, G. B. *Chem. Rev.* **1997**, *97*, 2879.

(8) Shul'pin, G. B.; Shilov, A. E.; Suss-Fink, G. *Tetraheron Lett.* **2001**, *42*, 7253.

(9) Lindsay Smith, J. R.; Shul'pin, G. B. *Tetrahedron Lett.* **1998**, *39*, 4909.

(10) Shul'pin, G. B.; Suss-Fink, G.; Shul'pina, L. S. *J. Mol. Catal., A: Chem.* **2001**, *170*, 17.

(11) Shul'pin, G. B.; Süss-Fink, G.; Shul'pina, L. S. *J. Mol. Catal., A: Chem.* **2001**, *170*, 17.

(12) Shul'pin, G. B. *Pet. Chem.* **2001**, *41*, 405.

(13) Süss-Fink, G.; Gonzalez, L.; Shul'pin, G. B. *Appl. Catal., A: Gen.* **2001**, *217*, 111.

(14) Shul'pin, G. B. *J. Mol. Catal. A: Chem.* **2002**, *189*, 39.

(15) Shul'pin, G. B. *C.R. Chim.* **2003**, *6*, 163.

(16) Shul'pin, G. B.; Golfeto, C. C.; Suss-Fink, G.; Shul'pina, L. S.; Mandelli, D. *Tetrahedron Lett.* **2005**, *46*, 4563.

(17) Shul'pin, G. B.; Kudinov, A. R.; Shul'pina, L. S.; Petrovskaya, E. A. *J. Organomet. Chem.* **2006**, *691*, 837.

(18) Kozlov, Y. N.; Nizova, G. V.; Shul'pin, G. B. *J. Phys. Org. Chem.* **2008**, *21*, 119.

(19) Shul'pina, L. S.; Kirillova, M. V.; Pombeiro, A. J. L.; Shul'pin, G. B. *Tetrahedron* **2009**, *65*, 2424.

(20) Kirillova, M. V.; Kozlov, Y. N.; Shul'pina, L. S.; Lyakin, O. Y.; Kirillov, A. M.; Talsi, E. P.; Pombeiro, A. J. L.; Shul'pin, G. B. *J. Catal.* **2009**, *268*, 26.

(21) Shul'pin, G. B. *Mini-Rev. Org. Chem.* **2009**, *6*, 95.

(22) Wong, L.-L. *Curr. Opin. Chem. Biol.* **1998**, *2*, 263.

(23) Westerheide, L.; Pascaly, M.; Krebs, B. *Curr. Opin. Chem. Biol.* **2000**, *4*, 235.

(24) Merkx, M.; Kopp, D. A.; Sazinsky, M. H.; Blazyk, J. L.; Müller, J.; Lippard, S. J. *Angew. Chem. Int. Ed.* **2001**, *40*, 2782.

(25) Ross, M. O.; Rosenzweig, A. C. *J. Biol. Inorg. Chem.* **2016**, 1.

(26) Friedle, S.; Reisner, E.; Lippard, S. J. *Chem. Soc. Rev.* **2010**, *39*, 2768.

(27) Yoshizawa, K.; Shiota, Y. *J. Am. Chem. Soc.* **2006**, *128*, 9873.

(28) Soobramoney, L.; Bala, M. D.; Friedrich, H. B. *Dalton Trans.* **2014**, *43*, 15968.

(29) Furniss, B. S.; Hannaford, A. J.; Smith, P. W. G.; Tatchell, A. R. *Vogel's textbook of practical organic chemistry*; 5th ed.; J. Wiley and sons: New York, 1989.

(30) SAINT Version 7.60a, Bruker AXS Inc., Madison, WI, USA, 2006.

(31) G. M. Sheldrick, SHELXS-97, SHELXL-2014 and SADABS version 2.05, University of Göttingen, Germany, 1997.

(32) Barbour, L. J. *Supramol. Chem.* **2001**, *1*, 189.

(33) Atwood, J. L. and Barbour., L. J. *Cryst. Growth Des.* **2003**, *3*, 3.

(34) Linden, A.; Petridis, A.; James, B. D. *HeIv. Chim. Acta* **2009**, *92*, 29.

(35) Shastri, K.; Cheng, E. W. C.; Motevalli, M.; Schofield, J.; Wilkinson, J. S.; Watkinson, M. *Green Chem.* **2007**, *9*, 996.

(36) Bai, S.-Q.; Koh, L. L.; Hor, T. S. A. *Inorg. Chem.* **2009**, *48*, 1207.

(37) Ball, R. J.; Genge, A. R. J.; Radford, A. L.; Skelton, B. W.; Tolhurst, V.-A.; White, A. H. *J. Chem. Soc., Dalton Trans.* **2001**, 2807.

(38) Blomenkemper, M.; Schröder, H.; Pape, T.; Hahn, F. E. *Inorg. Chim. Acta* **2012**, *390*, 143.

(39) Bai, S.-Q.; Jiang, L.; Zuo, J.-L.; Hor, T. S. A. *Dalton Trans.* **2013**, *42*, 11319.

(40) Escriche, L.; Sanz, M.; Casabo, J.; Teixidor, F.; Molins, E.; Miravitlles, C. *J. Chem. Soc., Dalton Trans.* **1989**, 1739.

(41) Miecznikowski, J. R.; Lynn, M. A.; Jasinski, J. P.; Lo, W.; Bak, D. W.; Pati, M.; Butrick, E. E.; Drozdoski, A. E. R.; Archer, K. A.; Villa, C. E.; Lemons, E. G.; Powers, E.; Siu, M.; Gomes, C. D.; Bernier, N. A.; Morio, K. N. *Polyhedron* **2014**, *80*, 157.

(42) Wang, Q.; Wang, D.-Q.; Sun, Y.-Y. *Acta Crystallogr. Sect. E* **2007**, *63*, m3010.

(43) Qian, J.; Xie, M.-J.; Feng, L.; Tian, J.-L.; Shang, J.; Zhang, Y.; Yan, S.-P. *J. Coord. Chem.* **2010**, *63*, 2239.

(44) Feng, X. D.; Zhang, R.; Wang, X. Y.; Zhang, X. X.; Wang, J. X.; Xing, Y. H.; Sun, L. X. *Polyhedron* **2015**, *90*, 69.

(45) Wong, W.-K.; Chen, X.-P.; Guo, J.-P.; Chi, Y.-G.; Pan, W.-X.; Wong, W.-Y. *J. Chem. Soc., Dalton Trans.* **2002**, 1139.

(46) Naicker, D.; Friedrich, H. B.; Omondi, B. *RSC Adv.* **2015**, *5*, 63123.

(47) Roy, P.; Manassero, M. *Dalton Trans.* **2010**, *39*, 1539.

(48) Kirillov, A. M.; Kopylovich, M. N.; Kirillova, M. V.; Karabach, E. Y.; Haukka, M.; da Silva, M. F. C. G.; Pombeiro, A. J. L. *Adv. Synth. Catal.* **2006**, *348*, 159.

(49) Kirillova, M. V.; Kirillov, A. M.; Mandelli, D.; Carvalho, W. A.; Pombeiro, A. J. L.; Shul'pin, G. B. *J. Catal.* **2010**, *272*, 9.

(50) Mac Leod, T. C. O.; Kirillova, M. V.; Pombeiro, A. J. L.; Schiavon, M. A.; Assis, M. D. *Appl. Catal., A: Gen.* **2010**, *372*, 191.

(51) Wijayati, N.; Siadi, K.; Wijaya, H.; Suhartono, M. T. *Int. J. Chem. Eng. Appl.* **2015**, *6*, 53.

(52) Björkling, F.; Godtfredsen, S. E.; Kirk, O. *J. Chem. Soc., Chem. Comm.* **1990**, 1301.

(53) Kirk, O.; Christensen, M. W.; Damhus, T.; Godtfredsen, S. E. *Biocatalysis* **1994**, *11*, 65.

(54) Skouridou, V.; Stamatis, H.; Kolisis, F. N. *J. Mol. Catal. B: Enzym.* **2003**, *21*, 67.

(55) Skouridou, V.; Stamatis, H.; Kolisis, F. N. *Biocatal. Biotransform.* **2003**, *21*, 285.

(56) Fernandes, T. A.; André, V.; Kirillov, A. M.; Kirillova, M. V. *J. Mol. Catal. A: Chem.* **2017**, *426, Part B*, 357.

(57) Gupta, S.; Kirillova, M. V.; Guedes da Silva, M. F.; Pombeiro, A. J. L. *Appl. Catal., A: Gen.* **2013**, *460–461*, 82.

(58) Kitajima, N.; Koda, T.; Iwata, Y.; Morooka, Y. *J. Am. Chem. Soc.* **1990**, *112*, 8833.

(59) Hatcher, L. Q.; Lee, D.-H.; Vance, M. A.; Milligan, A. E.; Sarangi, R.; Hodgson, K. O.; Hedman, B.; Solomon, E. I.; Karlin, K. D. *Inorg. Chem.* **2006**, *45*, 10055.

(60) Halime, Z.; Kieber-Emmons, M. T.; Qayyum, M. F.; Mondal, B.; Puiu, S. C.; Chufán, E. E.; Sarjeant, A. A. N.; Hodgson, K. O.; Hedman, B.; Solomon, E. I.; Karlin, K. D. *Inorg. Chem.* **2010**, *49*, 3629.

(61) Comba, P.; Haaf, C.; Helmle, S.; Karlin, K. D.; Pandian, S.; Waleska, A. *Inorg. Chem.* **2012**, *51*, 2841.

(62) Karlin, K. D.; Cruse, R. W.; Gultneh, Y. *J. Chem. Soc., Chem. Comm.* **1987**, 599.

(63) Tyeklar, Z.; Jacobson, R. R.; Wei, N.; Murthy, N. N.; Zubieta, J.; Karlin, K. D. *J. Am. Chem. Soc.* **1993**, *115*, 2677.

(64) Kirillov, A. M.; Kirillova, M. V.; Pombeiro, A. J. L. *Coord. Chem. Rev.* **2012**, *256*, 2741.

(65) Pham, A. N.; Xing, G.; Miller, C. J.; Waite, T. D. *J. Catal.* **2013**, *301*, 54.

CHAPTER FOUR

Application of thiophene-based NSN ligands in paraffin oxidation catalysis: *in situ* generation of the active catalyst

4.1 Summary

New types of NSN ligands have been synthesised based on a thiophene backbone with amide linkages. These are thiophene-2,5-dicarboxylic acid di(R)amide (**L3**) R = methyl (**a**), butyl (**b**), pentyl (**c**), cyclohexyl (**d**) and benzyl (**e**). Techniques that involve NMR spectroscopy, CHN analyses and single crystal X-ray crystallography for compounds **L3a**, **L3b** and **L3e**, were utilised to characterise the prepared compounds. Molecular structures of **L3a** and **L3e** revealed highly symmetrical and ordered arrangements, whereas **L3b** displayed an unsymmetrical structure due to the flexible butyl substituents. Disorder within the butyl group was also found, which was attributed to the flexibility and free rotation of the long alkyl chain. The potential catalytic activity of ligands **L3b** and **L3e** combined with various simple metal salts and H_2O_2 as the oxidant were tested *in situ*. A significant ligand effect was observed with $CuCl_2$, resulting in yields of 21 and 27% for the **L3b**/$CuCl_2$ and **L3e**/$CuCl_2$ systems respectively. Furthermore, an enhanced primary carbon selectivity was seen with the *in situ* generated systems.

4.2 Introduction

The transformation of saturated alkanes into more reactive products is a demanding field for which an array of catalysts have been invested.[1-13] One of the key requirements desired for a typical catalytic system is an economical and efficient catalyst that is stable and selective. This is why a systematic and carefully planned design of the catalyst is so imperative. Pincer ligands are advantageous in this regard because of several key features that include variable flexibility, ability for steric and electronic tuning as well as greater stability brought about by chelation of the three donor atoms to metal centres.

Pincer type ligands containing S- and N-donor atoms in varying combinations have been extensively explored.[14-38] However, despite its potential features, the NSN backbone in particular has been among the least studied of the pincer family and, thus, limited literature is available. The NSN donor set can be regarded as a relatively robust backbone, since it consists of two hard nitrogen donors and a central soft sulfur donor atom. This makes it a ligand system to be favourably considered in catalyst design. The NSN backbone may consist of asymmetric or symmetric substituents as described in literature reports.[39-41] As a general observation, aromaticity is often introduced into the backbone to increase rigidity and stability. The length of the spacer between the N- and S-donor atoms affect the binding mode of the ligand. Therefore, if there is no spacer group, the ligand will tend to coordinate in a bidentate fashion as shown in work by Lui *et al.*[42] Thiophene Schiff based NSN ligands have been reported by Pedras *et al.* who successfully coordinated these ligands to palladium(II) and nickel(II) to yield mononuclear complexes.[43] The incorporation of a thiophene backbone has been known to increase the thermal stability of ligands.[44]

This work aims to develop a new range of NSN ligands obtained via simple synthesis and cost effective routes. A thiophene (S-donor) with amide (N-donor) linkages was selected to form the central core of the NSN moiety with electronic and steric variation achieved through the variety of substituents bonded to the N-donor atoms. Potential catalytic activity of the prepared ligands was tested (in combination with simple metal salts) in the oxidation of *n*-octane using H_2O_2 as the oxidant.

4.3 Experimental Section

4.3.1 General

The ligands were prepared under an inert nitrogen atmosphere employing standard Schlenk techniques. Solvents were dried according to established methods[45] and purged with high purity nitrogen gas prior to use. Tetrahydrofuran (THF) was dried over sodium wire and benzophenone, absolute ethanol (EtOH) and methanol (MeOH) were dried over magnesium turnings and iodine, and dichloromethane (DCM) was dried over phosphorous pentoxide. The ligand precursor thiophene-2,5-dicarbonyl dichloride was synthesized according to a procedure adapted from the literature.[46] All other reagents were obtained commercially and used as received. NMR spectra were recorded using a Bruker Avance III 400 MHz spectrometer at ambient temperature. The ^{1}H NMR data are reported as chemical shift (δ, ppm) and referenced to the solvent peak $CDCl_3$. The attached proton test (APT) ^{13}C NMR, which distinguishes between quaternary C, CH, CH_2 and CH_3 carbons, are listed as chemical shift (δ, ppm) and positive (pos) or negative (neg) with the corresponding carbons in parentheses and referenced to the solvent peak $CDCl_3$. The IR spectra were recorded on a Perkin Elmer Attenuated Total Reflectance (ATR) spectrophotometer and elemental analyses were performed on a Thermo-Scientific Flash 2000 CHNS/O elemental analyzer, while the melting points were determined using a Stuart Scientific melting point apparatus.

4.3.2 Synthesis and characterisation of ligands

General procedure:

Thiophene-2,5-dicarbonyl dichloride was dissolved in a 80 ml mixture of DCM/THF (1:1 v/v). The respective amine was then added in excess (1:12) to this solution via a syringe and the resultant white turbid mixture was allowed to stir at room temperature overnight. Thereafter the mixture was suspended in 100 ml of double-distilled water, filtered and washed with 10% HCl followed by a $NaHCO_3$ solution. After a final wash with water, the solid was dried under vacuum for several

days to yield a white powder, identified as the product. All the ligands were synthesised by following this general procedure. Specific reagents and quantities are highlighted below:

Synthesis of thiophene-2,5-dicarboxylic acid dimethylamide (L3a). Thiophene-2,5-dicarbonyl dichloride (0.440 g, 2.11 mmol) and methylamine (2.19 ml, 25.3 mmol) was used to synthesise **L3a**. Single crystals were grown by slow evaporation of a concentrated solution of **L3a** in methanol. Yield: 71%. Melting point: 332-333 °C. ^{1}H NMR (400 MHz, $(CD_3)_2SO$): δ 2.76 (d, 6H, C*H*$_3$-N), 7.63 (s, 2H, C*H*-thiophene), 8.55 (d, 2H, N*H*). ^{13}C APT NMR (400 MHz, $(CD_3)_2SO$): δ 26.02 (*C*H$_3$-N) neg, 127.82 (*C*H-thiophene) neg, 142.91 (*C*-thiophene) pos, 161.08 (*C*=O) pos. IR ν_{max} (cm^{-1}): 3342 (w), 3186 (w), 3084 (w), 2966 (w), 2780 (w), 1540 (s), 1508 (s), 1363 (s), 1338 (s), 1318 (s), 971 (m), 779 (s) 463 (s). Anal. (%) calc. for $C_8H_{10}N_2O_2S$: C, 48.2; H, 5.6; N, 14.1; found: C, 48.2; H, 5.2; N, 13.9.

Synthesis of thiophene-2,5-dicarboxylic acid dibutylamide (L3b). This ligand was synthesised using the following mass and volume of the starting materials: thiophene-2,5-dicarbonyl dichloride (0.334 g, 1.60 mmol) and 1 butylamine.(89 ml, 19.2 mmol). Single crystals were obtained from slow evaporation of a methanol solution of **L3b**. Yield: 69%. Melting point: 236-237 °C. ^{1}H NMR (400 MHz, $(CD_3)_2SO$): δ 0.90 (t, 6H, C*H*$_3$CH$_2$CH$_2$CH$_2$-N), 1.31 (m, 4H, CH$_3$C*H*$_2$CH$_2$CH$_2$-N), 1.52 (m, 4H, CH$_3$CH$_2$C*H*$_2$CH$_2$-N), 3.20 (q, 4H, CH$_3$CH$_2$CH$_2$C*H*$_2$-N), 7.64 (s, 2H, C*H*-thiophene), 8.56 (d, 2H, N*H*). ^{13}C APT NMR (400 MHz, $(CD_3)_2SO$): δ 13.64 (*C*H$_3$CH$_2$CH$_2$CH$_2$-N) neg, 19.57 (CH$_3$*C*H$_2$CH$_2$CH$_2$-N) pos, 31.13 (CH$_3$CH$_2$*C*H$_2$CH$_2$-N) pos, 38.79 (CH3CH2CH2*C*H$_2$-N) pos, 127.80 (*C*H-thiophene) neg, 143.15 (*C*-thiophene) pos, 160.52 (*C*=O) pos. IR ν_{max} (cm^{-1}): 3310 (m), 3086 (w), 2961 (w), 2929 (w), 2862 (w), 1618 (s), 1549 (s), 1518 (m), 1291 (s), 747 (m), 660 (s). Anal. (%) calc. for $C_{14}H_{22}N_2O_2S$: C, 59.5; H, 7.9; N, 9.9; found: C, 59.1; H, 8.1; N, 10.2.

Synthesis of thiophene-2,5-dicarboxylic acid dipentylamide (L3c). This ligand was prepared using the following: thiophene-2,5-dicarbonyl dichloride (0.417 g, 1.20 mmol) and pentylamine (2.77 ml, 23.9 mmol). Yield: 94%. Melting point: 188-190 °C. ^{1}H NMR (400 MHz, $(CD_3)_2SO$): δ 0.87 (t, 6H, C*H*$_3$CH$_2$CH$_2$CH$_2$CH$_2$-N), 1.29 (m, 8H, CH$_3$C*H*$_2$C*H*$_2$CH$_2$CH$_2$-N, 1.50 (q, 4H, CH$_3$CH$_2$CH$_2$C*H*$_2$CH$_2$-N), 3.20 (q, 4H, CH$_3$CH$_2$CH$_2$CH$_2$C*H*$_2$-N), 7.67 (s, 2H, C*H*-thiophene), 8.56 (t, 2H, N*H*). ^{13}C APT NMR (400 MHz, $(CD_3)_2SO$): δ 14.45 (*C*H$_3$CH$_2$CH$_2$CH$_2$CH$_2$-N) neg, 22.33 (CH$_3$*C*H$_2$CH$_2$CH$_2$CH$_2$-N) pos, 29.14 (CH$_3$CH$_2$*C*H$_2$CH$_2$CH$_2$-N) pos, 29.22 (CH$_3$CH$_2$CH$_2$*C*H$_2$CH$_2$-N), pos 39.62 (CH$_3$CH$_2$CH$_2$CH$_2$*C*H$_2$-N) pos, 128.35 (*C*H-thiophene) neg, 143.68 (*C*-thiophene) pos, 161.04 (*C*=O) pos. IR ν_{max} (cm^{-1}): 3442 (w), 3304 (m), 3085 (w), 2956 (w), 2930 (m), 2871 (m), 1615 (s), 1552 (s), 747 (w), 664 (m). Anal. (%) calc. for $C_{16}H_{26}N_2O_2S$: C, 61.9; H, 8.4; N, 9.0; found: C, 61.4; H, 8.4; N, 8.8.

Synthesis of thiophene-2,5-dicarboxylic acid dicyclohexylamide (L3d). The following mass and volume of the starting reagents were used to prepare **L3d**: thiophene-2,5-dicarbonyl dichloride (0.408 g, 1.95 mmol) and cyclohexylamine (2.68 ml, 23.4 mmol). Yield: 70%. Melting point: 330-331 °C. ^{1}H NMR (400 MHz, $(CD_3)_2SO$): δ 1.12 (m, 2H, C_6H_{12}-N), 1.28 (m, 8H, C_6H_{12}-N), 1.61 (m, 2H, C_6H_{12}-N), 1.77 (m, 8H, C_6H_{12}-N), 3.67 (m, 2H, C_6H_{12}-N), 7.73 (s, 2H, C*H*-thiophene), 8.31 (d, 2H, N*H*). ^{13}C APT NMR (400 MHz, $(CD_3)_2SO$): δ 24.84 (C_6H_{12}-N) pos, 25.15 (C_6H_{12}-N) pos, 32.33 (C_6H_{12}-N) pos, 48.44 (C_6H_{12}-N) neg, 127.84 (*C*H-thiophene) neg, 143.34 (*C*-thiophene) pos, 159.70 (*C*=O) pos. IR ν_{max} (cm^{-1}): 3312 (m), 3084 (w), 2935 (m), 2854 (m), 1626 (s), 1541 (s), 1519 (s), 1447 (m), 1324 (m), 747 (m), 669 (m). Anal. (%) calc. for $C_{18}H_{26}N_2O_2S$: C, 64.6; H, 7.8; N, 8.4; found: C, 64.4; H, 7.4; N, 8.8.

Synthesis of thiophene-2,5-dicarboxylic acid dibenzylamide (L3e). Thiophene-2,5-dicarbonyl dichloride (0.477 g, 2.28 mmol) and benzylamine (2.98 ml, 27.4 mmol) were used to prepare ligand **L3e**. Single crystals were grown by slow evaporation of an acetonitrile solution of **L3e**. Yield: 64%. Melting point: 243-244 °C. ^{1}H NMR (400 MHz, $(CD_3)_2SO$): δ 4.46 (d, 4H, C*H*$_2$-Ph), 7.25 (t, 2H, Ph), 7.32 (m, 8H, Ph), 7.76 (s, 2H, C*H*-thiophene), 8.31 (d, 2H, N*H*). ^{13}C APT NMR (400 MHz, $(CD_3)_2SO$): δ 42.55 (*C*H$_2$-Ph) pos, 126.88 (Ph) neg, 127.26 (Ph) neg, 128.32 (Ph) neg, 139.14 (Ph) pos, 143.04 (*C*-thiophene) pos, 160.65 (*C*=O) pos. IR ν_{max} (cm^{-1}): 3306 (m), 3083 (w), 3025 (w), 1626 (s), 1543 (s), 1515 (s), 1455 (m), 1429 (m), 1297 (s), 748 (m), 604 (m). Anal. (%) calc. for $C_{20}H_{18}N_2O_2S$: C, 68.5; H, 5.2; N, 8.0; found: C, 68.2; H, 4.9; N, 8.2.

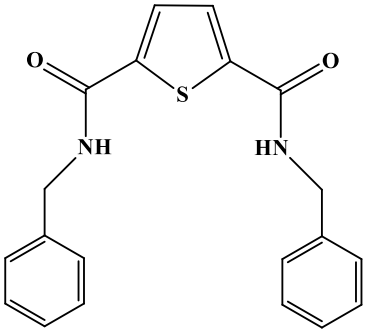

4.3.3 Crystallographic analyses

Single-crystal X-ray diffraction data were collected on a Bruker KAPPA APEX II DUO diffractometer using graphite-monochromated Mo-Kα radiation (χ = 0.71073 Å). Data collection was carried out at 173(2) or 295(2) K. The temperature was controlled using an Oxford Cryostream cooling system (Oxford Cryostat). Cell refinement and data reduction were performed using the program SAINT.[47] The data were scaled and absorption correction performed using SADABS.[48]

The structure was solved by direct methods using SHELXS-97[48] and refined by full-matrix least-squares methods based on F^2 using SHELXL-2014[48] and using the graphics interface program X-Seed[49]. The programs X-Seed and POV-Ray were both used to prepare molecular graphic images.

All non-hydrogen atoms were refined anisotropically and all, except the hydrogen H1N on N1, were placed in idealised positions and refined in riding models with U_{iso} assigned 1.5 or 1.2 times U_{eq} of their parent atoms. The bond distances were constrained at either 0.95 Å or 0.98 Å. The hydrogen H1N was located in the difference electron density maps and refined independently. Selected crystallographic and structural refinement data are presented in Table 4.1.

4.3.4 *In situ* oxidation studies

Oxidation reactions were performed in duplicate using two-neck pear shaped flasks (25 ml capacity) which were equipped with a condenser. In a typical reaction the following components were added: acetonitrile (solvent), cyclopentanone (internal standard), *n*-octane (substrate), hydrogen peroxide (H_2O_2) as the oxidant, the ligand, and the metal salt so that the total volume equated to 5 ml. The ligand and metal salt were introduced in the form of stock solutions with varying volumes in order to keep the no. of moles constant at 9.56×10^{-6} mol. The ligand to metal to substrate ratio was kept constant at 1:1:100 and a substrate to oxidant ratio of 1:9 was used. All reactions were carried out at a temperature of 50 °C which was maintained using an oil bath and a hot plate connected to a thermocouple. After a period of 24 h, an aliquot was removed, treated with PPh_3 and filtered through a Celite plug. Thereafter, 0.5 µl of the sample was injected into the GC for product analysis and quantification. A PerkinElmer Auto System gas chromatograph equipped with a flame ionisation detector (FID), which was set at 260 °C, was used for the analysis of the products. The injector temperature was set at 240 °C and a Pona column (50 m x 0.20 mm x 0.5µm) was employed to efficiently separate the products. Yields were calculated based on the total moles of products formed divided by the initial moles of substrate added into the reaction mixture and was expressed as a percentage while the percentage selectivity was expressed as moles of each product divided by the total moles of all products in the stream.

Table 4.1: Selected crystallographic and structure refinement data for compound **L3a**, **L3b** and **L3e**.

	L3a	**L3b**	**L3e**
Empirical formula	$C_8H_{10}N_2O_2S$	$C_{14}H_{22}N_2O_2S$	$C_{20}H_{18}N_2O_2S$
Formula weight	198.24	282.39	350.42
Temperature (K)	173(2)	173(2)	295(2)
Crystal system	monoclinic	monoclinic	orthorhombic
Space group	I2/a	P*n*	Pbcn
a (Å)	8.9361(14)	9.7350(8)	10.4596(11)
b (Å)	9.8978(14)	15.9958(14)	9.5313(12)
c (Å)	9.810(2)	9.8642(8)	18.800(2)
α (°)	90	90	90
β (°)	90.263(2)	97.541(2)	90
γ (°)	90	90	90
Volume ($Å^3$)	867.7(3)	1522.8(2)	1874.2(4)
Z	4	4	4
ρ_{calc} (g/cm^3)	1.518	1.232	1.242
μ (mm^{-1})	0.339	0.213	0.187
F(000)	416	608.0	736.0
Crystal size (mm^3)	0.09 x 0.11 x 0.22	0.150 × 0.120 × 0.100	0.380 × 0.280 × 0.090
2Θ range for data collection (°)	5.848 to 56.832	4.882 to 53.544	4.334 to 55.784
Index ranges	$-11 \le h \le 11$, $-13 \le k \le 13$, $-13 \le l \le 13$	$-12 \le h \le 12$, $-20 \le k \le 20$, $-11 \le l \le 12$	$-7 \le h \le 13$, $-12 \le k \le 12$, $-24 \le l \le 24$
Reflections collected	7398	14407	29523
Independent reflections	1088 [R(int) = 0.047]	5915 [R(int) = 0.0379	2243 [R(int) = 0.0458
Data / restraints / parameters	1088/0/65	5915/121/392	2243/48/118
Goodness-of-fit on F^2	1.105	1.032	1.042
Final R indices [I >=2σ (I)]	R1 = 0.0322, wR2 = 0.0787	R1 = 0.0459, wR2 = 0.1031	R_1 = 0.0454, wR_2 = 0.1191
Final R indices (all data)	R1 = 0.0390, wR2 = 0.0824	R1 = 0.0624, wR2 = 0.1106	R_1 = 0.0636, wR_2 = 0.1344
Largest diff. peak and hole ($e.Å^{-3}$)	0.34/-0.21	0.64/-0.22	0.23/-0.24

4.4 Results and discussion

4.4.1 Synthesis and characterisation of NSN ligands

In this study, five NSN ligands were prepared based on a rigid thiophene backbone containing amide functionalities on the 2- and 5-positions of the heterocycle. Varying substituents were introduced on the N-donor arms to investigate the steric and electronic properties of the ligand. These are thiophene-2,5-dicarboxylic acid di(R)amide (**L3**) where R = methyl (**a**), butyl (**b**), pentyl (**c**), cyclohexyl (**d**) and benzyl (**e**). Synthetic routes to the ligands, as displayed in Scheme 4.1, involved reacting the ligand precursor thiophene-2,5-dicarbonyl dichloride (**1**) with 12 equivalents of the respective amine (**2**) to obtain the products in 64-94% yield.

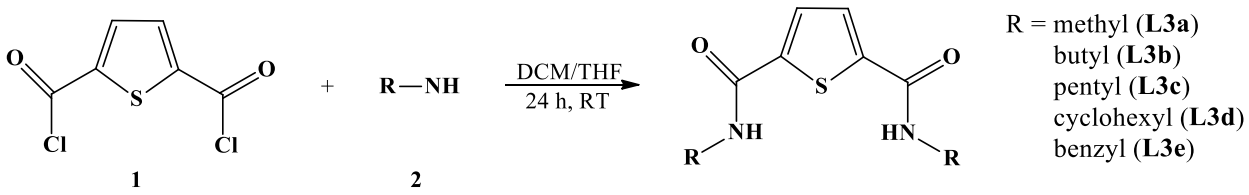

Scheme 4.1: Synthetic route for the preparation of the NSN ligands.

The reaction work up consisted of the suspension of the mixture in double-distilled water, followed by filtration and a series of washing, first with HCl to remove excess amine and then with a solution of $NaHCO_3$ to neutralise the acid. After a final wash with water and drying under vacuum, the products were obtained as white powders. Sharp melting points, clean NMR spectra as well as accurate CHN analyses indicated that the ligands were synthesised in high purity. A representative ^{1}H NMR spectrum of **L3b** is shown in Fig. 4.1. The characteristic amine proton peak (**f**) resonated at 8.56 ppm and appeared as a triplet. This signal was split by the two adjacent protons (**d**) and consequently protons **d** were split by **f** and **c**, therefore giving rise to a quartet resonating at 3.20 ppm. The same trend was observed for the other ligands in the series.

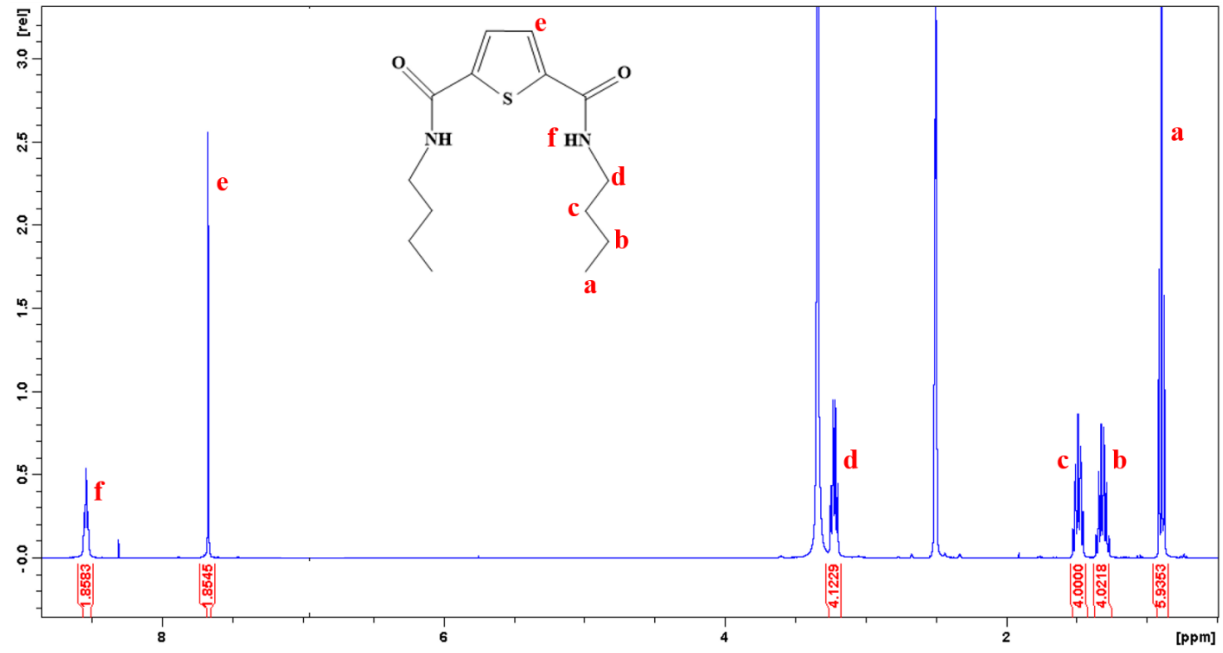

Figure 4.1: ^{1}H NMR spectrum of ligand **L3b** showing signals for the highlighted protons (**a-f**).

4.4.2 Molecular structural analysis by X-ray diffraction studies

Single crystals of **L3a**, **L3b** and **L3e** were obtained by slow evaporation of concentrated solutions of the respective ligands in either methanol or acetonitrile to yield colorless crystals. **L3a** and **L3b** respectively crystallised in the *I*2/*a* and *Pn* space groups of the monoclinic crystal system, while **L3e** belongs to the *Pbcn* space group of the orthorhombic crystal system. Analysis of the selected bond lengths and angles presented in Table 4.2, shows no differences of any significance between these values for all three ligands compared.

The asymmetric unit of **L3a** contains half a molecule with the remainder generated by symmetry 1.5-x, y, -z (displayed in Fig. 4.2). The entire molecule is mono planar, arranged in ordered parallel sheets in the crystal lattice. Every alternate sheet contains the molecules arranged in counter directions thus forming a 'top-to-bottom' arrangement when viewed along the *a*-axis (Fig. 4.2). This ordered arrangement of the crystal units allows for efficient stacking of the adjacent sheets that contributed to the high melting point observed (332-333 °C) for **L3a** due to long range interactions.

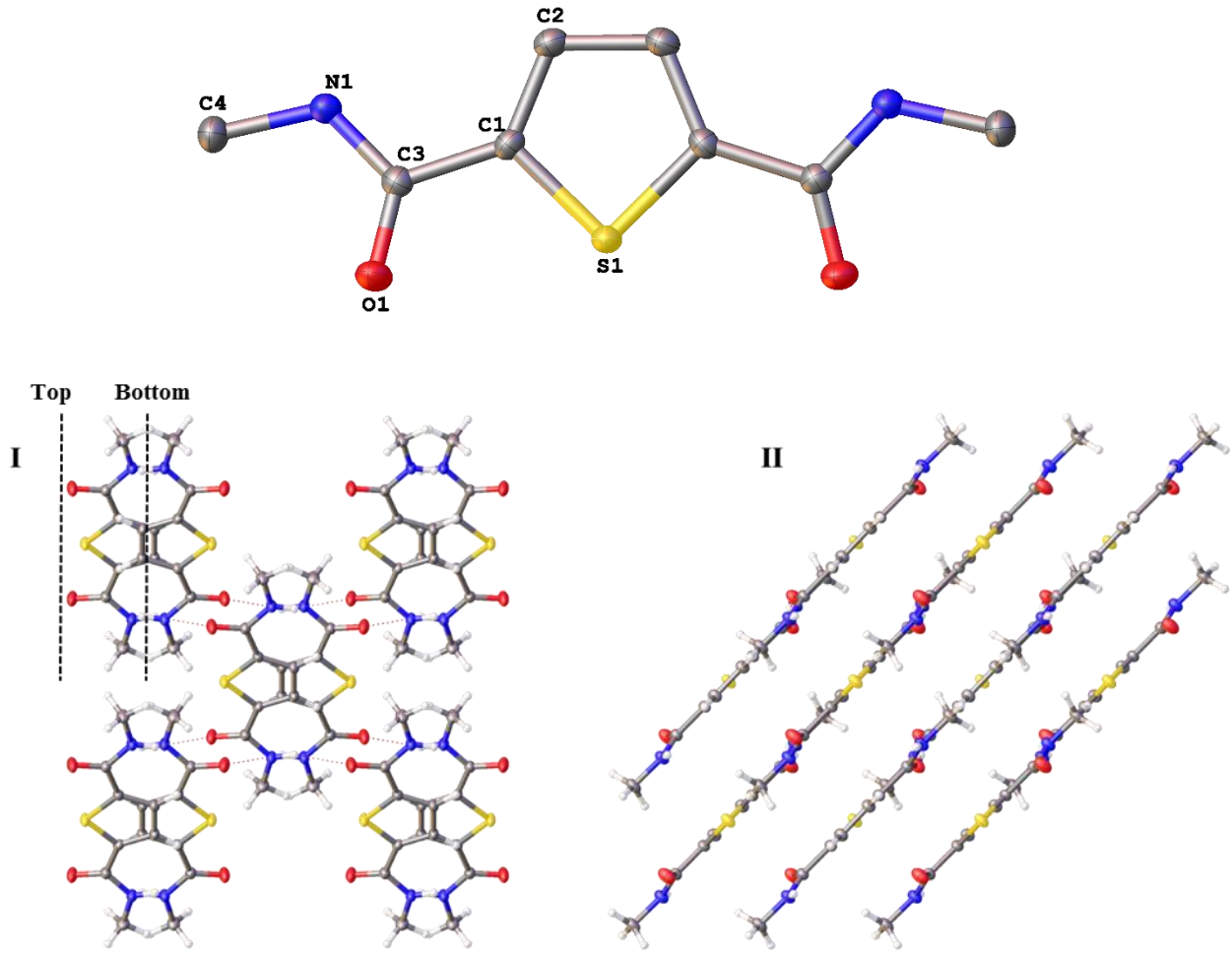

Figure 4.2: Molecular structure of **L3a** with hydrogen atoms omitted for clarity and thermal ellipsoids at drawn at the 50% probability level and crystal packing viewed along 100 (I) and 101 (II).

Table 4.2: Selected bond lengths (Å) angles (°) for ligands **L3a**, **L3b** and **L3e**.

		L3a	
S(1)−C(1)	1.7142(14)	C(3)−C(1)−S(1)	117.79(10)
O(1)−C(3)	1.2375(17)	O(1)−C(3)−N(1)	122.79(13)
N(1)−C(3)	1.3262(18)	O(1)−C(3)−C(1)	120.58(13)
N(1)−C(4)	1.4506(19)	N(1)−C(3)−C(1)	116.63(12)
		L3b	
S(1)−C(1)	1.721(5)	C(5)−C(1)−S(1)	118.4(3)
S(1)−C(4)	1.722(5)	O(1)−C(5)−N(1)	124.1(4)
O(1)−C(5)	1.247(5)	O(1)−C(5)−C(1)	118.9(4)
O(2)−C(10)	1.242(5)	O(2)−C(10)−N(2)	123.3(4)
N(1)−C(5)	1.319(6)	O(2)−C(10)−C(4)	120.3(4)
N(1)−C(6)	1.451(6)	N(1)−C(5)−C(1)	117.0(4)
N(2)−C(10)	1.331(5)	N(2)−C(10)−C(4)	116.4(4)
N(2)−C(11)	1.467(6)		
		L3e	
S(1)−C(9)	1.7162(16)	C(8)−C(9)−S(1)	117.16(10)
O(1)−C(8)	1.2333(18)	O(1)−C(8)−N(1)	122.41(17)
N(1)−C(8)	1.326(2)	O(1)−C(8)−C(9)	117.82(13)
N(1)−C(7)	1.454(2)	N(1)−C(8)−C(9)	116.63(12)

The molecular structure of **L3b** is presented in Fig. 4.3 in which the asymmetric unit cell contains two similar but independent molecules, and for clarity only one molecule is shown. Unlike **L3a**, **L3b** is asymmetric due to the high flexibility of the butyl groups. Consequently, disorder of the butyl chain was observed. Due to the presence of two molecules in nonequivalent positions in the crystal lattice, a unique packing motif was observed. The packing reveals a combination of zig-zag and linear arrangements of the molecules in alternating rows (Fig. 4.3), viewed along the *c* axis or 001.

Similar to **L3a**, the asymmetric unit of **L3e** contains one half of the molecule with the remainder generated by the symmetry operation, –x, y, 0.5-z. Furthermore, disorder within the phenyl rings

were noted. The thiophene ring and the amide linkage reside on a single basal plane with the phenyl ring lying on a separate plane that intersects the basal plane at an angle of 79.53°. The crystal packing of **L3e**, shown in Fig. 4.4, indicates an ordered zig-zag conformation with the phenyl groups in alternating planes.

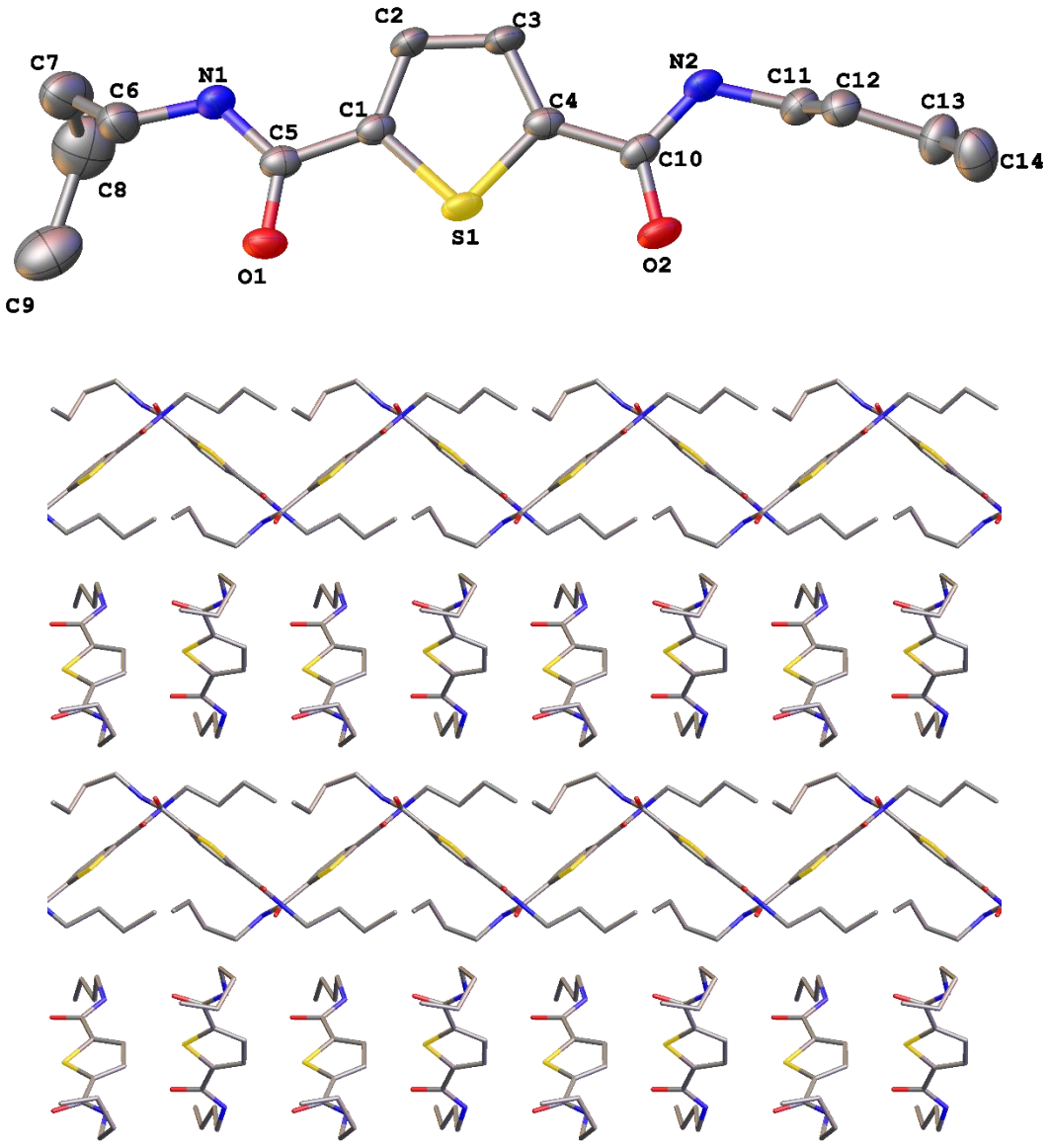

Figure 4.3: Molecular structure of **L3b** and crystal packing viewed along 001 with hydrogen atoms omitted for clarity and thermal ellipsoids drawn at the 50% probability level.

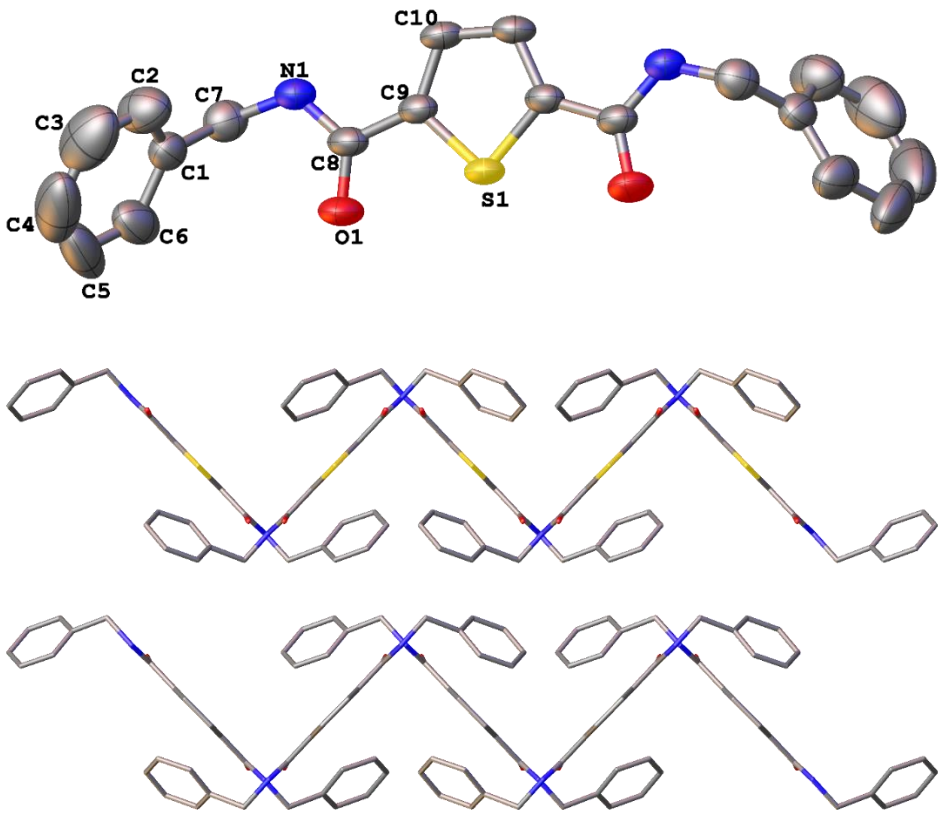

Figure 4.4: Molecular structure of **L3e** and crystal packing viewed along 010 with hydrogen atoms omitted for clarity and thermal ellipsoids drawn at the 50% probability level.

Complexation of these ligands to various metal precursors of iron, cobalt, nickel, copper and zinc was attempted with no success in the isolation of a stable complex. In most cases, only the unreacted ligand was recovered from the reaction, whilst in other reactions an oily residue was recovered, which did not correspond to a complex with the ligand. Presumably, the delocalisation of electrons between the carbonyl group of the amide linkage and the thiophene ring weakened the donor ability of the nitrogen atom. Furthermore, the sulfur on the thiophene ring is already a weak donor and hence the ability of this set of ligands to bind to the first row transition metals (mostly hard Lewis acidic centres) utilised in this study is hindered by their chemistry. In an effort to increase the binding ability of the ligand, reduction of the carbonyl group to form an imine bond using lithium aluminium hydride was attempted using literature procedures[50,51] with no success. Moreover, reactions in the presence of various bases were performed in an attempt to abstract the amide proton to increase the possibility of coordination, but this was also unsuccessful.

4.4.3 *In situ* catalytic studies

In order to test potential catalytic activity involving this ligand set, *in situ* studies were carried out using simple chloride metal salts of iron, cobalt, nickel and copper with two of the prepared ligands: **L3b** and **L3e**. These specific ligands were chosen simply because of their solubility in acetonitrile, which is the solvent of choice in this catalytic study. H_2O_2 was selected as the source of oxygen because it is a cheaper and "greener" oxidant, since the only by products are water and oxygen. Control experiments containing only the metal salt, the ligand or just the substrate (*n*-octane) with the oxidant were carried out. The blank reaction containing no catalyst gave a combined product yield of 2% in 24 h, whilst a reaction with only the ligand as the catalyst yielded the same amount of product as the blank run, indicating that the ligand is inactive on its own as a metal-free catalyst for this reaction. In a typical catalytic reaction, stoichiometric amounts of the metal salt and the ligand were combined together with the substrate, *n*-octane, and H_2O_2 so that the ratio was 1:1:100:900.

No improvement in the catalytic activity often associated with *in situ* generated metal complexes was observed with iron, nickel or cobalt metal salts, thus indicating that the ligand did not coordinate to the metal during the catalytic reaction. However, a significant difference was noted for the ligands in combination with $CuCl_2$ as shown in Fig. 4.5.

In 24 h, $CuCl_2$ as the catalyst gave a yield of C-8 oxygenates (secondary octanols, octanones and C(1) products) of 12%, whereas **L3b**/$CuCl_2$ and **L3e**/$CuCl_2$ produced much improved yields of 21 and 27% respectively. This certainly implies that the ligand formed some sort of synergistic or cooperative union (possible coordination) with the copper metal centre during the course of the catalytic reaction, thereby forming an intermediate complex, which is likely involved in enhancing the yield of the reaction. Furthermore, a ligand effect based on the N-donor substituents is observed in that the ligand with the benzyl side group (**L3e**) gave a higher yield in comparison to the butyl substituted ligand (**L3b**). Both steric and electronic effects could be cited as responsible for the catalytic activity, because the benzyl group is sterically bulkier and more electron donating than the butyl side chain.

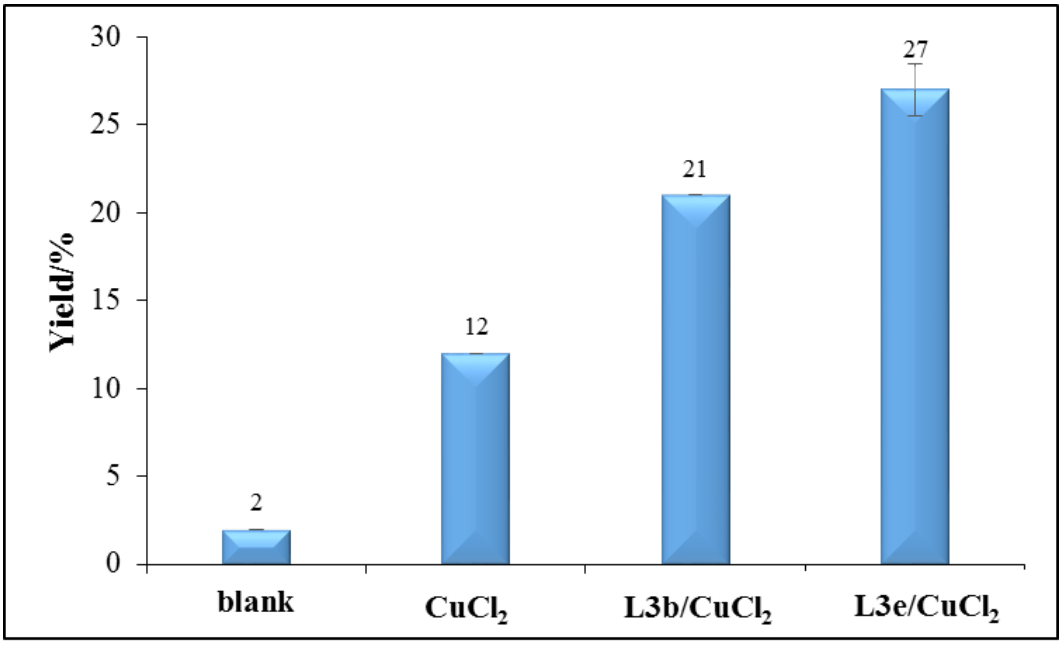

Figure 4.5: Product yield obtained for **L3b** and **L3e**/$CuCl_2$ in comparison to the blank and $CuCl_2$ at 50 °C in 24 h with an octane to H_2O_2 ratio of 1:9.

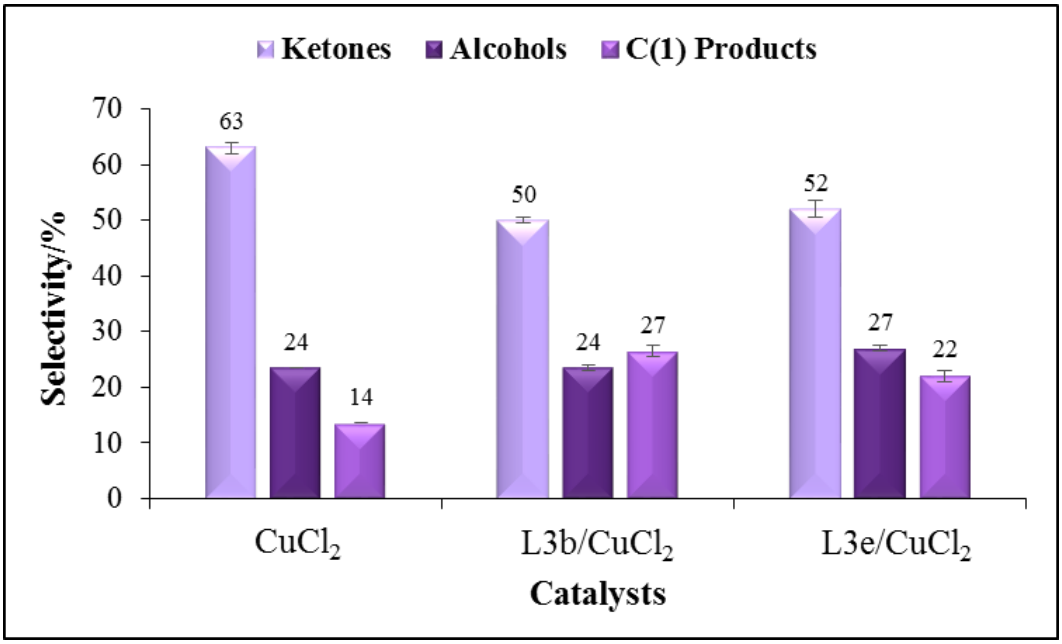

Figure 4.6: Product distribution for the oxidation of *n*-octane. Conditions: 50 °C, 24 h, octane:H_2O_2 = 1:9. (The alcohols include only those of the internal carbons while C(1) includes the 1-ol and acid products).

From the product distribution depicted in Fig. 4.6, it is evident that the selectivity profiles are different for the *in situ* catalyst systems in comparison to $CuCl_2$ alone. This result strongly suggests that the ligands influence the selectivity, particularly with regards to the ketone and primary or C(1) products (1-octanol and octanoic acid). A lower selectivity to the ketones is observed for the **L3b** and **L3e**/$CuCl_2$ systems compared to just $CuCl_2$, implying that the ligands play some role in slowing down the auto-oxidation of the initial alcohols to the corresponding ketones. Moreover, a higher selectivity to the C(1) products suggest that the ligands aid in the activation of the primary (terminal) carbons. The **L3b**/$CuCl_2$ system, in particular, displays a higher selectivity to the C(1) products in comparison to **L3e**/$CuCl_2$, which implies that the selectivity to the primary products are more influenced by steric factors. More specifically, the less sterically demanding, long chain butyl groups of **L3b** promoted primary product selectivity, whereas, the cyclic aromatic nature of the benzyl substituents in **L3e** seem to slightly hinder catalytic activation at the primary carbon.

4.5 Conclusion

This work reports the synthesis of five NSN ligands based on a thiophene backbone with a variation of the substituents bonded to the N-donor atoms. Single crystal X-ray diffraction analyses of **L3a** and **L3e** revealed symmetric structures with ordered arrangements of the molecules, whilst **L3b** displayed an unsymmetrical structure due to the flexible butyl side chains. Various attempts were made to coordinate this ligand set to several metal precursors with no success, possibly due to the weak donor ability of the thiophene sulfur and the amide nitrogens. The oxidation of *n*-octane with ligands **L3b** and **L3e** in combination with metal salts of iron, cobalt, nickel and copper, revealed a strong ligand effect with the copper salt, however no effect was observed with the other metal salts. The **L3b** and **L3e**/$CuCl_2$ systems produced total product yields of 21 and 27% respectively, which was considerably higher than for $CuCl_2$ alone (yield of 12%) in 24 h. Furthermore, the selectivity profile showed that the ligands enhanced the primary carbon selectivity. This work is still in progress and further studies on the possible catalytic intermediates and mechanisms are required for understanding the fundamentals of the catalysis.

4.6 References

(1) Clerici, G. M. *Appl. Catal.* **1991**, *68*, 249.

(2) Shul'pin, G. B.; Lindsay-Smith, J. R. *Russ. Chem. Bull.* **1998**, *47*, 2379.

(3) Shul'pin, G. B.; Süss-Fink, G.; Lindsay Smith, J. R. *Tetrahedron* **1999**, *55*, 5345.

(4) Shul'pin, G. B.; Süss-Fink, G.; Shul'pina, L. S. *J. Mol. Catal. A: Chem.* **2001**, *170*, 17.

(5) Süss-Fink, G.; Gonzalez, L.; Shul'pin, G. B. *Appl. Catal., A: General* **2001**, *217*, 111.

(6) Brazdil, J. *Top. Catal.* **2006**, *38*, 289.

(7) Nagataki, T.; Ishii, K.; Tachi, Y.; Itoh, S. *Dalton Trans.* **2007**, 1120.

(8) Mirkhani, V.; Moghadam, M.; Tangestaninejad, S.; Mohammadpoor-Baltork, I.; Rasouli, N. *Catal. Commun.* **2008**, *9*, 2411.

(9) Kozlov, Y. N.; Nizova, G. V.; Shul'pin, G. B. *J. Phys. Org. Chem.* **2008**, *21*, 119.

(10) Shul'pina, L. S.; Kirillova, M. V.; Pombeiro, A. J. L.; Shul'pin, G. B. *Tetrahedron* **2009**, *65*, 2424.

(11) Fernandes, R. R.; Kirillova, M. V.; da Silva, J. A. L.; Fraústo da Silva, J. J. R.; Pombeiro, A. J. L. *Appl. Catal., A: General* **2009**, *353*, 107.

(12) Mac Leod, T. C. O.; Kirillova, M. V.; Pombeiro, A. J. L.; Schiavon, M. A.; Assis, M. D. *Appl. Catal., A* **2010**, *372*, 191.

(13) Kirillova, M. V.; Kirillov, A. M.; Mandelli, D.; Carvalho, W. A.; Pombeiro, A. J. L.; Shul'pin, G. B. *J. Catal.* **2010**, *272*, 9.

(14) Abbenhuis, R. A. T. M.; del Río, I.; Bergshoef, M. M.; Boersma, J.; Veldman, N.; Spek, A. L.; van Koten, G. *Inorg. Chem.* **1998**, *37*, 1749.

(15) Mastrostamatis, S. G.; Papadopoulos, M. S.; Pirmettis, I. C.; Paschali, E.; Varvarigou, A. D.; Stassinopoulou, C. I.; Raptopoulou, C. P.; Terzis, A.; Chiotellis, E. *J. Med. Chem.* **1994**, *37*, 3212.

(16) Nock, B. A.; Maina, T.; Yannoukakos, D.; Pirmettis, I. C.; Papadopoulos, M. S.; Chiotellis, E. *J. Med. Chem.* **1999**, *42*, 1066.

(17) Canovese, L.; Visentin, F.; Chessa, G.; Niero, A.; Uguagliati, P. *Inorg. Chim. Acta* **1999**, *293*, 44.

(18) Ball, R. J.; Genge, A. R. J.; Radford, A. L.; Skelton, B. W.; Tolhurst, V.-A.; White, A. H. *J. Amer. Chem. Soc., Dalton Trans.* **2001**, 2807.

(19) Canovese, L.; Visentin, F.; Chessa, G.; Gardenal, G.; Uguagliati, P. *J. Organomet. Chem.* **2001**, *622*, 155.

(20) McGuinness, D. S.; Wasserscheid, P.; Keim, W.; Morgan, D.; Dixon, J. T.; Bollmann, A.; Maumela, H.; Hess, F.; Englert, U. *J. Am. Chem. Soc.* **2003**, *125*, 5272.

(21) McGuinness, D. S.; Wasserscheid, P.; Morgan, D. H.; Dixon, J. T. *Organometallics* **2005**, *24*, 552.

(22) Temple, C.; Jabri, A.; Crewdson, P.; Gambarotta, S.; Korobkov, I.; Duchateau, R. *Angew. Chem.* **2006**, *118*, 7208.

(23) Shaffer, D. W.; Szigethy, G.; Ziller, J. W.; Heyduk, A. F. *Inorg. Chem.* **2013**, *52*, 2110.

(24) Saghatchi, F.; Ahmadi, E.; Mohamadnia, Z.; Hajifatheali, H.; Tabebordbar, H.; Karimi, F. *Chem. Pap.* **2014**, *68*, 1555.

(25) Funasako, Y.; Kaneshige, K.; Inokuchi, M.; Hosokawa, H.; Mochida, T. *J. Organomet. Chem.* **2015**, *797*, 120.

(26) Mejia-Rivera, F.; Alvarado-Rodríguez, J.; Andrade-López, N.; Cruz-Borbolla, J.; Jancik, V.; Moreno-Esparza, R.; Pandiyan, T. *Struct Chem* **2015**, *26*, 189.

(27) Hajifatheali, H.; Ahmadi, E.; Wojtczak, A.; Jaglicic, Z. *Macromol. Res.* **2015**, *23*, 977.

(28) Chen, X.; Jing, Y.; Yang, X. *Chem. Eur. J.* **2016**, *22*, 1950.

(29) Shimokawa, R.; Kawada, Y.; Hayashi, M.; Kataoka, Y.; Ura, Y. *Dalton Trans.* **2016**.

(30) Das, U. K.; Daifuku, S. L.; Gorelsky, S. I.; Korobkov, I.; Neidig, M. L.; Le Roy, J. J.; Murugesu, M.; Baker, R. T. *Inorg. Chem.* **2016**, *55*, 987.

(31) Albrecht, M.; Dani, P.; Lutz, M.; Spek, A. L.; van Koten, G. *J. Am. Chem. Soc.* **2000**, *122*, 11822.

(32) Okamoto, K.; Kanbara, T.; Yamamoto, T.; Wada, A. *Organometallics* **2006**, *25*, 4026.

(33) Majumder, P.; Baksi, S.; Halder, S.; Tadesse, H.; Blake, A. J.; Drew, M. G. B.; Bhattacharya, S. *Dalton Trans.* **2011**, *40*, 5423.

(34) Niu, J.-L.; Hao, X.-Q.; Gong, J.-F.; Song, M.-P. *Dalton Trans.* **2011**, *40*, 5135.

(35) Ito, J.-i.; Kaneda, T.; Nishiyama, H. *Organometallics* **2012**, *31*, 4442.

(36) Chen, T.; He, L.-P.; Gong, D.; Yang, L.; Miao, X.; Eppinger, J.; Huang, K.-W. *Tetrahedron Lett.* **2012**, *53*, 4409.

(37) Ghorai, D.; Kumar, S.; Mani, G. *Dalton Trans.* **2012**, *41*, 9503.

(38) DeMott, J. C.; Dekarske, J. R.; McCulloch, B. J.; Ozerov, O. V. *Inorg. Chem. Frontiers* **2015**, *2*, 912.

(39) Mylonas, I.; Triantis, C.; Panagiotopoulou, A.; Patsis, G.; Raptopoulou, C. P.; Terzis, A.; Psycharis, V.; Komiotis, D.; Pelecanou, M.; Pirmettis, I.; Papadopoulos, M. *Inorg. Chim. Acta* **2013**, *400*, 2.

(40) Graf, D. D.; Schrock, R. R.; Davis, W. M.; Stumpf, R. *Organometallics* **1999**, *18*, 843.

(41) Fandos, R.; Fernández-Gallardo, J.; Otero, A.; Rodríguez, A.; Ruiz, M. a. J. *Organometallics* **2011**, *30*, 1551.

(42) Liu, B.; Li, L.; Sun, G.; Liu, J.; Wang, M.; Li, S.; Cui, D. *Macromolecules* **2014**, *47*, 4971.

(43) Pedras, B.; Santos, H. M.; Fernandes, L.; Covelo, B.; Tamayo, A.; Bértolo, E.; Capelo, J. L.; Avilés, T.; Lodeiro, C. *Inorg. Chem. Comm.* **2007**, *10*, 925.

(44) Agapie, T.; Day, M. W.; Bercaw, J. E. *Organometallics* **2008**, *27*, 6123.

(45) Furniss, B. S.; Hannaford, A. J.; Smith, P. W. G.; Tatchell, A. R. *Vogel's textbook of practical organic chemistry*; 5th ed.; J. Wiley and sons: New York, 1989.

(46) Coles, S. J.; Gale, P. A.; Hursthouse, M. B.; Light, M. E.; Warriner, C. N. *Supramol. Chem.* **2004**, *16*, 469.

(47) SAINT Version 7.60a, Bruker AXS Inc., Madison, WI, USA, 2006.

(48) G. M. Sheldrick, SHELXS-97, SHELXL-2014 and SADABS version 2.05, University of Göttingen, Germany, 1997.

(49) Barbour, L. J. *Supramol. Chem.* **2001**, *1*, 189.

(50) DeVries, V. G.; Bloom, J. D.; Dutia, M. D.; Katocs, A. S.; Largis, E. E. *J. Med. Chem.***1989**, *32*, 2318.

(51) Ravinder, B.; Rajeswar Reddy, S.; Panasa Reddy, A.; Bandichhor, R. *Tetrahedron Lett.* **2013**, *54*, 4908.

CHAPTER FIVE

Summary and Conclusion

The development of efficient homogeneous catalytic systems for the oxidation of saturated alkanes has remained a difficult task, which many research groups have tried to address over the last decades. Significant progress has been made in this field, however the development of an economically viable system that is highly active and selective and is still a challenge. This work presents efforts towards the development of such catalytic systems, with the synthesis of new types of biologically inspired SNS pincer ligands and their coordination to cheap, earth abundant, first row transition metals, nickel and copper. The prepared complexes were applied as catalysts in the oxidation of *n*-octane, as the alkane substrate, using either TBHP or H_2O_2 as an oxidant.

The prepared SNS ligands were classified into two series based on the type of N-donor substituent, i.e. a methyl (**L1**) or phenyl (**L2**) group. The ligand backbone was symmetric with ethylene spacers bridging the central N-donor to the S-donors to create a degree of flexibility. In addition, the substituents bound to the S-donor atoms were varied in order to establish possible stereoelectronic effects on the resultant complexes. A total of ten SNS ligands were synthesised and characterised in this study.

Coordination of most of these ligands to nickel were successful, yielding six new complexes which were fully characterised. The methyl N-substituted complexes (**1.1**) were formed as homobimetallic dimers bridged through three chloro groups, whereas the phenyl N-substituted complexes (**1.2**) were monomeric, with five coordinate, trigonal bipyramidal geometries around the metal centres.

All ten ligands were coordinated to copper to yield five new complexes with the methyl (**2.1**) and five with the phenyl (**2.2**) substituted on the N-donor atom, all of which also crystallised as five coordinate monomeric species. The exception was **2.2b**, containing an ethylene substituent on the S-donor atoms, which crystallised in an unusual dimeric fashion, bridged through a metallic $[CuCl_4]^{2-}$ anion. One of the differences observed between the two series of complexes (based on

the N-donor substituents) was their symmetry or lack thereof. The phenyl N-substituted nickel and copper complexes exhibited higher symmetry and order within the crystal lattice, due to the rigid aromatic ring, in comparison to the asymmetric methyl N-substituted ones.

After optimisation, all the catalytic oxidation reactions were conducted under relatively mild conditions at ambient pressure and a temperature of 50 °C, catalyst loading of 1 mol% and substrate to oxidant ratios of 1:12 (TBHP) and 1:9 (H_2O_2).

The activity of the nickel catalysts **1.1** and **1.2** were higher in comparison to the simple nickel salts, producing total yields to oxygenated products of 6-10% at 48 h with TBHP as the oxidant. The product distribution was a mixture of secondary octanols and octanones (major product) with no terminal carbon activation observed. Reactions with H_2O_2 as the oxidant produced yields of 1-2% over 24 h, which was equivalent to the blank, thus implying catalyst decomposition with this oxidant.

Catalytic data for the copper complexes with TBHP as the oxidant gave yields of ~15% for all the catalysts, which was similar to or less than that obtained with the uncomplexed $CuCl_2$ salt, after 24 h. The selectivity profile of the copper salt and the catalysts were also similar, therefore suggesting no effect of the ligand with the TBHP system. However, with H_2O_2 as the oxidant, considerably higher yields of 23-35% and 48-57% were obtained at 1 h, for series **2.1** and **2.2** respectively, with the major products as the alcohols (after reduction with PPh_3), as well as substantial terminal carbon activation. It is also worth noting that the **2.1**/H_2O_2 system gave comparable selectivity and activity to $CuCl_2/H_2O_2$, indicating that the methyl N-substituted ligand dissociated from the metal centre upon addition of the oxidant. On the other hand, the **2.2**/H_2O_2 catalytic series showed significantly higher yields as compared to $CuCl_2/H_2O_2$. More importantly, the profile of products obtained was different, implying a strong influence of the SNS ligands on the **2.2**/H_2O_2 catalytic systems. In addition, a possible copper-peroxo species was identified (using UV-vis) as the reactive intermediate which may have influenced the higher activity of catalyst **2.2**. Furthermore, the results showed that the catalytic activity is dominated by electronic effects since catalyst **2.2d**, containing the electron rich cyclohexyl S-substituents, gave the highest yield of 57% at 1 h. Remarkably high TONs of 2270-3180 were achieved with **2.2**/H_2O_2, indicating that this system was very efficient, in fact this is one of the most efficient *n*-octane oxidation catalysts reported to date. Overall, the phenyl N-substituted copper complexes were more active,

presumably due to the higher stability offered by the rigid and electron rich aromatic ring, in comparison to the methyl N-substituted copper complexes. This result therefore indicates that the ligand backbone does indeed play a significant role in the activity of the catalyst.

One of the major obstacles faced with the SNS ligand donor set is their instability under oxidizing environments. Therefore, a more robust NSN donor set was investigated in an effort to overcome this limitation. A series of NSN ligands (**L3**), containing a thiophene backbone and amide linkages, were synthesised and characterised. Attempts were made to coordinate these ligands to various first row transition metals, with no success. Hence, 'one pot' *in situ* catalytic studies with the ligands and metal salts of iron, cobalt, nickel and copper were investigated, using H_2O_2 as the oxidant. An improvement in the total yield from 12% for $CuCl_2/H_2O_2$ to 21-27% for **L3**/$CuCl_2/H_2O_2$ at 24 h was observed, suggesting that the ligand possibly coordinated to the metal centre during the catalytic cycle, forming a reactive intermediate. A mixture of octanols and octanones were also formed in these reactions, and an enhanced terminal activation was observed with the addition of the ligands. No positive effect was seen with the other metal salts containing Fe, Co or Ni.

A comparison of the results obtained for two of the best catalysts in each series, i.e. nickel catalysts (**1.1**, **1.2**), copper catalysts (**2.2**) and the *in situ* system (**L3**/$CuCl_2/H_2O_2$) is summarised in Table 5.1. It is clear that the copper catalysts were significantly more active, producing substantially higher yields within 1 h, with good selectivity to the alcohols and terminal products. The *in situ* systems also exhibited reasonable activity, with comparable terminal selectivities, but a higher selectivity to the ketone products at 24 h. The nickel catalysts were the least active and most selective to the ketones, presumably due to over-oxidation of the alcohols as a consequence of the prolonged reaction time (48 h).

This study has presented the synthesis and catalytic application of new coordination compounds in the activation of *n*-octane. From the work reported herein, it is evident that the copper-based SNS catalysts have considerable potential. Although further work is required to bring an understanding into the pathways involved in these catalytic systems, it is safe to conclude that this study has contributed significantly towards the development of economically viable systems capable of functioning at mild reaction conditions with high activity and efficiency. This work is indeed a major advancement of the field of alkane oxidation catalysis.

Table 5.1: A summary of the catalytic data for two of the most active catalysts in each study.

Catalyst	Yield/%	Reaction time/h	Product selectivity/%		
			Terminal (C(1))	Secondary octanols	Octanones
1.1a/TBHP	9	48	-	22	78
1.2b/TBHP	10	48	-	26	74
2.2c/H_2O_2	55	1	26	59	15
2.2d/H_2O_2	57	1	27	58	14
L3b/$CuCl_2$/H_2O_2	21	24	27	23	50
L3e/$CuCl_2$/H_2O_2	27	24	22	26	52

Appendix

The supporting information includes data on ^{1}H and ^{13}C APT NMR, IR, HRMS and elemental analysis for the prepared compounds, which are provided as individual pdf documents on the compact disc accompanying this dissertation. In addition, selected catalytic data and representative GC chromatograms for the catalytic reactions are provided. The data is presented in the same order corresponding to the chapter arrangement of the thesis report. This is to ensure that the total volume of the printed text is manageable and within the acceptable limit. Readers are encouraged to access the raw data for further information.